UNIVERSITÀ DEGLI STUDI DI PADOVA

DIPARTIMENTO DI INGEGNERIA INDUSTRIALE

CORSO DI LAUREA MAGISTRALE IN
INGEGNERIA CHIMICA E DEI PROCESSI INDUSTRIALI

Tesi di Laurea Magistrale in
Ingegneria Chimica e dei Processi Industriali

DEVELOPMENT OF A PHENOMENOLOGICAL MODEL OF AN ADSORPTION PROCESS FOR CAPTURING CO_2 FROM AIR

Relatore: Prof. Fabrizio Bezzo

Correlatore: Prof. Martin Van Sint Annaland

Correlatore: Prof. Fausto Gallucci

Correlatore: Ing. Francesco Sabatino

Laureando: FRANCESCO DESTRO

ANNO ACCADEMICO 2017 – 2018

Abstract

In the fight to global warming, it will not be enough to reduce or even to completely eliminate carbon dioxide emissions to fulfill the objectives set by the Paris Agreement: CO_2 must be removed from the atmosphere. Direct Air Capture (DAC) is the most promising technique for this purpose. KMG30 is a relatively cheap hydrotalcite, which demonstrated to have good carbon capture properties at low concentrations of CO_2, making it an interesting sorbent for DAC adsorption processes. In this work, the possibility to exploit KMG30 as sorbent for capturing CO_2 from air was investigated. A literature kinetic model for the sorption of CO_2 in KMG30 at high temperature was adapted to DAC conditions and validated with experimental data. It was found out that it was necessary to study the internal mass transfer in the sorbent particles to reduce the model-experimental data mismatch. A parametric study was then performed, to further improve the accuracy of the model. The parameters optimization was also extended to adsorption of CO_2 in presence of steam, which was proven to enhance the Cyclic Working Capacity (CWC) for CO_2 in KMG30. The final model validation led to very high accuracies in the reproduction of experimental data.

Sorption experiments between 25°C and 200°C were then designed and executed, to try to extend the model to low temperatures. On the basis of the model previously developed and on the collected experimental data, the CWC for the process was calculated for different conditions, to try to optimize the process yield.

Results showed that a Temperature Swing Adsorption (TSA) is the most convenient approach, with the adsorption step executed at room temperature. In these conditions, the higher contribution to the adsorption capacity is due to physisorption. The optimal regeneration condition seems to be achieved with steam at 150-200°C.

Riassunto

Il surriscaldamento globale è un problema affrontato dalla comunità scientifica internazionale ormai da decenni. Molti studi hanno documentato un aumento di temperatura di almeno 0,85°C negli ultimi 130 anni, che ha avuto conseguenze negative sul pianeta, come lo scioglimento dei ghiacciai e l'innalzamento del livello del mare (0.19 m tra il 1901 e il 2010). La causa principale del fenomeno è stata individuata nell'effetto serra, con un ruolo fondamentale attribuito all'aumento della concentrazione atmosferica di CO_2 rispetto all'era pre-industriale. Sarà necessario ridurre le emissioni di CO_2 del 30-85% entro il 2050, per non superare il limite di 450 ppmv di CO_2 nell'aria, determinato dal Gruppo intergovernativo sul cambiamento climatico (*Intergovernmental Panel on Climate Change*, IPCC) come "punto di non ritorno". Nel lungo termine, le risorse rinnovabili potranno prendere il posto dei combustibili fossili, tuttavia nel medio termine una sostituzione completa non sarà possibile, e il cambiamento climatico potrà essere mitigato unicamente riducendo le emissioni di CO_2. L'IPCC stesso ha proposto l'utilizzo di tecnologie di cattura e stoccaggio della CO_2 (*Carbon Capture and Storage*, CCS) per ridurre le emissioni atmosferiche nei processi di combustione. Per mantenere l'aumento di temperatura al di sotto di 1,5°C (limite posto dall'Accordo di Parigi del 2015), non sarà però sufficiente ridurre le emissioni: sarà necessario rimuovere CO_2 dall'aria. Gli attuali processi di CCS non sono adatti a questo scopo, perché sono efficienti per flussi di gas in cui la CO_2 è concentrata, come nei fumi di scarico di un impianto di produzione di energia elettrica tramite combustione. Al contrario, la CO_2 nell'aria è molto diluita (400 ppm), ed è necessario sviluppare processi appositi per queste condizioni. Le tecnologie di cattura della CO_2 atmosferica diretta (*Direct Air Capture*, DAC) sono le più promettenti per questo scopo, perché permettono di rimuovere la CO_2 direttamente dall'aria, con la possibilità in futuro di raggiungere emissioni negative. Un altro vantaggio è che, al contrario dei processi di CCS, le tecnologie di DAC non devono essere collocate necessariamente in corrispondenza dei punti di emissione di CO_2 (cattura distribuita). Ciò consente di sfruttare processi DAC in impianti in cui la CO_2 è utilizzata come reagente, evitando di dover trasportare tramite *pipelines*, intrinsecamente associate ad un costo e ad un rischio, la CO_2 sequestrata tramite CCS.
I primi processi di DAC sfruttavano tecniche di assorbimento in soluzioni acquose alcaline, tuttavia questo tipo di tecnologia sembra avere costi energetici troppo elevati. Le soluzioni devono infatti essere riscaldate durante la rigenerazione, con un elevato dispendio energetico. Sono in seguito stati sviluppati processi di adsorbimento con diversi tipi di materiali solidi, quali ammine supportate, zeoliti e strutture metallorganiche, che hanno dimostrato di permettere di ottenere

prestazioni migliori. Infatti, a parità di CO_2 catturata, i materiali solidi richiedono una quantità di energia per la rigenerazione significativamente inferiore.

Lo scopo di questo lavoro di tesi è lo studio di un processo di DAC tramite adsorbimento con KMG30, un particolare tipo di idrotalcite relativamente economico che ha dimostrato buone capacità di cattura della CO_2. Un modello cinetico disponibile in letteratura (Coenen *et al.*, 2018d) per le reazioni di adsorbimento e desorbimento di CO_2 e H_2O in KMG30 tra 300°C e 500°C è stato implementato in un modello monodimensionale pseudo-omogeneo di un reattore impaccato, al fine di simulare il processo per determinare le condizioni operative ottimali. Una prima convalida con dati sperimentali a 400°C ha mostrato che il modello non era sufficientemente accurato per descrivere esperimenti a basse concentrazioni di CO_2. Il modello di letteratura era infatti mirato a descrivere le reazioni in ampi intervalli di concentrazioni di CO_2 e H_2O, e non nelle specifiche condizioni di interesse per la DAC. Per migliorare l'accuratezza, è stato analizzato il trasporto di materia all'interno delle particelle di sorbente tramite un modello numerico che risolve i bilanci radiali di materia ed energia all'interno di una particella di KMG30. I risultati hanno dimostrato che le reazioni di adsorbimento e desorbimento della CO_2 sono limitate dal trasporto di materia. Una volta che le equazioni del trasporto di materia sono state implementate nel modello del reattore, l'accuratezza nella riproduzione dei dati sperimentali è aumentata, ma ancora non a sufficienza. È stato dunque deciso di effettuare una analisi di sensibilità sui principali parametri cinetici, per ridurre l'errore rispetto ai dati sperimentali. Lo studio parametrico ha dimostrato che il modello cinetico originario sottostimava la capacità di adsorbimento, soprattutto a basse pressioni di CO_2. Allo stesso tempo, le leggi cinetiche sovrastimavano la velocità di desorbimento e alcune reazioni di carbonatazione della massa della particella non erano correttamente implementate. In seguito all'introduzione di valori ottimizzati per i parametri legati a questi problemi, l'accuratezza di riproduzione dei dati sperimentali è stata migliorata significativamente. Lo studio parametrico è stato poi esteso al fine di ottimizzare la parte del modello che descrive le reazioni della CO_2 in presenza di H_2O. È infatti importante ottenere un'elevata accuratezza anche in queste condizioni, perché la rigenerazione del sorbente viene tipicamente effettuata inviando al reattore vapore acqueo.

Una volta che è stato verificato che il modello era convalidato dai dati sperimentali a 400°C sia in presenza che in assenza di H_2O, lo studio è proseguito al fine di individuare le condizioni ottimali per il processo di DAC. È stato verificato che comprimere l'aria in alimentazione al reattore è uno spreco di energia, perché non comporta alcun effettivo aumento di capacità di adsorbimento. Conviene pertanto effettuare il processo a pressione atmosferica. Per quanto riguarda la rigenerazione, il desorbimento tramite invio al reattore di vapore acqueo è la soluzione migliore

rispetto all'utilizzo di azoto, perché H_2O aumenta la capacità ciclica di adsorbimento (*Cyclic Working Capacity*, CWC) e può essere separata facilmente dalla CO_2 prodotta.
Lo studio della temperatura ottimale del processo è una questione più complicata. Dato che alcuni risultati di letteratura avevano dimostrato che la capacità di adsorbimento della CO_2 in idrotalciti è più elevata a basse temperature, è stata valutata la possibilità di effettuare il processo di DAC a due diverse temperature. Operando la fase di adsorbimento a temperatura ambiente e rigenerando invece a temperature più alte, è teoricamente possibile risparmiare energia rispetto ad un processo isotermo a temperatura elevata, come quello precedentemente simulato per la validazione del modello. Dato che non erano disponibili dati sperimentali a bassa temperatura, sono stati effettuati esperimenti di analisi termogravimetrica a 25°C, 100°C e 200°C, che hanno permesso di stimare che la capacità di adsorbimento di KMG30 a temperatura ambiente è di circa 2,80 mol/kg, delle quali 2,00 mol/kg sono adsorbite fisicamente, mentre 0,80 mol/kg sono adsorbite chimicamente. Sono stati effettuati esperimenti a 25°C anche su un reattore a letto impaccato, contenente particelle di sorbente. In questo caso, è stata misurata una capacità di adsorbimento inferiore del 30-40% rispetto all'analisi termogravimentrica. Ciò significa che in un reattore la capacità effettiva di adsorbimento può essere inferiore rispetto alle condizioni di adsorbimento ottimale della TGA, probabilmente a causa di limitazioni dovute al trasporto di materia e a problemi di distribuzione disomogenea della fase gas. Un'altra possibilità per la differenza dei risultati dei due esperimenti è che durante l'analisi termogravimetrica parte dei gas N_2 e O_2 contenuti nell'aria si adsorbano nel materiale, causando una sovrastima parziale della capacità di adsorbimento della CO_2. Anche se questo fenomeno non è documentato in letteratura, per avere conferma della capacità di adsorbimento a temperatura ambiente sarebbe opportuno effettuare ulteriori esperimenti, sia di analisi termogravimetrica che con letto impaccato.
Gli esperimenti hanno dimostrato che a bassa temperatura l'adsorbimento fisico è il maggior responsabile della cattura di CO_2. Pertanto, dato che il modello precedentemente ottimizzato non tiene conto dell'adsorbimento fisico, non può essere usato per simulare l'adsorbimento a bassa temperatura, a meno che non vengano implementate ulteriori equazioni per descrivere questo fenomeno. Il modello è però valido ad alte temperature (superiori a 250°C), ed è quindi utile per analizzare le condizioni di rigenerazione, che avvengono a temperature elevate. Grazie all'utilizzo combinato dei dati sperimentali a bassa temperatura e del modello, è stato possibile effettuare un'analisi delle condizioni ottimali di processo.
La prima situazione analizzata consiste in un processo isotermo a 400°C, nelle condizioni in cui il modello permette di ottenere simulazioni perfettamente affidabili. I risultati hanno dimostrato che la CWC rigenerando con vapore acqueo è compresa tra 0,15 e 0,50 mol/kg.

Si è poi rivolta l'attenzione al processo TSA, con adsorbimento a temperatura ambiente. La CWC è stata calcolata per due diverse temperature di rigenerazione: 200°C, con solo desorbimento fisico, e 400°C, con desorbimento sia fisico che chimico. Secondi i dati sperimentali, rigenerando a 200°C la CWC raggiunge 2 mol/kg, considerando unicamente il desorbimento fisico. Questo valore potrebbe essere ulteriormente aumentato per effetto della presenza di vapore acqueo durante la rigenerazione, come è provato che succeda a 300°C, ma sono necessari ulteriori dati sperimentali per confermare che ciò avvenga anche a 200°C. Rigenerando a 400°C, la CWC aumenta, perché anche la CO_2 adsorbita chimicamente viene desorbita. Tuttavia, le simulazioni effettuate con il modello ottimizzato hanno dimostrato che la capacità aggiuntiva è di solo 0,50-0,85 mol/kg.

Lo studio realizzato permette di concludere che conviene operare la cattura diretta di CO_2 dall'aria mediante particelle di KMG30 con un approccio di TSA. Effettuando la fase di adsorbimento a temperatura ambiente, la CWC è nettamente superiore che operando a 400°C, con l'ulteriore vantaggio del risparmio energetico. Dai risultati ottenuti, sembrerebbe che convenga rigenerare il materiale saturo a 200°C, rilasciando così solo la CO_2 adsorbita fisicamente. È necessario effettuare un'analisi economica del processo per valutare se valga la pena utilizzare vapore acqueo a 400°C, più costoso, per rigenerare anche la CO_2 adsorbita chimicamente.

I valori di CWC ottenuti (attorno a 2 mol/kg) sono simili alle capacità di adsorbimento dei materiali più performanti per la cattura diretta di CO_2, come le strutture metallorganiche e le ammine solide supportate, nonostante le idrotalciti siano generalmente più economiche. Sembra dunque conveniente continuare a studiare il processo. Innanzitutto, è necessario svolgere ulteriori misurazioni per determinare la capacità di adsorbimento a bassa temperatura, dato che gli esperimenti effettuati hanno restituito un valore approssimativo, sebbene sufficientemente accurato per determinare le condizioni ottimali di processo. Inoltre, sarebbe utile implementare all'interno del modello delle equazioni per descrivere l'adsorbimento fisico, per poter effettuare simulazioni anche con cicli di adsorbimento a temperatura ambiente. Un approccio di modellazione di tipo "*black-box*" è consigliato, in quanto una descrizione fenomenologica dell'adsorbimento fisico appare essere troppo complessa per essere implementata all'interno di un modello già oneroso in termini computazionali.

Index

Introduction

In the latest years, several studies and publications demonstrated that the temperature of the planet rose of at least 0.85°C from 1880 to 2012. The anthropogenic contribution to global warming is universally acknowledged upon the scientific community. Recent international policies have endorsed the reduction of the emissions in the atmosphere of CO_2, which is the main contributor to the greenhouse effect. Carbon Capture and Storage (CCS) technology allows to successfully sequestrate CO_2 from point sources, such as power plants, where the concentration of CO_2 in gas streams is significant. However, latest studies demonstrated that this will not be enough to achieve the objectives set by international climate change policies: it will be necessary to remove CO_2 from air, where its concentration is only 400 ppm. Direct Air Capture (DAC) is the most promising category of processes which are aimed to sequestrate carbon from the atmosphere.

The objective of this work is to investigate and quantitively assess the performance of an adsorption technique for DAC. The possibility to exploit KMG30 pellets, a mineral of the hydrotalcites group, as sorbent in a packed bed reactor (PBR) is explored, and an optimization of the process conditions is carried out. The thesis is structured as follows.

In Chapter 1, after introducing the connection between global warming and CO_2 emissions, the advantages and disadvantages of DAC with respect to CCS are presented. The state of the art of DAC is then summarized, with a particular focus on adsorption processes, which seem to be the most promising ones. The main characteristics of hydrotalcites are further presented, with special attention to the carbon capture properties of KMG30. The detailed objectives of this thesis work are then set.

In Chapter 2 the models exploited during this work are introduced. A kinetic model for CO_2 and H_2O sorption in KMG30 valid between 300°C and 500°C taken from literature is presented, together with a model for a PBR used in previous research works. These models were then adapted to the situation of this project. The equations and the main conditions of a particle model which was used to study the mass transfer inside the sorbent pellets are then presented. A final paragraph is dedicated to the description of the experimental setup which was used to perform experiments in the attempt to extend the validity of the model to low temperature.

In Chapter 3 an initial validation of the aforementioned kinetic model with experiments close to DAC feed conditions is performed. Since the kinetic model was meant to give appreciable results in wide ranges of composition of the gas streams, the accuracy in the particular conditions of low CO_2 concentrations was not satisfying. Hence, a study of the intra-particle mass transfer and a

sensitivity analysis on the main parameters of the model were carried out. Results led to propose changes to the model, which allowed to reduce the model-experimental data mismatch within an acceptable error.

In Chapter 4 the performance of DAC with KMG30 in a PBR is evaluated for different process conditions. An isothermal high temperature process is first simulated, using the model optimized in the previous chapter. Then, the possibility to work at room temperature during the adsorption step and to use steam at 200°C or 400°C for the regeneration is assessed. For these calculations, both the model and new data acquired from experiments at low temperature are used.

Final conclusions are then drawn about the optimal process conditions among the analyzed ones, and the limits of the study are accounted for. Suggestions for the development of future work are finally addressed.

Chapter 1

CO_2 capture and objective of the thesis

1.1 Global warming and CO_2 emissions

Land and ocean temperatures rise in the past decades has been documented by several scientists and institutions. An increment of at least 0.85 °C from 1880 to 2012 can be demonstrated on the basis of datasets from different sources. The Intergovernmental Panel on Climate Change in its Fifth Report (IPCC, 2014) clearly states that, in the Northern Hemisphere, the past 30 years have been the warmest in the last 800 years. In Figure 1.1 annual and decadal average temperatures over the period 1850-2012 are reported. Climate change brought harmful effects to the environment, including glaciers melting and a sea level rise of 0.19 m in the period 1901–2010 (IPCC, 2014).

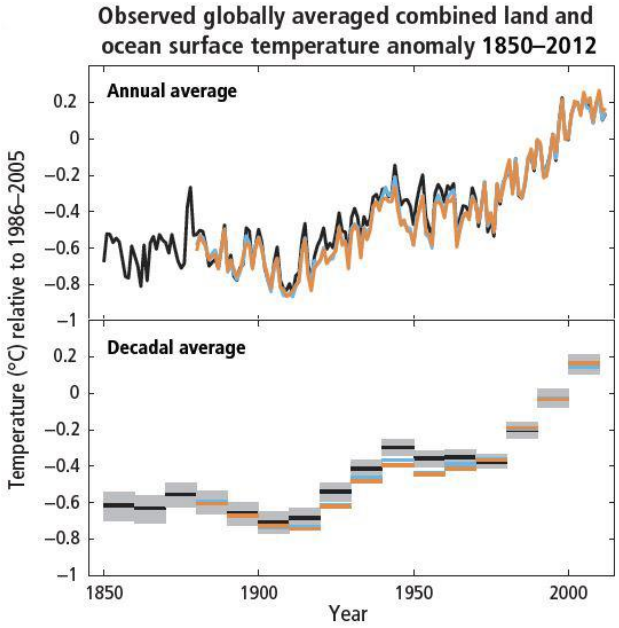

Figure 1.1 *Average annual and decadal temperature deviations from the average temperature in the period 1850-2012. Image taken from the IPCC AR5 (2014)*

The anthropogenic contribution to climate change is unanimously agreed upon within the scientific community (Anderegga *et al.*, 2010). The accumulation of greenhouse gases (GHG) in the atmosphere is the main cause for radiative forcing, with carbon dioxide (CO_2) as the largest single

contributor (IPCC, 2014). Concentration of CO_2 saw a +40% rise since 1750, with an increasing rate in the last decade (IPCC, 2014). Anthropogenic CO_2 emissions are mostly due to the combustion of fossil fuels, which still underpin the transport and power sector of our society. CO_2 represents the largest contributor of all the global anthropogenic GHG emissions, with percentages as high as 75%. An additional criticality related to CO_2 emissions is the high residence time in the atmosphere: the lifetime of CO_2 in the atmosphere might be 300 years, plus 25% that lasts forever (IPCC, 2013). For these reasons climate change discussions have mainly focused on the reduction of CO_2.

CO_2 emissions should be reduced by 30-85% by 2050 not to cross the 450 ppmv of CO_2 in the air, the "non-return limit" set by the IPCC (2014). On the long-term, fossil fuel combustion could be replaced by sustainable resources. On the midterm, however, fossil fuels will still play an important role for power generation and transportation, thus the effect on the climate change can only be mitigated by decreasing CO_2 emissions. Energy savings and efficiency improvements in both power production and consumer products are important means to achieve this goal, but will not be enough to fulfil the new international climate policies. Carbon capture technologies represent a possible solution to compensate for this problem in the short and mid-term.

1.2 CO_2 Capture Techniques

Carbon Capture and Storage (CCS) has been proposed for reducing the emissions of CO_2 in the atmosphere (IPCC, 2005). This kind of technologies has been widely studied in the past decades, and includes pre-combustion, oxyfuel combustion and post-combustion CO_2 capture, that can be then stored in dedicated sites or exploited as feed for chemical processes.

However, to keep the temperature rise below 1.5 °C (Paris agreement) it will not be enough to decrease, and eventually eliminate, carbon dioxide emissions. As shown in Figure 1.2, to achieve the goal set during Paris conference, CO_2 must be removed from the atmosphere.

Current CCS technology would not be effective for capturing CO_2 from the air, where CO_2 molar concentration is 0.04%, because in all the three classes of processes, CO_2 concentration in the gas stream is much higher, and also the operating conditions are far from normal air (Table 1.1). This is the reason for which CCS can be effectively used only in CO_2 point sources, such as power plants.

The Direct Air Capture (DAC) concept was first introduced for climate change mitigation in 1999 (Lackner *et al.*, 2008). It acquired rising importance in the last years as researches demonstrated its feasibility (Holmes and Keith, 2012; Lackner *et al.*, 2012) both with new processes and by adapting existing processes to DAC conditions.

Table 1.1 *Main operative conditions of the most exploited CCS techniques (Tzimas and Peteves, 2003)*

	pre-combustion	oxy-fuel combustion	post-combustion
pressure (atm)	>5	>50	1
temperature (°C)	>100	<50	<100
CO_2 concentration (vol %)	~35	>90	4−14

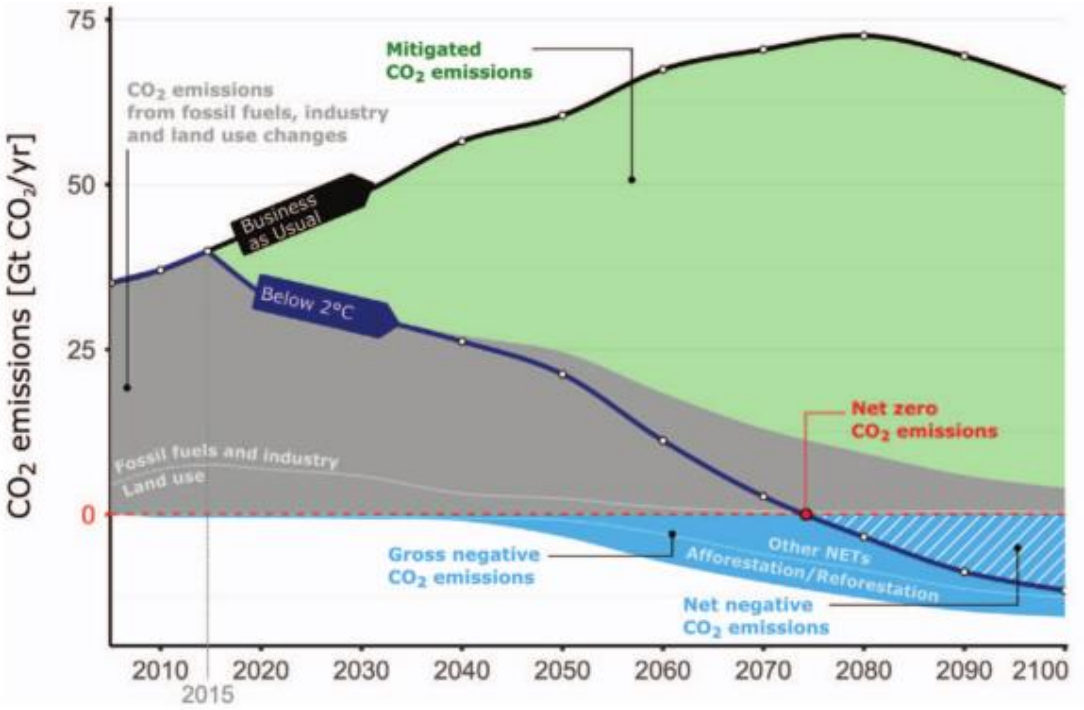

Figure 1.2 *CO_2 emissions road map to keep the temperature rise in the planet below 2°C. Mitigating CO_2 emissions and introducing substantial changes in the emissions from fossil fuels, industry and land use will not be enough: net negative CO_2 emissions technologies must be exploited as well. Image taken from Fuss et al. (2018)*

DAC processes have important advantages over CCS:

- it is a negative emissions technology, which could potentially allow to reduce the concentration of CO_2 from the air. Other examples of negative emissions techniques are ocean fertilization, bioenergy with carbon capture and storage, biochar, afforestation and reforestation. DAC is however the most promising way to make the human impact on climate reversible: CCS can only reduce emissions;
- DAC is the most promising technology for distributed air capture, able to compensate for emissions caused by distributed sources, such as automotive and aviation (which account for 50% of emissions). This aspect is of essential importance. Even if in the future transportation will be electricity-based, fossil fuels will have to be used for long distances and DAC will still be useful. Finally, leakage of CO_2 from geological sites where CO_2

captured through CCS processes is stored could only be compensated through DAC. This is an important feature, because if there were no means to make up for disruptive leakages, CCS effectiveness to fight climate change could be vain;

- DAC allows to obtain streams with concentrated CO_2 which can be exploited as raw material for the synthesis of chemicals. An example of application is the closure of the carbon cycle by fixing the CO_2 into fuel, through renewable H_2 using processes powered by solar energy (Armaroli and Balzani, 2015);
- DAC units can be located everywhere, so they could be built in the proximity of plants where CO_2 is used as reactant. CCS makes instead use of pipelines for CO_2 transportation from point sources (such as power plants), associated with an intrinsic cost and risk;
- In air there are no high concentration of impurities (NO_x, SO_x, …) often found in exhausted streams, that damage the devices used in the process, such as sorbents;
- The development of DAC techniques would allow the law to force who violates emission limits or is responsible for leakages from CO_2 storage sites to compensate via DAC.

It is important to underline the fact that DAC is not an alternative to CSS, but they are supposed to be used in a complementary fashion. Actually, an 80% reduction of CO_2 emissions by 2050 in developed countries cannot be achieved even if all point-source emissions were captured (Lackner *et al.*, 2012). Still, at the moment DAC presents some challenges, mainly related to the high cost and due to the low concentration of CO_2 in air. According to Lackner *et al.* (2012), DAC would be economically convenient compared to the other techniques for reducing CO_2 emissions if it were cheaper than 100 $/ton$_{CO_2}$, and extremely interesting below 50$/ton$_{CO_2}$. Though there are different examples of applications, also at pilot scale, there are no technologies completely mature and a precise costs evaluation is difficult for processes which are still at R&D stages. At the moment the cheapest technology is produced by Carbon Engineering Ltd and it is estimated to cost 240$/ton$_{CO_2}$, including both the costs for the carbon capture (60$/ton$_{CO_2}$ according to the studies of the company (Holmes and Keith, 2012)) and those related to the regeneration (180 $/ton$_{CO_2}$ according to APS (Socolow *et al.*, 2011)). Carbon Engineering Ltd process is based on an absorption process that employs a liquid alkaline solution in a large air-liquid contactor to sequestrate CO_2 from air (Holmes and Keith, 2012). Analysis on studies on current DAC processes showed however that an adsorption process should be more convenient (Sanz-Pérez *et al.*, 2016). As a matter of fact, Climeworks AG built a pilot plant for DAC in Switzerland, using an adsorption process based on diamines supported on a silica gel. At the moment the cost of carbon sequestration for the facility

is 600$/ton$_{CO_2}$, but the company is confident to be able to reach 100$/ton$_{CO_2}$ by scaling-up the process (*Nature website*).

1.3 Direct Air Capture state of the art

Spending energy in heating or pressurizing a large volume of air for separating CO_2 is not convenient, because it is very diluted and the waste of energy would be consistent. Actually, the Gibbs free energy required to separate one mole of carbon dioxide from a gas mixture is proportional to the logarithm of CO_2 partial pressure.

Sorption processes are more convenient, because energy is required only for regeneration, and it depends on the mass of the sorbent rather than on the initial concentration in the gas stream. The amount of adsorbed CO_2 per mass of sorbent does not depend on the dilution level, but only on the process conditions and on the sorbent binding power.

Sorption processes can make use of a liquid sorbent (absorption) or of a solid one (adsorption), and they can involve only physical bonds (physisorption) or even chemical ones (chemisorption). All combinations are currently studied by different research groups. Physisorbents bind CO_2 weakly compared to chemisorbents. Therefore, for a fixed concentration in a gas stream, physisorbents uptake less CO_2 but require less energy for regeneration. Actually, chemisorbents usually require $T > 100°C$ for regenerations, while some physisorbents could potentially work also at ambient temperature. Chemisorption is usually promoted by high temperatures, because most reaction kinetic constants increase with temperature (Arrhenius law). Instead, physisorption capacity is reduced by increases of temperature, as weak bonds are less strong at high temperatures.

Carbonation of liquid amines, alkali and alkali-earth solutions ($Ca(OH)_2$, NaOH, …) were first studied, because they represent traditional ways to industrially capture CO_2 from gas streams with concentrated CO_2. These processes present a very high efficiency because of a strong bounding power. However, regeneration costs proved to be too much energy-demanding, due to the high enthalpy of the solutions and to the high binding power itself, while adsorption processes appear to be intrinsically cheaper (Sanz-Pérez *et al.*, 2016). Therefore the focus will be from now on about these processes. The state of the art (Sanz-Pérez *et al.*, 2016; Yuan *et al.*, 2016) of DAC adsorption technologies is further presented.

The main solid physisorbents currently used for CO_2 capture include natural materials, activated carbons, zeolites and Metal-Organic Frameworks (MOFs). Activated carbons are too weak to be used at low CO_2 concentrations, therefore they are not suitable for DAC. Zeolites have been tested, and they are not stable in the presence of moisture. Furthermore, a time- and energy-consuming temperature swing adsorption (TSA) is necessary to maintain the cyclic working capacity. MOFs, however, appear to be promising sorbents.

MOFs are materials characterized by highly ordered structure. They are composed of metallic nodes connected by bridges of organic species. MOFs properties can be easily tuned based on the desired application. For CO_2 adsorption, a greater pore size is desirable. The most interesting MOF for CO_2 capture is MOF-74, which can be synthesized with different metals elements (Sanz-Pérez *et al.*, 2016). Open metal sites are often included, to increase CO_2 uptakes at very concentrations. Using magnesium as one of the metal species leads to the greatest CO_2 loadings. Presence of moisture interferes with the adsorption, because H_2O competes with CO_2 in the bonding to the sites. Despite some solutions were proposed, the moisture issue, together with an unclear long-term stability and the high cost of MOFs, is still an open problem and further research is needed.

Chemisorption has been applied to CO_2 capture for several years in industrial problems. It guarantees an efficient uptake for diluted gas streams like air. The main chemisorption processes that were applied to DAC are summarized in Table 1.2 with the main advantages and disadvantages.

Since aqueous amine solutions are the oldest and most used approach for CO_2 removal, a great interest arose in supported amines for DAC. The strong bond between the amine group and CO_2 allows to obtain significant uptakes even at low concentrations. Primary amines provide the strongest bonds compared to secondary and tertiary amines, however they also have a high regeneration cost. Secondary amines appear to be the most convenient compromise between uptake and energy demand. Polymeric amines are usually employed, since low molecular weight amines are too volatile and the loss over time is too high. The most commonly used amine is poly(ethylenimine) (PEI) on supports such as silica and alumina. There are different classes of supported amines (Figure 1.3): class I amines are adsorbed on oxide supports, while class II amines are covalently bind to supports, with an improved stability of the material. New studies (Didas *et al.*, 2015) focus on the adoption of the so-called class III amines, which are amine-based polymers directly polymerized on the support from monomers.

They present an improved CO_2 uptake cyclic working capacity compared to other classes of amines. The main disadvantage of solid amines based processes is that long times are required in most of the reported studies to saturate the material, due to the slow adsorption kinetics. New projects in different research groups are testing combinations of amines of different classes with different supports to try to overcome the problem. Also, amine-ingrafted MOFs caught the interest of researchers, since they combine high CO_2 uptake with fast adsorption kinetics. The cost is however still high, and the stability not fully predictable (Darunte *et al.*, 2016). The adsorption capacity of the most studied CO_2 sorbents is reported in Figure 1.4.

Table 1.2 Summary of the characteristics of the main sorbents for CO_2

material	advantage	disadvantage
alkaline solutions	high CO_2 loading, known technology, cheap material	high energy demanding regeneration
supported alkaline solids	high adsorption capacity, reduced regeneration energy expense	air pre-heating is needed and is still too energy expensive
solid-supported amines	reduced energy requirements for regeneration, high capacity	slow adsorption kinetics, possible degradation at relatively high temperatures
MOFs	lowest regeneration costs, easily tailorable properties	low uptake in normal conditions, not fully understood long-term stability, high cost
amine-grafted MOF	fast saturation, high CO_2 uptake	stability not known, expensive material

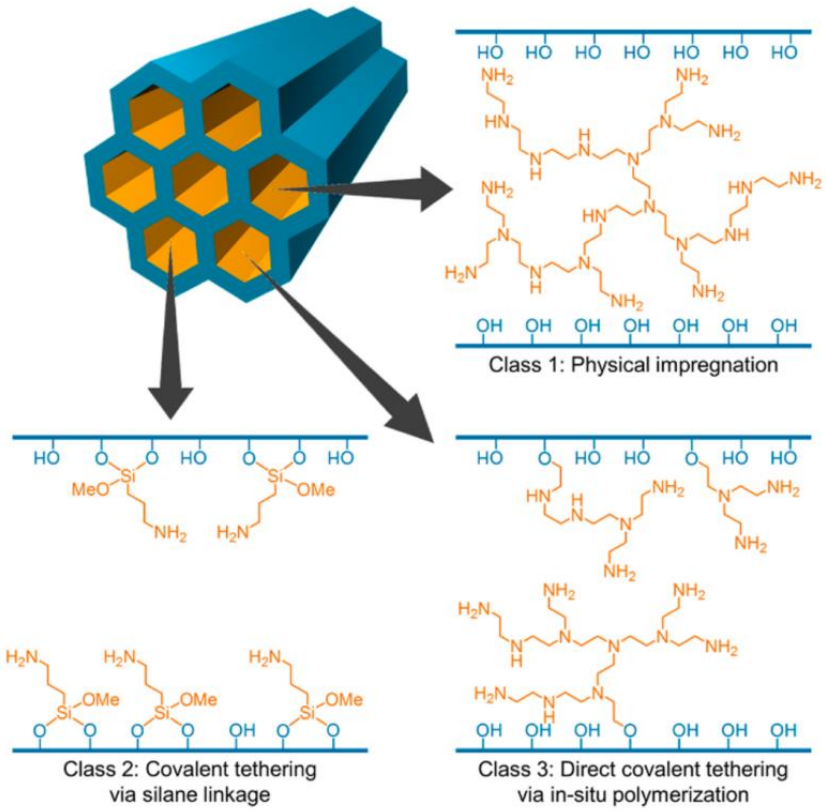

Figure 1.3 *Chemical structure of the three classes of amines used for CO_2 adsorption. Image taken from* Didas *et al.* (2015)

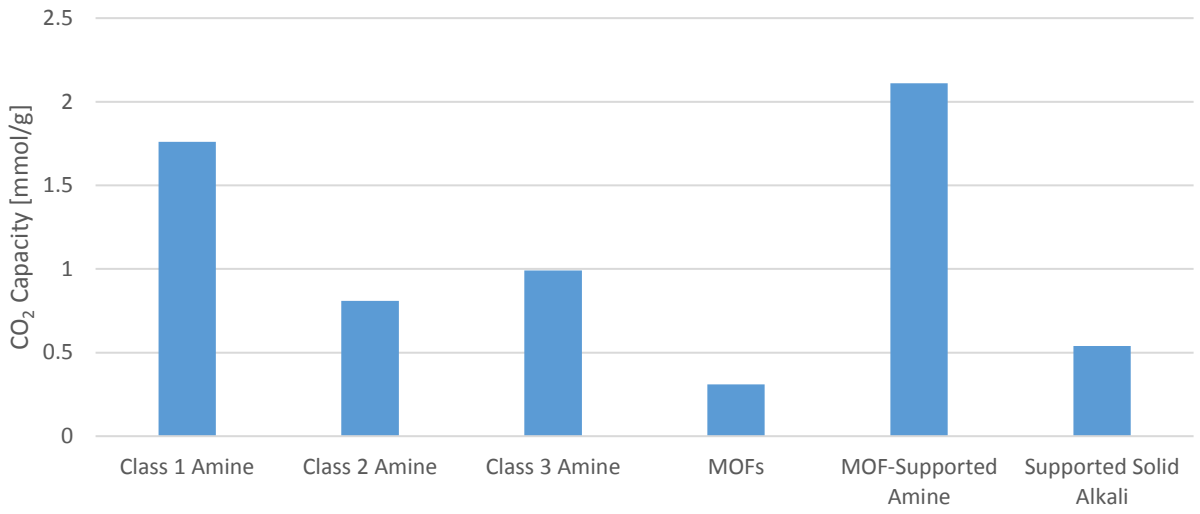

Figure 1.4 *CO_2 adsorption capacity of the most important solid CO_2 adsorbent. Data taken from literature* (Sanz-Pérez *et al.*, 2016; Yuan *et al.*, 2016)

Also carbonation of alkali and alkali-earth based solids was object of studies (Sanz-Pérez *et al.*, 2016) for DAC, since liquid solutions with these species demonstrated to be able to absorb much CO_2, though with too high regeneration costs. Experiments showed that energy demand for regeneration is lower. $Ca(OH)_2$ was found to perform better than other Ca and Na oxides and hydroxides. Studies were made also with reactors powered by solar power to accomplish both the carbonation and regeneration steps, but the energy demand was found to be still high, greater than the one required by alkali metal hydroxide solutions. The main reason is that pre-heating air prior to adsorption to at least 350°C is usually necessary to enhance carbonation kinetics. This conclusion moved research to supported solid alkali carbonates, to increase the exposed alkali surface and increase carbonation rates. A lot of combinations of active materials and supports were tried, with γ-Al_2O_3 as a support showing promising results. Better performances than in previous cases were achieved, in some cases as good as the ones obtained with solid-supported amine materials.

1.4 Hydrotalcites for CO_2 capture

1.4.1 Hydrotalcites main properties

Hydrotalcites are natural materials that gained attention for their use in carbon capture in the latest years. An important review on the main properties dates back to 1991 (Cavani *et al.*, 1991), when they were studied for their catalytic properties.

Hydrotalcites, belonging to the group of anionic clays, are made of octahedra of hydroxyl groups with a magnesium cation in the center (Figure 1.5). The octahedra are lined along their edges to form infinite brucite-like planes, one on top of the other, with hydrogen bonds keeping the structure together. Mg^{2+} can be substituted by bivalent cations (e.g.: Cu, Ni, Mn) or by trivalent cations of about the same size, such as Al^{3+}. This way a charge imbalance is generated. Compensation occurs in the interlayers, where water is usually present with counterions (often carbonates, but also chlorides, nitrates, …). The amount of water between the layers depends on temperature, water pressure and the on the type of ions and counterions. The total structure has a rhombohedral orientation, with unit cell $Mg_6Al_2(HO)_{16}CO_3^{2-} \cdot 4\ H_2O$. The Mg content is the main responsible for the basicity of hydrotalcites and of derived materials, and it influences the capacity of adsorption of acidic gases like CO_2. However, too high Mg content leads to mechanical stability issues at high pressures of steam and CO_2, because of the formation of $MgCO_3$. Basicity of hydrotalcites-like materials can be increased by promotion with K_2CO_3, enhancing the sorption capacity of acid gas such as CO_2 of even more than one order of magnitude.

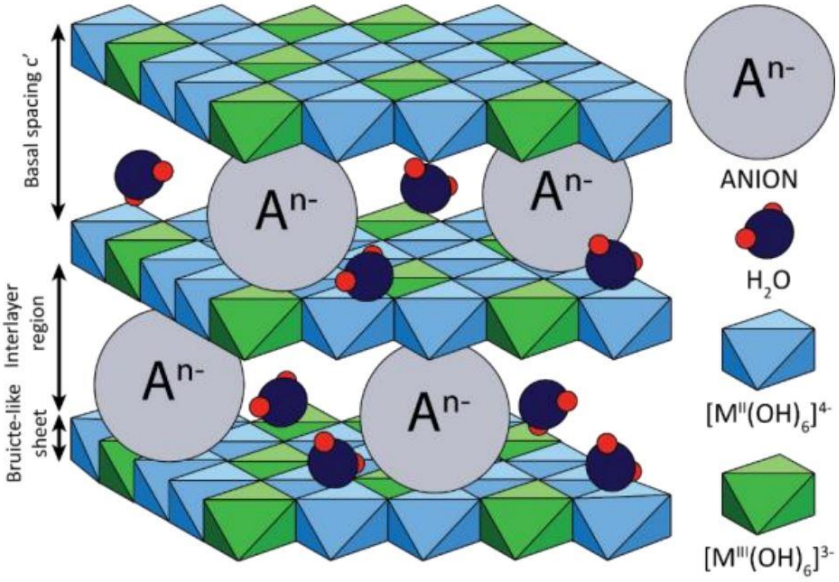

Figure 1.5 *Structure of hydrotalcite-based materials. Image taken from Dębek et al. (2017)*

They are not the most performant materials as far as the CO_2 adsorption capacity is concerned, but their low cost and stability over many cycles and up to 600°C make them interesting candidates for DAC. In addition, in recent studies (Coenen *et al.*, 2016) quick adsorption kinetics and high selectivity towards CO_2 was observed. Another important advantage of studying CO_2 adsorption on hydrotalcites is that kinetic and equilibrium data are available (Coenen *et al.*, 2018d) for process simulation and optimization.

1.4.2 CO_2 and H_2O adsorption mechanism and capacity

Studies (Coenen *et al.*, 2016, 2017, 2018a, 2018b, 2018c) on some types of hydrotalcites were developed to explore its use for Sorbent Enhanced Water Gas Shift (SEWGS) processes, in which the WGS reaction is promoted through CO_2 adsorption. The results are, however, also interesting for the application of hydrotalcites for carbon capture in general and specifically for DAC. In particular, SASOL hydrotalcites MG30 and MG70 were investigated during the experiments, after impregnation on K_2CO_3. The impregnated materials are further referred to as KMG30 and KMG70. KMG30 showed a high adsorption capacity for CO_2, with different types of carbonates that can be formed (Figure 1.6). The MgO/Al_2O_3 ratio is 30/70 by weight (so the Mg/Al molar ratio is 0.54 according to the material chemical formula), with a potassium loading of approximately 20 wt.%.

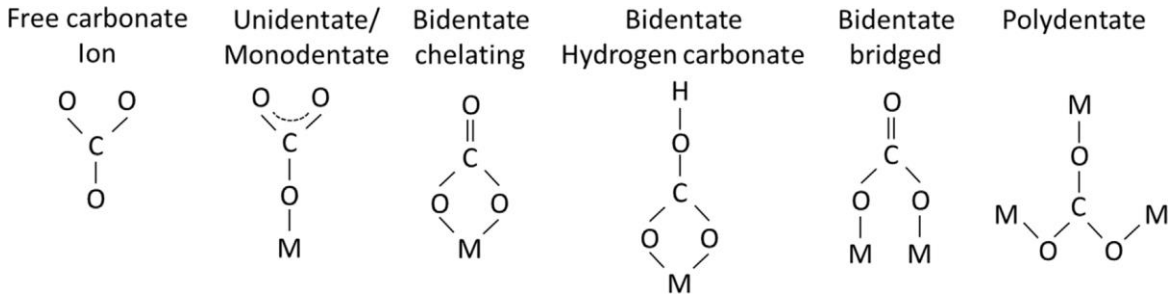

Figure 1.6 *Different types of carbonates that are formed upon adsorption of CO_2 in hydrotalcites. Figure taken from Coenen et al.(2018a)*

The adsorption mechanism appears to be predominantly chemisorption, because the cyclic working capacity increase with temperature (typical behavior of chemisorbents, as discussed in Paragraph §1.3). The acid-base interaction between CO_2 and the basic sites of KMG30 is responsible for chemisorption, though a fast physisorption probably occurs as well. In Figure 1.7 cyclic and first cycle CO_2 adsorption working capacities at different temperatures (300°C, 400°C and 500°C) and cycles durations are reported. Regeneration was carried out in dry conditions with nitrogen. A pre-treatment at 600°C was performed before the actual experiments to desorb as much CO_2 and H_2O as possible from the material. Cyclic capacity is lower than the capacity at the first cycle after the pre-treatment, therefore the history of the material is of great importance to evaluate its adsorption performance. At higher temperatures and cycles durations, the cyclic capacity increases, while the first cycle capacity is almost constant. This phenomenon was explained considering that the cyclic capacity has a strong dependence on the amount of sites regenerated during desorption steps, while fresh pre-treated KMG30 always presents the same amount of available sites. The adsorption reaction presents a slower continuous adsorption rate after the first initial fast adsorption rate (especially for high Mg content in the material), but it is in any case much faster than desorption.

It does not seem to be influenced significantly by temperature and adsorption time: equilibrium is reached quickly even at low temperature, so it appears clear that the conditions of the desorption step have the greatest impact over the cycling working capacity.
Since desorption kinetics is enhanced by an increase of temperature, and a longer regeneration step allows to reach a greater extent of reaction, temperature and cycle duration are the important operating variables for the process. As a matter of fact, below 200-250°C, the desorption reaction is practically deactivated and very long times would be needed for sorbent regeneration.

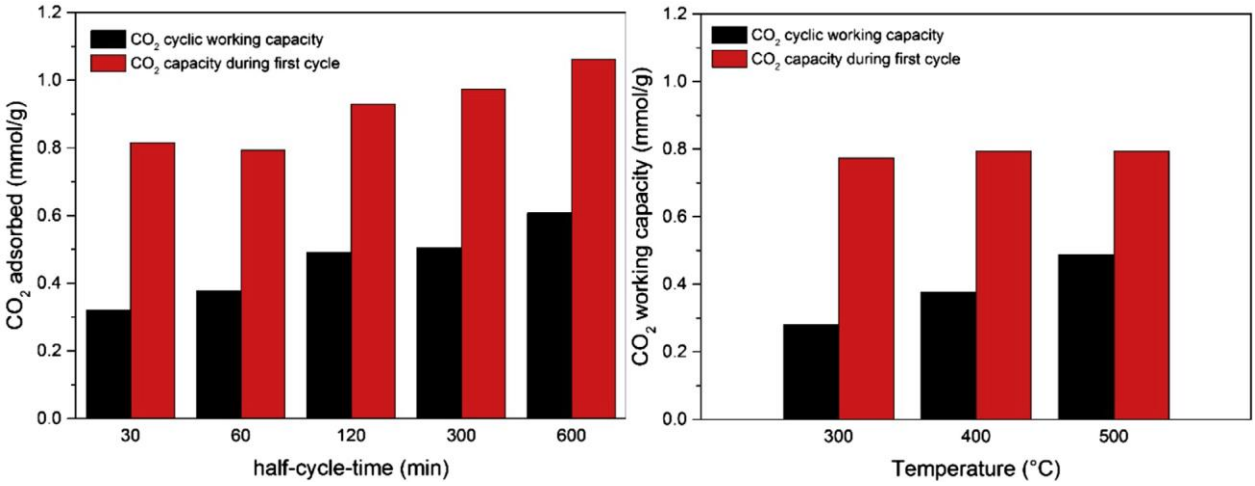

Figure 1.7 *Measured CO_2 working capacity of KMG30 for different half-cycle times (left) and temperatures (right). Image taken from Coenen et al. (2016)*

Moisture degree is another important variable for the process: hydrotalcites adsorb steam, too, and its presence greatly affects CO_2 sorption, both in the adsorption and in the desorption step. Cyclic working capacity is strongly enhanced by increasing the partial pressure of the adsorbate for both CO_2 and H_2O, but the increase for H_2O was measured to be way larger than for CO_2. The mechanism of adsorption seems to be physisorption for H_2O. The cycling working capacity for KMG30 was measured to be up to 0.47 mmol/g for CO_2 (p_{CO2} = 8 bar) and 1.06 mmol/g for H_2O (p_{H2O} = 4.2 bar) with half-cycle time of 30 minutes at 400°C, using dry nitrogen for regeneration.
Since the presence of steam during CO_2 adsorption and desorption appeared to be significant, further studies (Coenen *et al.*, 2017) with TGA and PBR experiments were developed to try to quantitively assess its effect on the CO_2 adsorption kinetics for different materials. Experiments were performed with two hydrotalcites with different Mg/Al ratios (KMG30 and KMG70, composition summarized in Table 1.3).
Three main sites have been found, responsible for CO_2 and H_2O adsorption reactions. The obtained model for the adsorption sites with the respective reactions is reported in Figure 1.8.

Table 1.3 *KMG30 and KMG70 main chemical characteristics*

	Mg/Al	Al/K	Mg/K	K_2CO_3
KMG30	0.54	3.79	2.06	20%w
KMG70	2.95	1.63	4.80	20%w

In Site A only H_2O adsorption occurs, and it can be regenerated with N_2. Site B only adsorbs CO_2 and is more abundant on KMG70, that has higher MgO content. Hence, MgO is probably the main actor in the formation of basic adsorption sites on the surface of the sorbent. This site can be relatively easily regenerated with N_2. An additional adsorption site (site C) can adsorb both CO_2 and H_2O. After CO_2 adsorption, Site C can be regenerated only with steam (or with CO_2 after steam adsorption). Site C regeneration consists in an exchange of adsorbed species, and since N_2 cannot be adsorbed in the site, it has no effect on the desorption.

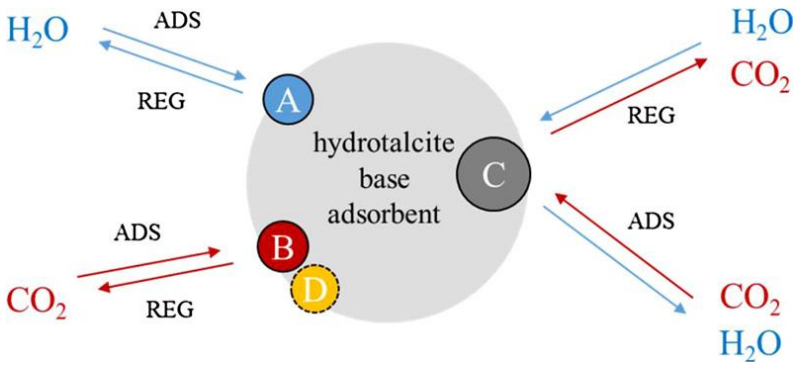

Figure 1.8 *Three adsorption sites (A, B, C) model used to describe CO_2 and H_2O sorption in hydrotalcites. The hypothesis of the existence of a fourth site (D) was originally introduced, but then dropped. Image taken from Coenen et al. (2018b)*

If both CO_2 and H_2O are fed during the adsorption step, they both adsorb in Site C, and the amount of CO_2 that can be adsorbed is increased with respect to the adsorption in dry conditions. Therefore, wet conditions increase the cyclic working capacity of Site C for the effect on both the adsorption and desorption steps. The interaction of K_2CO_3 with Al centers seems to be the main responsible for these reactions, since the cyclic working capacity of this site is greater for KMG30, which has the lowest MgO content. Hence, KMG30 should be used if the capture process occurs in wet conditions, while KMG70 performs better in dry conditions.

The existence of a fourth site (Site D) has been hypothesized (Coenen *et al.*, 2017). It is activated when it is exposed to both CO_2 and H_2O, but its capacity is decreasing with time. Further publications showed instead that experimental data can be described without Site D, only exploiting with the three previous sites, so the hypothesis of the existence of a fourth site was dropped (Coenen *et al.*, 2018d).

Studies (Moreira *et al.*, 2006) about CO_2 adsorption on hydrotalcites have been performed also at low temperatures, demonstrating that at room temperature the adsorption capacity of hydrotalcites is greater than at high temperatures. This trend is valid for all hydrotalcites, though the actual capacity depends on the characteristics of the material itself (Mg/Al ratio, pretreatment, impregnation with K_2CO_3, …). For example, in Figure 1.9 the adsorption isotherms for the hydrotalcite MG50 are reported at temperatures below 350°C, showing that the capacity is much higher at 29°C than at 350°C. The reason is that at low temperatures (below 100°C) the contribution of physisorption is significant and has to be considered together with the one of chemisorption. Physisorbed CO_2 desorbs at temperatures (150°C) lower than the one needed to decompose carbonates (at least 250-300°C).

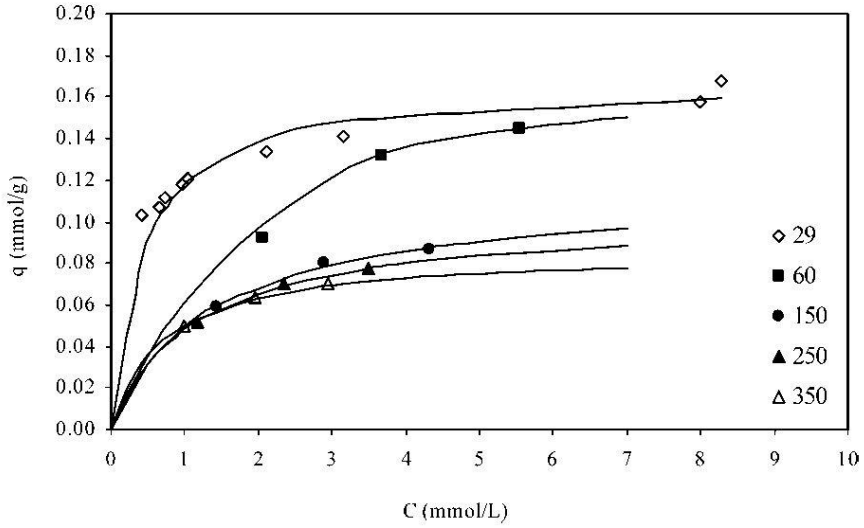

Figure 1.9 *Adsorption isotherms for MG50 at different temperatures below 350°C. Image taken from Moreira et al.(2006)*

Operating only at low temperatures, the regeneration of chemically adsorbed CO_2 cannot be obtained, while working only at high temperature the increased capacity at room temperature would not be exploited (and in addition energy would be wasted to operate the adsorption step at high temperature). Hence, the only possibility to exploit both the physical and chemical adsorption capacity of hydrotalcites is operating the adsorption and the desorption steps at different temperatures (Temperature Swing Adsorption, TSA).

1.5 Aim of the project

Since the results presented in Paragraph §1.4 showed that exploiting hydrotalcites for CO_2 capture leads to promising achievements, it was decided to evaluate the possibility to use these materials for direct air capture.

A kinetic model recently developed (Coenen *et al.*, 2018d) to describe CO_2 and H_2O adsorption on hydrotalcites is the starting point for this thesis work. The model was obtained from experiments with gas feed different from normal air (2.5% CO_2 and steam up to 10% in a nitrogen atmosphere), because it was intended to be used for optimization of SEWGS processes. The parameters of the model were regressed with experimental data obtained between 300°C and 500°C, the optimal range for the regeneration step for DAC (Moreira *et al.*, 2006; Coenen *et al.*, 2016). However, since it is probably more advantageous to carry out the adsorption step of CO_2 from air at room temperature, exploiting the increased adsorption capacity (Moreira *et al.*, 2006), further work is needed to have the model correctly reproducing experimental data in wider ranges of temperature and in DAC feed conditions.

Hence, the objectives of the thesis project were set to be:

1. Implementation of the aforementioned kinetic model in a dynamic packed-bed reactor (PBR) model;
2. Validation of the model with available PBR breakthrough experimental data in the same operative conditions in which the model was developed;
3. Improvement of the accuracy by studying mass transfer limitations using a particle model;
4. Extension of the kinetic model to DAC conditions to perform a phenomenological analysis on DAC at high temperature, exploiting the final model;
5. Design and execution of DAC experiments at room temperature. Attempts to extend the phenomenological model to these conditions will be performed;
6. The optimal conditions for the process will be investigated making use of the sorption model and the collected data. The possibility to carry out the adsorption and the desorption steps at different temperatures will be explored. A particular focus will be given to the regeneration step, as far as the optimal temperature, pressure and step duration are concerned. The effect of exploiting steam for the regeneration will be analyzed: usually pure nitrogen is used, but the use of steam demonstrated to lead to an increased CO_2 cyclic adsorption capacity.

Chapter 2

Materials and methods

In this chapter, after describing the kinetic model reported in literature for CO_2 and H_2O sorption in KMG30 at high temperature, the model used for simulating a PBR in the following chapters is presented. The particle model used in Chapters 3 and 4 for studying the internal mass transfer is then introduced. Finally, the experimental procedure for the DAC breakthrough experiments whose results are reported in Paragraph 5.3.1 is described.

2.1 Kinetic model

The kinetic model describing CO_2 and H_2O adsorption and desorption on a potassium-promoted hydrotalcite was provided by previous works (Coenen *et al.*, 2018d) on the topic. The three adsorption sites structure proposed for KMG30 has already been discussed in §1.4. Some parameters were changed during the course of this work (Paragraph §3.3) to better reproduce the experimental datasets that were provided to validate the model.

The original kinetic model was obtained based on experimental results on KMG30. Some experiments had also been carried out to be sure that neither external nor internal mass transfer limitations were present during the experimental procedures. TGA experiments were performed with feeds of different compositions of CO_2, H_2O and N_2 in different sequences, in order to understand the influence of steam on the adsorbed CO_2. More information on the experimental setup and on the experiments carried out to develop this kinetic model can be found in previous publications (Coenen *et al.*, 2017, 2018d). Measurements were performed with a fresh sample, which had been pretreated at 600°C for 2 hours under N_2. The assumption made in the development of the model is that all CO_2 and H_2O were desorbed during the pre-treatment. The range of validity of the model is between 300 – 500 °C and from 0.1 to 20 bar. The kinetic model was actually developed for studying SEWGS reactions, which show the best yields in these operating conditions. One of the goals of this work is to prove that the model can also be used for assessing the performance of DAC at these conditions.

The kinetic constants of the different adsorption reactions are described with the Arrhenius law:

$$k_{rxn} = k_{rxn}^{0} \exp\left(\frac{-Ea}{RT}\right) \tag{2.1}$$

where k_{rxn}^{0} is the pre-exponential factor, of the same unit of measurement of the kinetic constant k_{rxn}, E_a is the activation energy (J mol^{-1}), R is the gas constant (J mol^{-1} K^{-1}) and T is the temperature (K). In any case, for the adsorption reactions the value proposed for the activation energy is zero, as it has been observed that adsorption takes place also at low temperatures.
The Elovich Equation, which is effective for describing the behavior of heterogeneous surfaces, has been proposed to describe the dependence of the activation energy for the desorption reactions on the surface coverage θ of the sorption sites:

$$Ea = Ea^{0} - \beta\theta \quad , \tag{2.2}$$

where Ea^{0} is the activation energy at null coverage (J mol^{-1}), β is the Elovich parameter (J mol^{-1}) and θ is the ratio between the number of occupied sites and the maximum number of sites.
The adsorption capacity of the sites was described with a Freundlich Isotherm:

$$q_{site}^{eq} = k_{f,site}\, p_i^{n_{f,site}}\, \rho_s \quad , \tag{2.3}$$

where q_{site}^{eq} is the equilibrium concentration of the adsorbed species in a site (mol m^{-3}), ρ_s is the solid bulk density (kg m^{-3}), while $k_{f,site}$ (mol m^{-3}) and $n_{f,site}$ (adimensional) are the specific Freundlich constants for the site and p_i is the partial pressure of species i. For Site A the dependence is on steam partial pressure, for Site B on carbon dioxide partial pressure, while for Site C is on the partial pressure of both species, always expressed in bar.
The reactions and their rates for the different sorption sites are further reported.

In Site A steam adsorption and desorption reactions occur:

$$H_2O + A[\ ] \leftrightarrows A[H_2O] \tag{2.4}$$

The rates of the reactions are described with a first order Langeren model: below the equilibrium sorption capacity for hydrates (q_A^{eq}), only steam adsorption occurs, while above q_A^{eq} only steam desorption reaction proceeds:

$$\frac{dq_A}{dt} = \begin{cases} k_{ads,A}\left(q_A^{eq} - q_A\right) & \text{if } q_A < q_A^{eq} \\ -k_{des,A}\, q_A & \text{if } q_A > q_A^{eq} \end{cases} \tag{2.5}$$

$$q_A^{eq} = k_{f,A}\, p_{H_2O}^{n_{f,A}}\, \rho_s \tag{2.6}$$

The model of the reactor (presented in §2.2) becomes too slow in the case in which an "If cycle" is introduced for the reaction kinetics, which would be very handy in this situation. To overcome the problem, the adsorption rate has been implemented as:

$$rate_{ads,A} = 0.5\, k_{ads,A}\left(q_A^{eq} - q_A + \left|q_A^{eq} - q_A\right|\right) \tag{2.7}$$

which is different from zero only if q_A is smaller than the equilibrium value, as wanted.
For the desorption rate a smooth transition coefficient was introduced in the reaction rate:

$$rate_{des,A} = n_T \, k_{des,A} \, q_A \ , \tag{2.8}$$

$$\text{with } n_T = 0.5 + 0.5 \tanh\left(\frac{q_A - q_A^{eq}}{0.1}\right) \tag{2.9}$$

According to Equation 2.8, n_T (adimensional) is equal to zero when desorption should not occur, and instead equals to one when the number of occupied sites is bigger than the equilibrium value. The transition is however not very steep and n_T acquires values between 0 and 1 around q_A^{eq}. The denominator inside the parenthesis in Equation 2.8 defines the smoothness of the transition. The smaller the denominator, the smoother the transition, however instability issues arise for too small values. The implemented value for the denominator (0.1) is the compromise which was found between steepness and stability.

Site B reactions and their kinetics are very similar to the ones described for Site A. The reactions are:

$$CO_2 + B[\ ] \leftrightarrows B[CO_2], \tag{2.10}$$

with enthalpy of the reaction ΔH_R = -160 ÷ - 100 kJ/mol (Coenen *et al.*, 2018d).
A Langeren model and a Freundlich isotherm are adopted also for these reactions:

$$\frac{dq_B}{dt} = \begin{cases} k_{ads,B}\left(q_B^{eq} - q_B\right) & if\ q_B < q_B^{eq} \\ -k_{des,B}\, q_B & if\ q_B > q_B^{eq} \end{cases} \tag{2.11}$$

$$q_B^{eq} = k_{f,B}\, p_{CO_2}^{n_{f,B}} \rho_s \tag{2.12}$$

For the implementation, an approach analog to Equations 2.6, 2.7 and 2.8 was adopted, obviously using the concentrations of carbonates q_B instead of the concentration of hydrates q_A.

An additional reaction has to be taken into account for CO_2 sorption: bulk carbonation. This reaction is responsible for the slow adsorption observed after a first fast adsorption, as described in §1.4.2. Bulk hydrates formation has not been considered, since H_2O adsorption does not present this second slow step. Most probably, this phenomenon is due to the migration of surface carbonates into the bulk of the material. The additional term introduced to account for the formation of bulk carbonates is:

$$rate_{bulk\ ads,B} = k_{bulk\ ads,B}\, p_{CO_2}^{n_b} \rho_s \tag{2.13}$$

Experiments showed that the bulk carbonates are fully desorbed within a regeneration step (provided that its long enough), so also a bulk desorption reaction rate has to be computed:

$$rate_{bulk\ des,B} = k_{bulk\ des,B}\ q_{bulk,B} \tag{2.14}$$

The proposed values of the parameters (Coenen *et al.*, 2018d) at 400°C for the reactions of sites A and B are reported in Table 2.1.

In Site C both CO_2 and H_2O adsorb, and an exchange between the occupied sites can occur. The single species reactions are:

$$H_2O + C[\ ] \leftrightarrows C[H_2O] \tag{2.15}$$

$$CO_2 + C[\ ] \leftrightarrows C[CO_2] \tag{2.16}$$

The desorption part of the reactions above presented occurs only upon thermal treatment, and will not be discussed. The adsorption kinetics for the reaction expressed by Equation 2.15 is:

$$\frac{dq_{C,H_2O}}{dt} = k_{C,ads}\ p_{H_2O}(q_{C,max} - q_{C,H_2O} - q_{C,CO_2}) \tag{2.17}$$

And for reaction (2.16):

$$\frac{dq_{C,CO_2}}{dt} = k_{C,ads}\ p_{H_2O}(q_{C,max} - q_{C,H_2O} - q_{C,CO_2}) \tag{2.18}$$

The equilibrium concentration of occupied sites is the same for both species and is calculated as:

$$q_{C,max} = (k_{C1}P_{CO_2} + k_{C2}P_{H_2O}^{n_C})\ \rho_s \tag{2.19}$$

Also the adsorption kinetic constant is the same for both Equations 2.17 and 2.18. Equations 2.17 and 2.18 are valid only if $q_{C,max} > q_{C,H_2O} + q_{C,CO_2}$: if this condition is not true, the rate of the reactions is null. The only way to desorb an adsorbed species is either with a thermal treatment or by replacing it with another species.

The exchange reaction between carbonates and hydrates and its kinetic law are further presented:

$$C[CO_2] + H_2O \leftrightarrows CO_2 + C[H_2O] \tag{2.20}$$

$$\frac{dq_{C,CO_2}}{dt} = -\frac{dq_{C,H_2O}}{dt} = k_{C,rep1}q_{C,H_2O}p_{CO_2}\rho_s - k_{C,rep2}q_{C,CO_2}p_{H_2O}\rho_s \tag{2.21}$$

The parameters for the kinetic laws at 400°C for Site C are reported in Table 2.2. For the replacement kinetic constants, Arrhenius law (Equation 2.1) parameters are available.

Table 2.1 *Kinetic parameters for sites A and B at 400°C*

$k^0_{ads,A}$	3.19	[s^{-1}]
$Ea^0_{ads,A}$	0	[J mol^{-1}]
$k^0_{des,A}$	564	[s^{-1}]
$Ea^0_{des,A}$	1.37E+05	[J mol^{-1}]
$\beta_{des,A}$	1.37E+05	[J mol^{-1}]
$Q_{max,A}$	1.612	[mol kg^{-1}]
$n_{f,A}$	0.124	[-]
$k_{f,A}$	1.113	[mol kg^{-1} $bar^{-0.124}$]
$k^0_{ads,B}$	0.16	[s^{-1}]
$Ea^0_{ads,B}$	0	[J mol^{-1}]
$k^0_{des,B}$	42.98	[s^{-1}]
$Ea^0_{des,B}$	1.10E+05	[J mol^{-1}]
$\beta_{des,B}$	8.45E+04	[J mol^{-1}]
$Q_{max,B}$	0.78	[mol kg^{-1}]
$n_{f,B}$	0.0825	[-]
$k_{f,B}$	0.6063	[mol kg^{-1} $bar^{-0.0825}$]
$k^0_{bulk\ ads,B}$	1.93E-04	[mol kg^{-1} $bar^{-0.5}$ s^{-1}]
$Ea^0_{bulk\ ads,B}$	0	[J mol^{-1}]
n_b	0.5	[-]
$k^0_{bulk\ des,B}$	2.233E-05	[s^{-1}]
$Ea^0_{bulk\ ads,B}$	4.497	[J mol^{-1}]

Table 2.2 *Kinetic parameters for site C at 400°C*

$k_{C,ads}$	0.10	[s^{-1}]
k_{C1}	0.156	[mol kg^{-1} bar^{-1}]
k_{C2}	0.691	[mol kg^{-1} $bar^{-0.591}$]
n_C	0.591	[-]
$k^0_{C,rep1}$	9.66E-04	[mol kg^{-1} $^{ba\text{-}1r}$ s^{-1}]
$Ea^0_{C,rep1}$	-14059	[J mol^{-1}]
$k^0_{C,rep2}$	0.034767	[mol kg^{-1} bar^{-1} s^{-1}]
$Ea^0_{C,rep2}$	6127.92	[J mol^{-1}]

2.2 Reactor model

A packed-bed dynamic reactor model was used to simulate breakthrough experiments with feeds of CO_2, H_2O and N_2 in different compositions, in order to validate the kinetic model presented in Paragraph §2.1 with the available datasets.

A pseudo-homogeneous model was used for most of the simulations. The governing equations are reported in Table 2.3, and they include energy and momentum balances. The meaning of the symbols for the variables of this table and the following ones can be found in the Nomenclature

section. The energy balance can also consider heat transfer to the external environment through the reactor walls. The main assumption is the absence of radial temperature and concentration gradients (1D model). The influence of axial dispersion of heat and mass is instead taken into account (the used axial transport properties are reported in Table 2.4). A very efficient finite difference technique with higher order temporal (SDIRK2) and spatial discretization (WENO3) with local grid and time step adaptation (Smit *et al.*, 2005) is adopted in order to simulate the reactor behavior in detail, obtaining axial temperature and concentration profiles. Newton-Raphson method based numerical techniques were used to solve the equations.

Table 2.3 *Pseudo-homogeneous PBR model*

Component mass balance for the gas phase: $\epsilon_g \frac{\partial(\rho_g w_{i,g})}{\partial t} = -v_g \frac{\partial(\rho_g w_{i,g})}{\partial x} + \frac{\partial}{\partial x}(\rho_g D_{eff,ax} \frac{\partial w_{i,g}}{\partial x}) + r_i MW_i$
Component mass balance for the solid phase: $\epsilon_s \frac{\partial(\rho_s w_{j,s})}{\partial t} = r_j MW_j$
Energy balance: $(\epsilon_g \rho_g C_{p,g} + \epsilon_s \rho_s C_{p,s}) \frac{\partial}{\partial t} T = -\rho_s v_g C_{p,g} \frac{\partial T}{\partial x} + \frac{\partial}{\partial x}\left(\lambda_{eff} \frac{\partial T}{\partial x}\right) + r_i \Delta H_{R,i} - \alpha \frac{4}{D_i}(T - T_{env})$ with α = 45 W m^{-2} K^{-1} from experimental studies in a similar reactor (Hamers, 2015)
Momentum balance: $-\frac{dp}{dx} = 150 \frac{\eta_g v_g (1-\epsilon_g)^2}{\epsilon_g^3} + 1.75 \frac{\rho_g v_g^2}{d_p} \frac{(1-\epsilon_g)}{\epsilon_g^3}$

Table 2.4 *Heat and mass dispersion descriptions for the PBR model*

Effective axial heat dispersion (Vortmeyer and Berninger, 1982) $\lambda_{eff} = \lambda_{bed,0} + \frac{Re\, Pr\, \lambda_g}{Pe_{ax}} + \frac{Re^2 Pr^2 \lambda_g}{6\,(1-\epsilon_g)\, Nu}$ $\lambda_{bed,0}$ is calculated with the Bauer and Schluender equation (1978)
Gunn and Misbah equation (1993) $Pe_{ax} = \frac{2\,(0.17+0.33\left(-\frac{24}{Re}\right)}{1-(0.17+0.33\left(-\frac{24}{Re}\right)}$
Gunn equation (1978) $Nu = (7 - 10\epsilon_g + 5\epsilon_g^2)(1 - 0.7 Re^{0.2} Pr^{0.33}) + (1.33 - 2.44\epsilon_g + 1.2\epsilon_g^2) Re^{0.2} Pr^{0.33}$
Axial mass dispersion (Edwards and Richardson, 1968) $D_{eff,ax} = \left(\frac{0.73}{Re\, Sc} + \frac{0.5}{\epsilon_g + \frac{9.7\,\epsilon_g^2}{Re\, Sc}}\right) v_g\, d_p$

A heterogeneous model accounting for external mass transfer limitations was used to study the influence of the mass transfer between the solid and the gas phase. The model solves the mass balances for the gas species in both the gas and solid phase. The new equations introduced with respect to the pseudo-homogeneous model are presented in Table 2.5.

The model was originally developed to describe chemical-looping packed bed reactors (Noorman *et al.*, 2007). Physical properties for KMG30 were taken from Soares *et al.* (2005) and from previous experimental studies (Coenen *et al.*, 2018b) on the same material. A summary of the used physical properties for solid species is reported in Table 2.6.

Table 2.5 *Heterogeneous PBR model mass balances*

Component mass balance for the gas phase: $\epsilon_g \rho_g \frac{\partial w_{i,g}}{\partial t} = -\rho_g v_g \frac{\partial w_{i,g}}{\partial x} + \frac{\partial}{\partial x}\left(\rho_g D_{eff,ax} \frac{\partial w_{i,g}}{\partial x}\right) - \dot{n}_{g \to s}$
Component mass balance for the solid phase: $\epsilon_s \rho_s \frac{\partial w_{j,s}}{\partial t} = r_j MW_j + \dot{n}_{i,g \to s}$
Mass transfer: $\dot{n}_{g \to s} = h_m \rho_g (w_g - w_s)$ $h_m = \frac{Sh}{Sc} \frac{\nu_g}{d_p}$ $Sc = \frac{\nu_g}{D_i}$ $Sh = 2 + 0.69\, Re^{0.5}\, Sc^{0.33}$ if $Re < 2000$ (Paterson and Hayhurst, 2000) $Sh = 0.015\, Re^{0.83} Sc^{0.42}$ if $Re > 2000$ $Re = \frac{\rho_g v_g d_p}{\eta_g}$

Table 2.6 *Components properties added to the model*

Free sites MW	0.4378 kg/mol
Carbonate MW	0.4818 kg/mol
Hydrate MW	0.4557 kg/mol
Free sites density	2450 kg/m^3
Carbonate density	2696 kg/m^3
Hydrate density	2551 kg/m^3
Mean particles diameter	0.0025 m
Particles porosity	0.64 $\frac{m^3_{void}}{m^3_{particle}}$
Specific heat for the solids	Temperature dependent equations taken from the NIST databank (2018). For sorption sites, the equation for MgO was exploited.
Conductivity for all solids[1]	33.22 exp(-1.33E-03 T) $\frac{W}{m\,K}$

The reactor properties (bed length, diameter and porosity) were implemented in the model according to those of the experiments that in every case had to be reproduced. The thermo-physical properties from gas components were calculated according to Daubert and Danner (1992). The chemical formula for the free sites of the hydrotalcites has been assumed to be $Mg_6Al_2K_2O_{10}$. The

[1] Value for alumina taken from the NIST databank (*National Institute of Standards and Technology website*, 2018)

carbonate species formed when CO_2 is adsorbed has been considered to be $Mg_6Al_2K_2O_9CO_3$, while $Mg_6Al_2K_2O_9(OH)_2$ is the hydrate assumed to be formed after H_2O adsorption. The introduced kinetic laws were already discussed in §2.1. The initial solid concentration of carbonates and hydrates in the different sites was not known and a trial and error procedure was carried out to assess it. A verification study was carried out after the changes introduced to the original model. A comparison of the numerical solution with a simplified analytical solution proved that the program solves the balances and the equations correctly. The verification study is reported in Appendix A.

2.3 Particle model

The internal diffusion limitations for some of the reactions presented in Paragraph §2.1 were studied with a mono-dimensional particle model (Noorman *et al.*, 2011). A very efficient finite difference technique with grid refinement near the external surface of the particle and automatic time-step adaptation are employed. The model was originally developed to describe the oxidation and the reduction of a particle composed only of a metal species, of a metal oxide and of an inert. Adaptations were introduced to describe the sorption reactions studied in this work.

The model is based on the following assumptions:

• The particle is spherical and porous;

• The volume of the particle is constant while the porosity of the particle changes.

The system is isobaric and the structure of the particle is uniform and can be locally represented by a porosity, a tortuosity and an average pore size.

The governing equations and the corresponding initial and boundary conditions of the model are reported in Table 2.7 and Table 2.8.

Table 2.7 *Particle model governing equations*

Gas phase components mass balance $\frac{\partial(\epsilon_g \rho_g w_{g,i})}{\partial t} = -\frac{1}{r^2}\frac{\partial(r^2 n_i)}{\partial r} + r_i MW_i$ where $n_i = j_i + w_{g,i} n_{tot} = -\rho_g \sum_{k=1}^{N_g-1} D_{eff,ik} \frac{\partial w_{g,k}}{\partial r} + w_{g,i}\, n_{tot}$
Solid phase components mass balance: $\frac{\partial(\epsilon_s \rho_s w_{s,j})}{\partial t} = \sum_{i=1}^{N_g} (r_i\, MW_i)$

Explanation of the introduced symbols can be found in the Nomenclature section. For the calculation of the diffusive mass fluxes n_i, the effect of both diffusion and drift fluxes were considered. Drift fluxes are included in the calculations to be able to account for the effect of mass change inside the particle. The total drift flux n_{tot} can be evaluated from the continuity equation, since the equations are in the mass reference frame. Pure species data for solid and gaseous

components are as for the reactor model (Paragraph §2.2). The diffusion matrix was built with the Maxwell-Stefan equations, that allow for the correct description of multi-component diffusion, also when high bulk concentrations are applied. The effect of tortuosity was included in the calculation of the effective diffusivity $D_{eff,ik} = D_{ik}\ \varepsilon_p\ \tau^{-1}$. Knudsen diffusion was taken into account, too, to assess the influence of the particle morphology, in particular of the particle pores diameters. For all the calculations, a particle diameter of 2.5 mm was used, with pore diameter equal to 186 Å, as measured for the particles with which breakthrough experiments were carried out (Coenen *et al.*, 2018b, 2018c, 2018d). The reactions of the kinetic model (§2.1) were studied one at the time, using their rates to calculate the production/consumption terms of the equations.

Table 2.8 *Initial and boundary conditions for the particle model*

Condition	Component balance (gas phase)
t = 0	$w_{g,N_2} = 1$ for the adsorption reactions $w_{g,N_2} = 0.9, w_{g,H_2O} = 0.1$ for the H_2O desorption reaction $w_{g,N_2} = 0.975, w_{g,CO_2} = 0.025$ for the CO_2 desorption reaction
r = 0 (center)	$\left.\frac{\partial w_{g,i}}{\partial r}\right\|_{(r=0)} = 0$
r = R (surface)	$\sum_{k=1}^{N_{g-1}} D_{eff,i,k}\ \frac{\partial w_{j,k}}{\partial r} = \sum_{k=1}^{N_{g-1}} k_{g,ik}(w_{g,k} - w_{bulk,k})$
where	$k_{g,ik} = \Xi_{i,k}\ k^0_{g,ik}$ (film model) $\Xi_{i,k} = \frac{\Phi_{ik}}{\exp(\Phi_{ik})-1}$, $\Phi_{ik} = \frac{m_{tot}}{\rho_g k^0_{g,ik}}$

After that the first simulations showed that the heat of the reactions does not significantly affect the temperature profile, it was decided to neglect the energy balance for simplifying the calculations. Hence, the system was considered isothermal at 400°C.

2.4 Experimental procedure and setup

Breakthrough experiments were carried out in a packed bed setup filled with KMG30 pellets, in order to collect data to validate the kinetic model presented in §2.1 at low temperatures. The results of the experimental procedure explained in this paragraph are reported in Paragraph §4.1.

The pellets, of cylindric shape, were provided as MG30 by Sasol Ltd. The chemical and physical properties were analyzed by Sasol prior to delivery (results are reported in Table 2.9). Before to place the material inside the reactor, it was impregnated with 20%w K_2CO_3 following the specific patented procedure (Nataraj *et al.*, 2000) used also in the previous works on the kinetic model

(Coenen *et al.*, 2018d), to obtain the same KMG30 whose sorption properties were already introduced in §1.4.2.

Table 2.9 *Properties of the MG30 pellets provided by Sasol. Analysis were carried out on the actual batch used in the experiments*

Analysis	Results
Al_2O_3 [%]	70.3
MgO [%]	29.7
Specific surface area [m^2/g]	246
Packed bulk density [g/ml]	0.84
Median diameter [mm]	3.07
Median length [mm]	2.90
Pore volume total [ml/g]	0.418

X-Ray Diffraction (XRD) analysis, conventionally used for identifying the solid phases of a material, was performed to assess that the impregnation procedure had been completed properly. Some pellets were ground in order to obtain a fine powder to be analyzed. One sample was prepared from unpromoted pellets, and one from the promoted sorbent particles. The Rigaku Miniflex 600 X-ray diffractometer was used for the study.

During the XRD analysis (Birkholz, 2006), X-rays are generated by a cathodic tube and conveyed towards the sample. The rays reflected by the sample after the collision are collected and measured, repeating the procedure for all the possible 2γ angles between the sample and the incident rays. The interaction between the X-rays with the material generates a diffraction pattern, where a constructive interference (represented by a peak in the collected X-rays intensity) is produced when the distance d (m) between the planes of the crystalline structure of the material satisfies the Bragg's Equation:

$$Z\,\delta = 2d\sin(\gamma) \tag{2.22}$$

where Z is a positive dimensionless integer, δ is the wavelength of the incident wave and is γ the diffraction angle. Hence, for a given crystallographic phase (fixed interplanar distance d), the peaks of intensity will be at the same values of 2γ: the phase composition of the sample can be identified by comparison with literature values of the angles at which peaks appear for a certain phase.

Hydrotalcites are not completely crystalline, so X-rays are scattered in many directions: instead of obtaining high intensity narrow peaks that can be easily analyzed, they are widened (Cullity and Weymouth, 1957). In any case, the most important objective for the performed analysis was spotting the difference between the material before and after the impregnation, to identify the new peak corresponding to K_2CO_3, so the widened peaks due to the amorphous phases were not a significant problem.

After the impregnation and the XRD characterization, the KMG30 pellets were put inside the reactor for the DAC experiments. The employed tubular reactor (length = 11 cm, internal diameter = 7 mm) had a diameter to small compared to the sorbent particles: the particle equivalent diameter was about half of the reactor diameter. In order to avoid channeling phenomena that cause an inhomogeneous distribution of the gas in the reactor, the equivalent diameter of the sorbent should be at least ten times smaller than the diameter of the reactor. Hence, the pellets were crushed to reduce their dimension, but not too much, not to have too high pressure drops within the reactor. The particles diameter was reduced with a milling machine, that exploits rotating metal spheres for crushing the sorbent pellets. The new mean diameter of the particles was measured with a Fritsch Analysette 22.

The Process Flow Diagram (PFD) of the experimental setup used for performing the breakthrough experiments is represented in Figure 2.1.

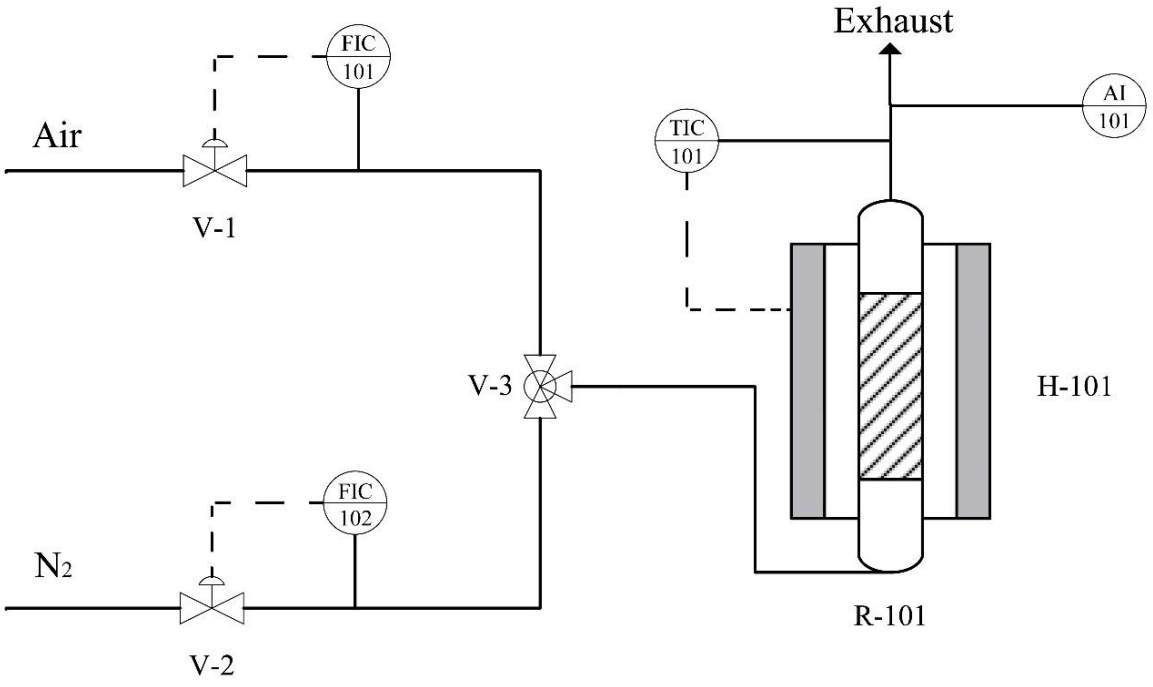

Figure 2.1 *PFD of the experimental setup used for Direct Air Capture breakthrough experiments at low temperature*

Flow controllers (FIC-101 and 102) were employed to switch the feed of the reactor from air during the adsorption step to pure nitrogen during the regeneration and to keep the inlet flow rate at the desired value. The reactor (R-101) was placed in a cylindrical electrical oven (H-101), which heats to the set regeneration temperature. Pictures of the reactor are reported in Figure 2.2. A layer of quartz pellets was placed at the beginning of the bed, in order to pre-heat the gas feed to the reactor temperature and to homogenize the distribution of the gas inside the reactor. The outlet composition was measured through Agilent 490-PRO Micro Gas Chromatograph.

Figure 2.2 *Pictures of the reactor used for the DAC experiments. Left: macroscopic view of the tubular reactor inside the cylindric oven. Right: close-up view of the reactor inside the oven. Before to execute the experiments, a layer of insulant was placed at the top and at the bottom of the oven not to disperse the produced heat*

Chapter 3

High temperature sorption model: validation and optimization

In this chapter the kinetic model presented in §2.1 will be validated and optimized on the basis of available experimental results at 400°C.

3.1 Datasets available for validation

The datasets available for validation of the kinetic model consist in the breakthrough curves (outlet concentrations as function of time) of CO_2 and H_2O from a PBR (maintained isothermal at 400°C through an oven) whose characteristics are as in Table 3.1. In the experiments, different steps were performed, changing the feed of the reactors. In Figure 3.1 and in Table 3.2 the breakthrough curves and the feed conditions are reported for a first experiment (Dataset 1, thirty-tree steps, each one lasting 1800s).

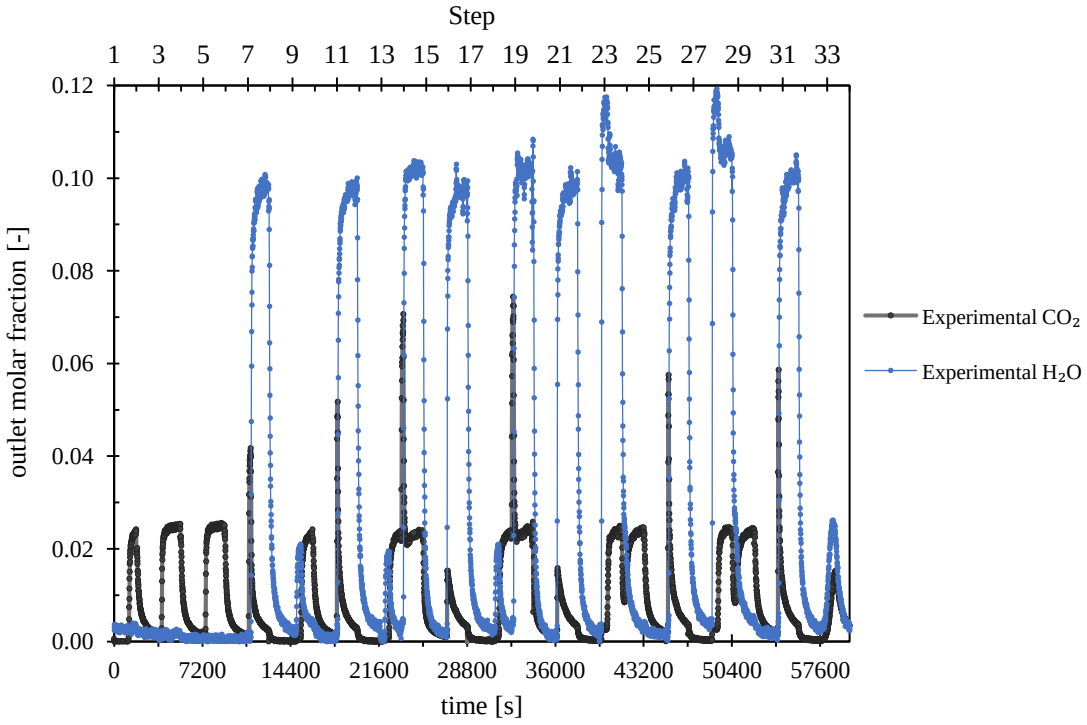

Figure 3.1 *Breakthrough curves from the PBR. Feed conditions as in Table 3.2*

It is possible to notice that the first six steps only involve CO_2 adsorption and desorption, so they will be useful for validating Site B kinetics. The following steps will then be exploited to validate the effect of steam during both the adsorption and the desorption steps.

Table 3.1 *Properties of the reactor used for the experiments in Datasets 1 and 2*

Bed porosity	0.40 $\frac{m^3_{void}}{m^3_{bed}}$
Bed length	0.176 m
Bed diameter	0.027 m

Table 3.2 *Feed conditions for the first dataset. Each step lasts 1800 s.*

Step	Feed	Step	Feed	Step	Feed
1	2.5% CO_2, 97.5% N_2	12	100% N_2	23	10% H_2O, 87.5% N_2, 2.5% CO_2
2	100% N_2	13	2.5% CO_2, 97.5% N_2	24	2.5% CO_2, 97.5% N_2
3	2.5% CO_2, 97.5% N_2	14	10% H_2O, 87.5% N_2, 2.5% CO_2	25	100% N_2
4	100% N_2	15	100% N_2	26	10% H_2O, 90% N_2
5	2.5% CO_2, 97.5% N_2	16	10% H_2O, 90% N_2	27	100% N_2
6	100% N_2	17	100% N_2	28	10% H_2O, 87.5% N_2, 2.5% CO_2
7	10% H_2O, 90% N_2	18	2.5% CO_2, 97.5% N_2	29	2.5% CO_2, 97.5% N_2
8	100% N_2	19	10% H_2O, 87.5% N_2, 2.5% CO_2	30	100% N_2
9	2.5% CO_2, 97.5% N_2	20	100% N_2	31	10% H_2O, 90% N_2
10	100% N_2	21	10% H_2O, 90% N_2	32	100% N_2
11	10% H_2O, 90% N_2	22	100% N_2	33	100% N_2

A second experiment (Dataset 2, Figure 3.2) only involved steam adsorption and desorption, and will then be useful to analyze Site A kinetics independently. Experimental conditions are the same as for the previous experiment, but for the different feed composition (Table 3.3).

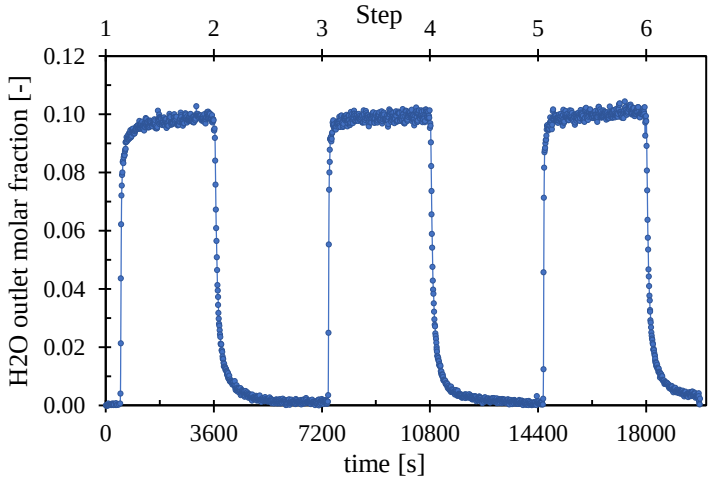

Figure 3.2 *Dataset 2 experimental data*

Table 3.3 *Feed conditions for the second dataset. Each step lasts 3600 s.*

Step	Feed	Step	Feed
1	10% H_2O, 90% N_2	4	100% N_2
2	100% N_2	5	10% H_2O, 90% N_2
3	10% H_2O, 90% N_2	6	100% N_2

3.2 Internal mass transfer at high temperature

The kinetic model presented in §2.1 was obtained with experiments not limited by the mass transfer (Coenen *et al.*, 2018d). In an actual PBR, however, mass transfer may play a role. While the external mass transfer limitations may be eliminated by increasing the inlet flow rate, the diffusion inside the sorbent particles may be more problematic.

The effectiveness factor η_{rxn} can be adopted to easily describe the internal mass transfer in the reactor model (§2.2), by multiplying the reactions rates by their own efficiencies. It is defined as the ratio between the actual average reaction rate in the sorbent particle and the rate obtained with a local concentration of the reactant gases equal to the bulk one in every point of the particle:

$$\eta_{rxn} = \frac{\int_0^{r_b} r^2 \dot{m}_{g\to s}(r)dr}{\int_0^R r^2\, \dot{m}_{g\to s,bulk}dr}, \tag{3.1}$$

where r (m) denotes the radial coordinate inside the particle, r_b is the point at which the boundary between the reaction zone and the diffusion zone is located, R (m) is the radius of the particle and $\dot{m}_{g\to s}$ is the mass transfer rate (kg m^{-2} s^{-1}). Both the adsorption and the regeneration processes are inherently transient, consequently the apparent reaction rate will change with time. For this reason, η_{rxn} will change while conversion proceeds. Indeed, the effectiveness factor will decrease with increasing conversion, as Equation 3.1 clearly states: with increasing conversion the reaction rate calculated with the local reactant concentration will decrease, while the reaction rate calculated at the bulk concentration will remain unchanged.

Sites A and B reactions were studied first, because these sorption sites have much bigger capacities than Site C. The given definitions of conversions for the reactions of Sites A and B are summarized in Table 3.4. The equilibrium mass fractions of adsorbed species are computed through the Freundlich Equations 2.6 and 2.12; the equilibrium mass fractions of free adsorbent sites are derived as:

$$w_{adsA}^{eq} = w_{adsA}^{0} - \left(w_{hydA}^{eq} - w_{hydA}^{0}\right)\frac{MW_{adsA}}{MW_{hydA}} \tag{3.2}$$

$$w_{adsB}^{eq} = w_{adsB}^{0} - \left(w_{carB}^{eq} - w_{carB}^{0}\right)\frac{MW_{adsB}}{MW_{carB}} \tag{3.3}$$

The given equations refer to relative conversions, which range from 0% to 100% for every bulk composition, despite the equilibrium concentration of adsorbed CO_2. This choice was adopted to be able to easily compare the results for different bulk conditions. In addition, since the initial mass fractions of the different types of free sites and of the adsorbed species are not known, these definitions allow to obtain relations valid for every initial composition.

Table 3.4 *Conversion definitions for the reactions of Site A and Site B*

Reaction	Conversion definition
H_2O adsorption Site A	$X_{ads,A} = \frac{w^0_{adsA} - w_{adsA}}{w^0_{adsA} - w^{eq}_{adsA}}$
H_2O desorption Site A	$X_{des,A} = \frac{w^0_{hydA} - w_{hydA}}{w^0_{hydA} - w^{eq}_{hydA}}$
CO_2 adsorption Site B	$X_{ads,B} = \frac{w^0_{adsB} - w_{adsB}}{w^0_{adsB} - w^{eq}_{adsB}}$
CO_2 desorption Site B	$X_{des,B} = \frac{w^0_{carB} - w_{carB}}{w^0_{carB} - w^{eq}_{carB}}$

Before obtaining the equations correlating the effectiveness factor to the conversion for the different reactions, it was decided to assess whether the internal mass transfer was actually limiting the kinetics or not. The particle model introduced in §2.3 was used to study the diffusion of CO_2 and H_2O inside the particles for different bulk concentrations during both the adsorption and the regeneration steps. The same process conditions (T=400°C, p=1 bar) of the experiments presented in §2.4 were used.

CO_2 adsorption kinetics is very fast. At the beginning of the adsorption step, only N_2 is present in the gas phase inside the particle. When the CO_2 adsorption step begins, the gas slowly diffuses inside the particle and begins to react, forming carbonates in the external layer of the particle. As the reaction goes on, CO_2 reaches inner shells of the particles, and carbonation begins also there. In Figure 3.3, y_{CO_2} simulated radial profiles inside the particle are reported for different conversions of carbonate and for a bulk molar fraction of CO_2 equal to 0.025. The profiles demonstrate that the reaction is limited by the diffusion: a flat concentration of CO_2 is reached only for complete conversion (in very long times). CO_2 desorption in Site B is less limited by mass transfer: for low conversions the reaction proceeds with the same velocity in every point of the particle, and the carbonates mass fraction radial profile is flat (Figure 3.4). However, for conversions above 30-40%, the reaction proceeds faster on the external layers of the particles. In addition, CO_2 concentration radial profiles (Figure 3.5) showed that for small conversions inside the particles the amount of CO_2 is significantly higher than outside. Therefore, for low conversions the desorption reaction proceeds with the same velocity in every point, but it is slowed down by the presence of a higher concentration of CO_2 than in the bulk. Experiments and simulations showed that the reaction

is slow, so it proceeds for a long time at these low conversions conditions. Hence, for this reaction internal mass transfer should be taken into account.

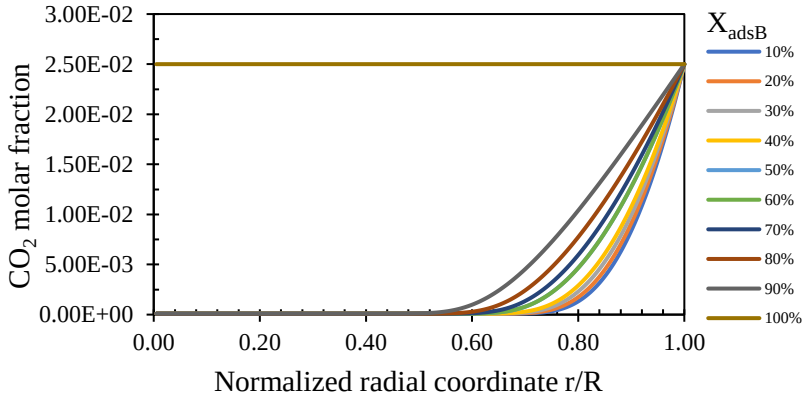

Figure 3.3 *Particle radial profile of CO_2 molar fraction during CO_2 adsorption with $y_{CO2,bulk}$=0.025 in nitrogen*

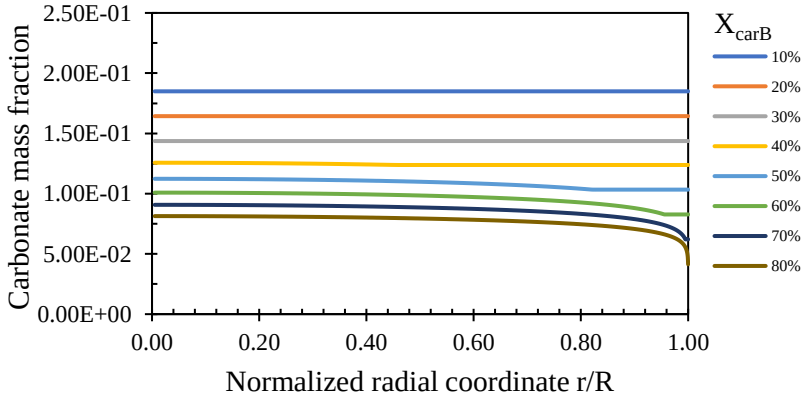

Figure 3.4 *Particle radial profile of Site B carbonates mass fraction during the regeneration step, with $y_{N2,bulk}$=1*

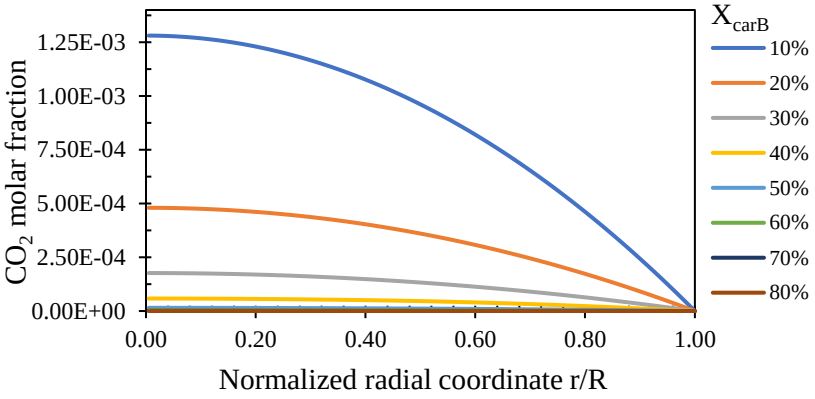

Figure 3.5 *Particle radial profile of CO_2 molar fraction during CO_2 desorption with $y_{N2,bulk}$=1*

Steam radial profiles during H_2O adsorption ($y_{H2O,bulk}$=0.10) are reported in Figure 3.6. The concentration inside the particle is lower than in the bulk for conversions below 45%, demonstrating a mass transfer limitation. Therefore, although this reaction is very fast and reaches high conversions in short times, the effectiveness factor for this reaction will be computed. Finally, the steam desorption reaction was analyzed. In this case, from the profiles of both y_{H2O} and w_{hydA}, it seems that the reaction proceeds in kinetic control. However, it was decided to proceed with the calculations of the effectiveness factor also for steam desorption to have further proof that the reaction is controlled by the kinetics.

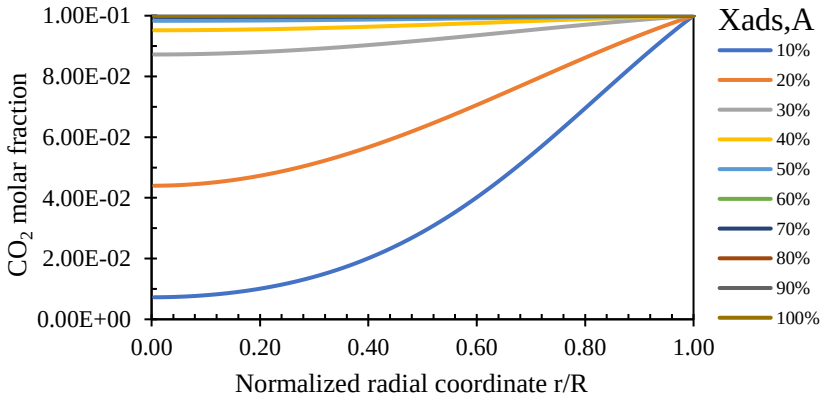

Figure 3.6 *Particle radial profile of H_2O molar fraction during H_2O adsorption with $y_{H2O,bulk}$=0.1 in nitrogen*

As far as Site C is concerned, the most important reaction for DAC is the exchange reaction (2.20). Regenerating the particles with steam actually allows to desorb CO_2 also from site C, and this is a possibility that may be explored for optimizing the process. Simulations were therefore carried out with the particle model to understand if the exchange reaction is limited by the intra-particle mass transfer. Different initial concentrations of adsorbed species were used in simulations, with various bulk gas compositions. In every case, mass transfer was proven to be very efficient. The particle radial profiles during the regeneration of the sorbent with N_2/H_2O mixtures after CO_2 adsorption were always flat, for all the different values of conversion of the carbonate. The conversion of carbonate in Site C was defined as:

$$X_{carC} = \frac{w^0_{carC} - w_{carC}}{w^0_{carC}} \tag{3.4}$$

The bulk composition is 10% H_2O and 90% N_2 and the initial solid composition is 5%w site C carbonate and 0% site C hydrate, the rest of the particle being composed by the other sites. The diffusions of CO_2 outside the particle and of H_2O inside the particle are very fast: concentrations profiles are flat. Results were found to be similar also for other process conditions, so the effectiveness factor was not calculated for site C exchange reaction.

Results showed that internal mass transfer limitations are worthy to be studied for the sorption reactions of both the gaseous species in the studied process conditions. The results presented from now on were obtained using a value for the tortuosity of the particle equal to 2. Calculations were performed also with other values (0.5, 1 and 3), but the effectiveness factor obtained with this value of tortuosity are the ones that give the better fitting of experimental data when they are used in the PBR model.

Since in the PBR the bulk composition of the gas phase is not uniform within the axial profile, attempts to obtain the relation between effectiveness factor and conversion as a function of the bulk composition were made. Instead of incorporating the particle model inside the reactor model, it is handier and more numerically convenient to use just an equation relating the effectiveness factor to the conversion and to the bulk composition, i.e. to exploit a $\eta_{rxn}(X, \overline{y}_{bulk})$ equation, regressed upon the data generated with the particle model. Hence, simulations with the particle model were carried out to obtain points of the $\eta_{rxn}(X, \overline{y}_{bulk})$ function for different values of conversion and bulk composition. Simulations were performed for at least ten different values of bulk concentration of the sorbent gases for each reaction. Based on the obtained $\eta_{rxn}(X, \overline{y}_{bulk})$ points, equations able to fit the generated data were guessed. Then, the equation parameters were regressed with the Sum of Squared Errors (SSE) method, using the error between the effectiveness factors calculated with the particle model and the proposed equations. The obtained results are further presented, starting from CO_2 reactions (the most important ones for DAC).

For CO_2 adsorption the equation is:

$$\eta_{ads,B} = \left(-0.60\, {X_{ads,B}}^2 - 0.58\, X_{ads,B} + 1.46\right) p_{CO_2}^{0.36} \tag{3.5}$$

In Figure 3.7 the curves calculated with the particle model and with Equation 3.5 are compared for some of the bulk CO_2 concentrations analyzed. Equation 3.5 can reproduce the particle model results with very good accuracy. The effectiveness factor for this reaction is quite low even at small conversions, confirming that the internal mass transfer is limiting the reaction. When the bulk concentration of CO_2 is lower, the effectiveness factor decreases. These relations were obtained using w_{adsB}^0 = 0.15 and w_{carB}^0 = 0.135. As already discussed, the actual solid composition prior to the adsorption step is not known a priori. For the given definitions of conversion (Table 3.4), the initial amount of adsorbate has no practical effect. The initial concentration of carbonates, instead, has an effect on the kinetic laws and accordingly on the effectiveness factor. Simulations were carried out to assess how much the effectiveness factor is affected by varying w_{carB}^0 for the bulk condition corresponding to $y_{CO2,bulk}$ = 0.025.

Results (Figure 3.8) showed that, if the initial composition is not varied much, the difference in the effectiveness factor for a given conversion is not significant. Hence, since the actual initial composition is not known *a priori* but only approximately, Equation 3.4 was assumed to be valid for a range of compositions close to the one with which it was obtained, instead of deriving the relation for all the different compositions. The same assumption was extended to the equations for the other reactions.

For the CO_2 desorption reaction, a more complicated equation had to be used to describe the results obtained with the particle model:

$$\eta_{des,B} = \left(X_{des,B}^2 \left(453\, p_{CO_2} - 5.82\right) + X_{des,B} \left(8.13 - 441\, p_{CO_2}\right)\right) \left(12.3\, p_{CO_2} - 0.32\right) + 1 \qquad (3.6)$$

The effectiveness factor calculated with the particle model and with E4quation 3.6 for CO_2 desorption are reported in Figure 3.9. Regression has been attempted for conversion only up to 80%, because CO_2 desorption is very slow. For this reaction, the effectiveness factor is high for low conversions, but then it goes down as the reaction proceeds. Also in this case, for lower bulk concentrations of CO_2 the mass transfer leads to a greater limitation to the reaction. The data calculated with the particle model are reproduced by Equation 3.6 with less accuracy with respect to the results obtained with Equation 3.5. However, the approximation was accepted, since it correctly describes the trend, which is more important than the actual value of the effectiveness factor.

After having studied the reactions of Site B, focus was given to Site A. The effectiveness factor for H_2O adsorption in Site A demonstrated to have only a slight dependence on the bulk composition, which was, therefore, neglected. The following simple linear equation is able to reproduce the relation with good accuracy, as demonstrated in Figure 3.10:

$$\eta_{ads,A} = -\,0.994\, X_{ads,A} + 0.992 \qquad (3.7)$$

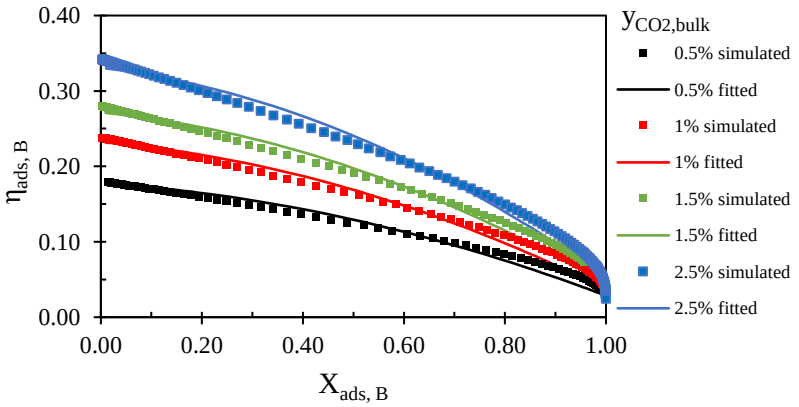

Figure 3.7 *Effectiveness factor for carbonates formation in Site B. The simulated points were calculated with the particle model, while the fitted curves with Equation 3.5*

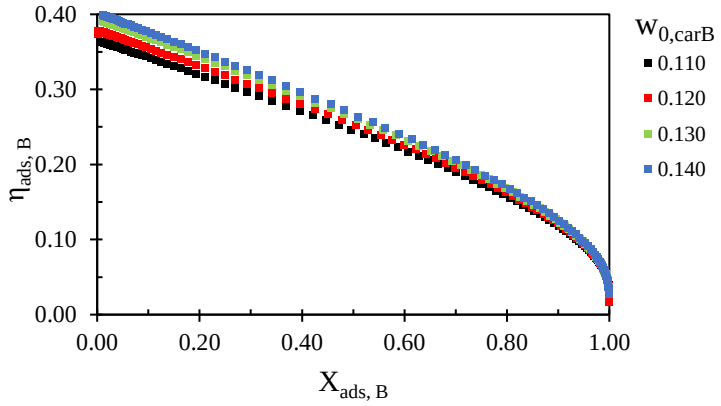

Figure 3.8 *Sensitivity analysis on the effect of a different carbonate initial mass fraction on* η_{adsB}

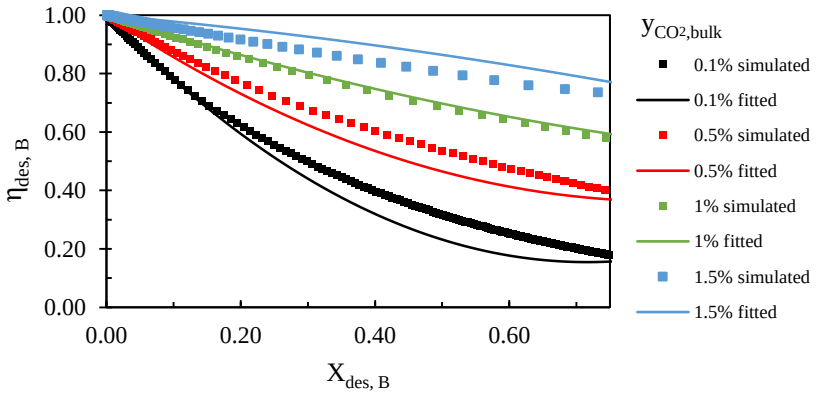

Figure 3.9 *Effectiveness factor for CO_2 desorption from Site B. The simulated points were calculated with the particle model, while the fitted curves with Equation 3.6*

The relation for the effectiveness factor for steam desorption from site A is much more complicated than the ones for the other reactions. Actually, many parameters had to be regressed in order to be able to fit with sufficient accuracy the points generated by the particle model, because the decrease of the efficiency with the bulk concentrations of steam was proven to be very significant. The obtained equation is:

$$\eta_{des,A} = 1 + ((4.19 - 69.49\ P_{CO2})\ X_{des,A}^3 + (142.11\ P_{CO2} - 9.67)\ X_{des,A}^2 + (7.35 - 60.92\ P_{CO2})\ X_{des,A})\ (5.16\ P_{CO2} - 0.53) \quad (3.8)$$

Regression was made for conversions up to 80%, because higher values were obtained only for very high times. The effectiveness factor calculated with the particle model and the regressed equation are reported in Figure 3.11. As already discussed, gas composition radial profiles showed that mass transfer is not limiting this reaction significantly, so model validation with experimental data will be performed both with and without using Equation 3.8, in order to evaluate if it is really

necessary to burden the model with such a complex equation, or if unitary efficiency is still adequate.

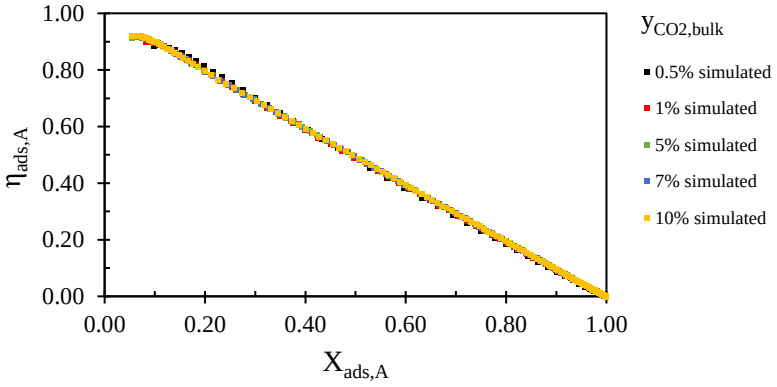

Figure 3.10 *Effectiveness factor for hydrates formation in Site A. For all the bulk concentrations of steam, the trend is similar*

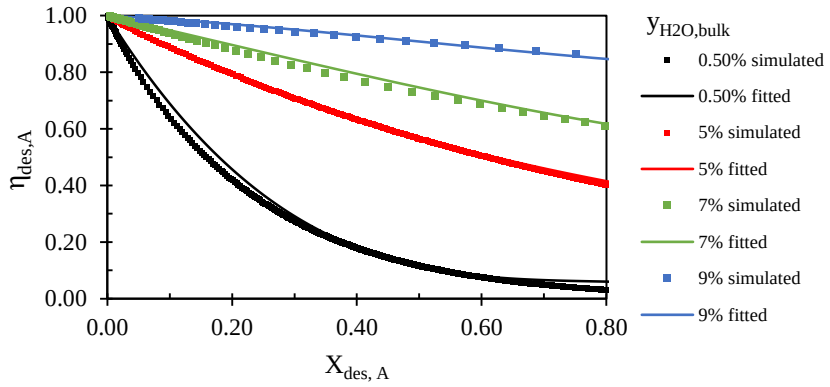

Figure 3.11 *Effectiveness factor for H_2O desorption from Site A. The simulated points were calculated with the particle model, while the fitted curves with Equation 3.8*

3.3 CO_2 sorption model

Since CO_2 sorption reactions are the most important for DAC, greater importance was given to the model validation for this species with respect to steam adsorption. For this purpose, the first six steps of Dataset 1 (Figure 3.1 and Table 3.2) can be exploited, since they only involve CO_2 adsorption and desorption. Adsorption on Site C occurs only during the first step, because CO_2 desorption from Site C can be obtained only by regenerating with steam, which does not happen in Steps 1-6. Site B reactions are the only responsible of the sorption in these steps, and, initially, they will be the only ones considered. The kinetic model presented in Paragraph §2.1 was used for simulations in the same conditions of Dataset 1 (Steps 1-6). One adsorption and one desorption steps are alternatively executed, starting from an adsorption step. Each step lasts 1800 s. Only CO_2

outlet concentration is considered for validation, since no steam is fed to the reactor. As already discussed, the original solid composition is not known beforehand. The original concentration of carbonate in Site B had to be guessed by trial and error, until the simulated breakthrough time matched the experimental one. Though with $w^0_{carB} = 0.13$ the breakthrough time is correctly predicted, the predicted shape of the breakthrough curves is not sufficiently accurate. The CO_2 outlet concentration after the breakthrough is underpredicted (1.9% vs 2.5% in the feed and in the experiments), and the breakthrough time for the second adsorption step is overpredicted.

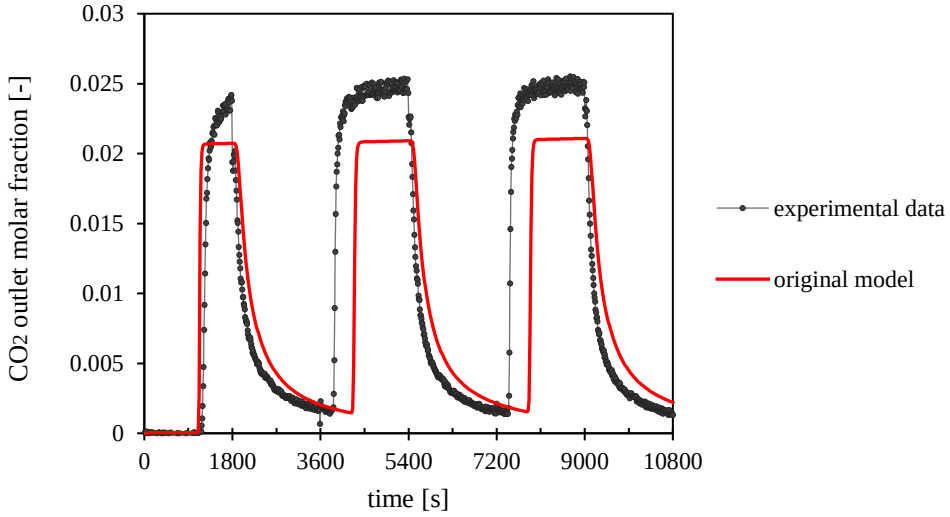

Figure 3.12 *Experimental and simulated curves for the first three cycles using the original model*

After carrying out several simulations and analysis, it was found out that the reason for the inaccurate simulations is an over-estimation of the bulk adsorption rate for CO_2. Adsorption and desorption rates axial profiles for bulk carbonates at the end of the first six steps, obtained through simulations with the original model, are reported in Figure 3.13. Bulk carbonates desorption rate is very low during all the steps, even during regeneration. On the other hand, the adsorption reaction goes on even during the regeneration steps, adsorbing the CO_2 released at the beginning of the reactor. It is possible to notice that the reaction rates at the end of an adsorption or desorption steps are the same for corresponding steps in every cycle. As a matter of fact, looking at the rate equations for bulk CO_2 sorption (Equations 2.14 and 2.15), reactions go on until an equilibrium between adsorption and desorption rates is reached for a certain bulk carbonates concentration. However, according to the model the equilibrium value is too high: the bulk carbonate concentration in the bed always keeps growing during all the first six steps, and even during the regeneration, as shown in Figure 3.14. Reducing the value of $k^0_{bulk\ ads,B}$ allowed to obtain very good improvements in the reproduction of experimental data. As a first attempt, it was divided by the value of the solid bulk density, reducing it from 1.93E-04 to 4.82E-07 [mol kg^{-1} $bar^{-0.5}$ s^{-1}]. This change led to satisfying

improvements (Figure 3.15), so the new value for $k^0_{bulk\ ads,B}$ was accepted initially, although its later optimization was planned.

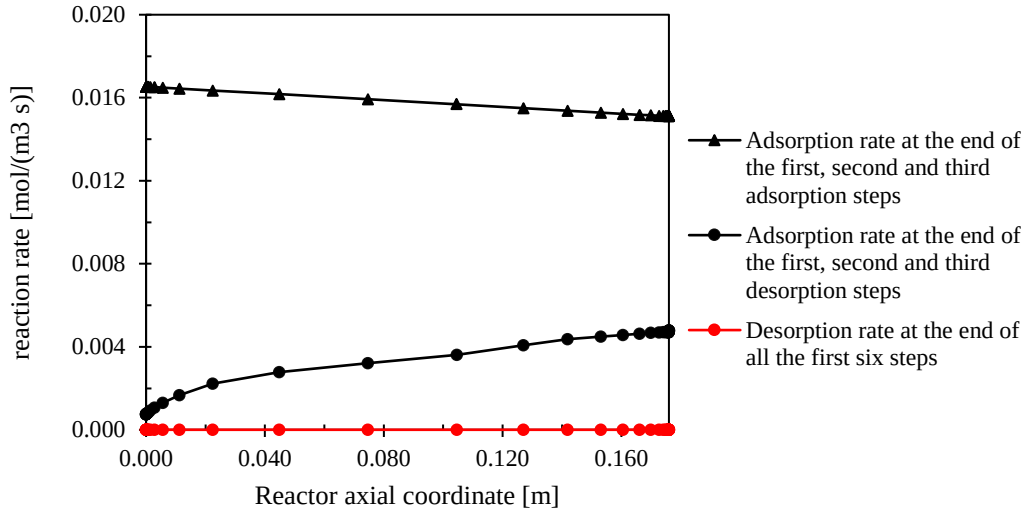

Figure 3.13 *Bulk CO_2 adsorption and desorption rates axial profiles at different times. Data obtained with simulations with the original kinetic model.*

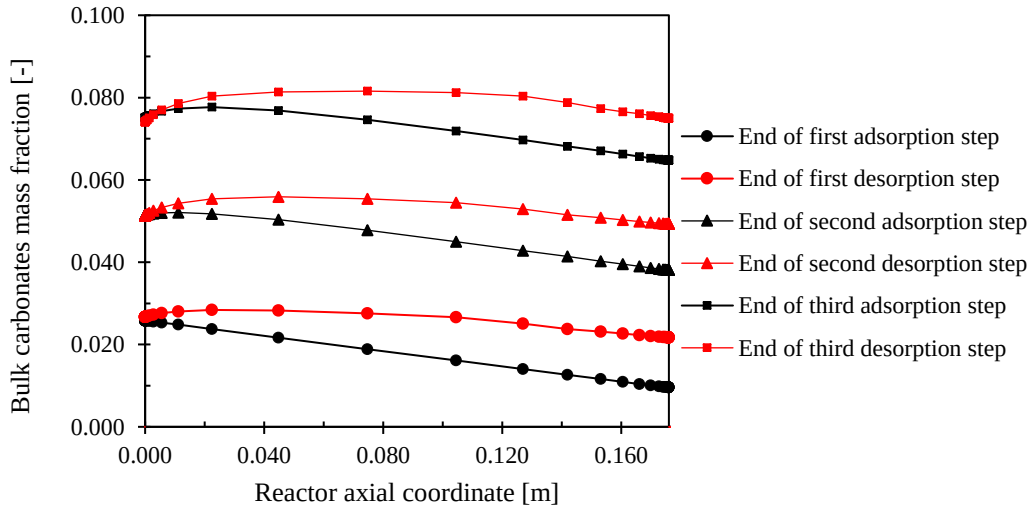

Figure 3.14 *Bulk carbonates mass fractions axial profiles at the end of each one of the first six steps. Data obtained with simulations with the original kinetic model*

From now on, any reference to the original kinetic model will consider this change. Though the breakthrough molar fraction of CO_2 is now able to reach 2.5% as in the experiments, the experimental data are not still reproduced appropriately. In particular, breakthrough curves are too steep, too much CO_2 is desorbed during the regeneration step and the breakthrough time for the second and the third adsorption steps are overpredicted, due to the excessive sites regeneration. In order to try to improve the accuracy of reproduction of the experimental data, mass transfer

limitations were taken into account. External mass transfer was proven to be very efficient, because no differences were obtained using the heterogeneous model (Paragraph §2.2) instead of the pseudo-homogeneous model, as it is possible to see in Figure 3.15.

The effect of the internal mass transfer was then considered, exploiting Equation 3.5 and Equation 3.6 to calculate the effectiveness factor to be multiplied by the reactions rates. New simulations were carried out and better results were obtained with respect to the ones without intra-particle diffusion limitations (Figure 3.16).

The peaks of the breakthrough curves are finally rounded, similarly to the experimental curves. The results show that the intra-particle mass transfer could be limiting the reaction kinetics for CO_2 adsorption and desorption in Site B, as predicted by the particle model (see Paragraph §3.2). From now on, the effect of internal mass transfer for Site B reactions will be always considered. Still, too much CO_2 is released during the desorption steps, and the breakthrough times for the second and the third breakthrough steps are overpredicted, even if less than without considering the mass transfer. The excessive CO_2 release and the shift in the predicted breakthrough times are actually linked: more sites are regenerated during a desorption step, more time is needed during the following adsorption step to reach the breakthrough.

Hence, accounting for the internal mass transfer and adopting the proposed correction on $k^0_{bulk\ ads,B}$ are not enough to obtain satisfying results. Therefore, it was decided to assess the influence of some significant parameters, to improve the fitting of experimental data. A sensitivity analysis was carried out, simulating the breakthrough experiments for different values of the parameters. New values were proposed, looking for a compromise between optimal reproduction of experimental data at the minimum change from the original model. In Table 3.5 the original values of the parameters considered in this sensitivity analysis are reported, together with the range of variation in which they were studied. Some considerations on the effect of changes on the analyzed parameters will be further presented.

First, the desorption kinetic constant $k^0_{des,B}$ and the parameter $\beta_{des,B}$ in the Elovich equation were varied, in order to try to reduce the amount of regenerated sites calculated by the model. This objective can be fulfilled by reducing either $k^0_{des,B}$ or $\beta_{des,B}$, as stated by Equations 2.1 and 2.2. In Figure 3.17 and Figure 3.18 some of the simulations carried out for different values of $k^0_{des,B}$ and $\beta_{des,B}$ are reported. The effect of acting on one parameter or the other is similar, the only difference being that $\beta_{des,B}$ has a stronger influence on the first part of the desorption curve, when the coverage of occupied sites is still high, while $k^0_{des,B}$ equally affects all the curve. In both cases, the desorption rate is reduced and the desorption curves are matched better. Also the breakthrough times of the second and the third curves are predicted with more accuracy, because less sites are regenerated and the overprediction shown with the original model (Figure 3.16) is reduced. However, it is not

possible to reduce the desorption rate as much as it would be needed for reproducing the experimental data, because, under certain values of $k^0_{des,B}$ and $\beta_{des,B}$, a step in the CO_2 outlet concentration appears at the beginning of the second and of the third adsorption steps. The reason is that if the concentration of available sites is not high enough, the equilibrium concentration of carbonates at the beginning of the new adsorption step is lower than the actual value of occupied sites, so the adsorption does not start and some CO_2 escapes from the reactor as soon as it is fed.

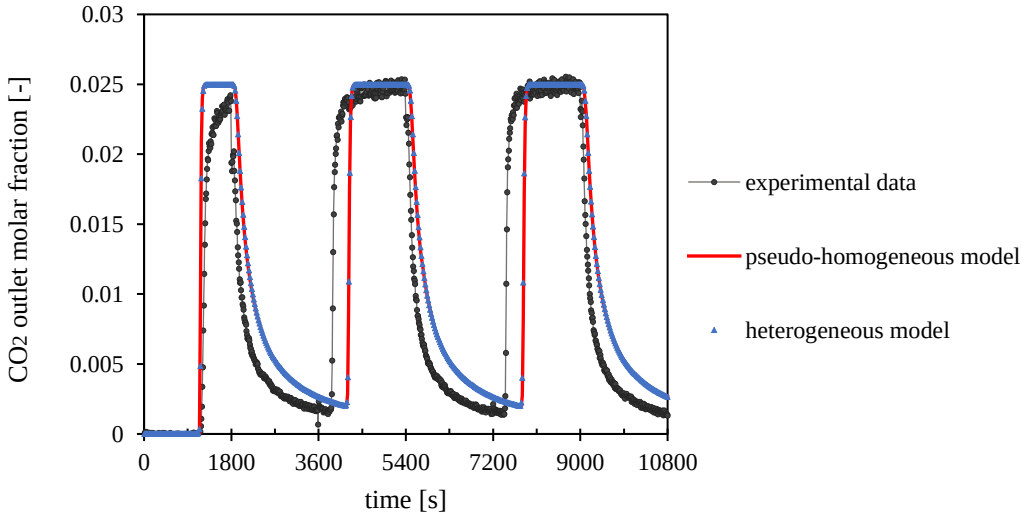

Figure 3.15 *Experimental breakthrough curves compared with curves simulated with both the pseudo-homogeneous and the heterogeneous reactor model at the new proposed reduced bulk carbonation rate.*

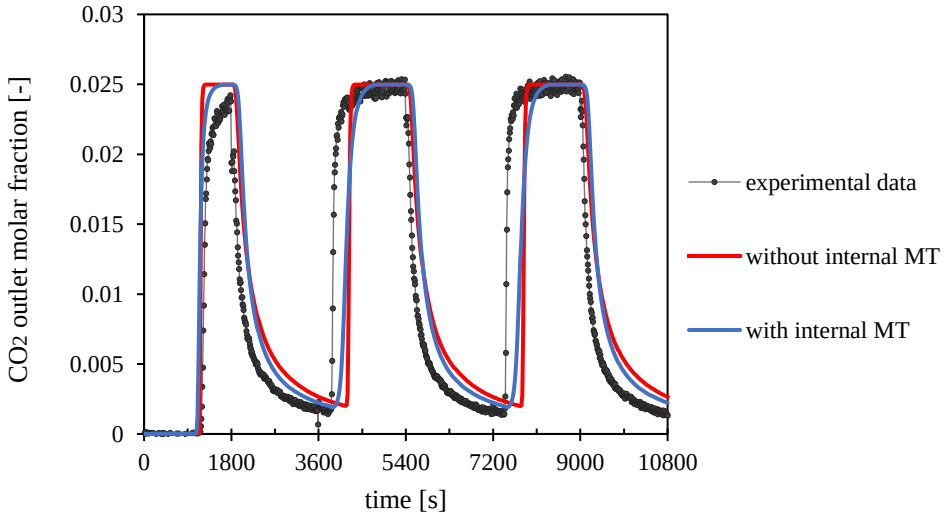

Figure 3.16 *Experimental breakthrough curves compared with curves simulated through the pseudo-homogeneous model with and without considering the internal mass transfer*

Table 3.5 *Parameters analyzed during the sensitivity analysis, together with the range in which their effect was explored. The proposed final changes are presented*

Parameter	Original value	Sensitivity analysis range	New proposed value
$k^0_{ads,B}$ [s^{-1}]	0.16	0.10 – 0.50	0.32
$k^0_{des,B}$ [s^{-1}]	42.98	1 - 50	5
$\beta_{des,B}$ [J mol^{-1}]	84544	70000-100000	92000
$k^0_{bulk\ ads,B}$ [mol kg^{-1} $bar^{-0.5}$ s^{-1}]	4.825E-07	4.00E-07 – 2.00E-04	1.206E-04
$k^0_{bulk\ des,B}$ [s^{-1}]	2.233E-05	2.233E-05 - 4.5E-03	1.34E-03
$n_{f,B}$ [-]	0.0825	0.025 – 0.100	0.034
$k_{f,B}$ [mol kg^{-1}]	0.6063	0.55 – 0.65	0.6063

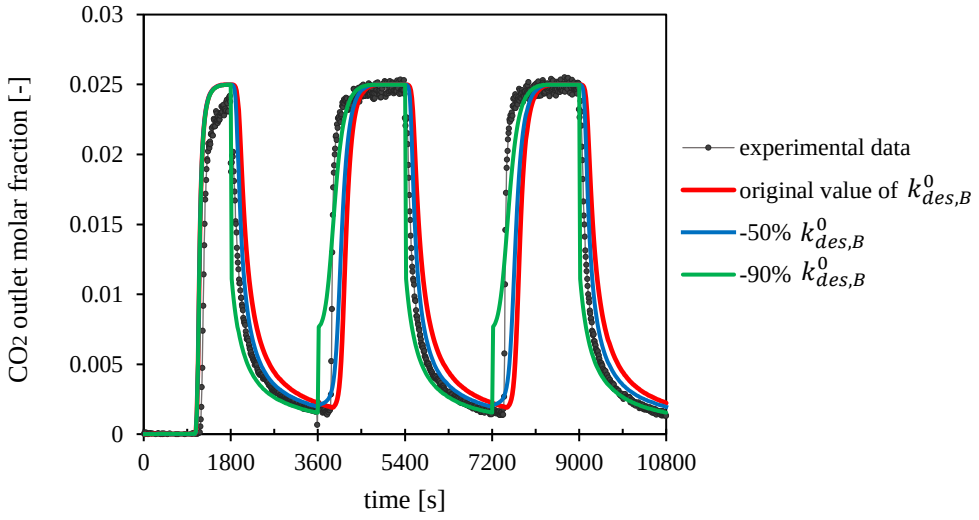

Figure 3.17 *Selected results of the sensitivity analysis on* $k^0_{des,B}$

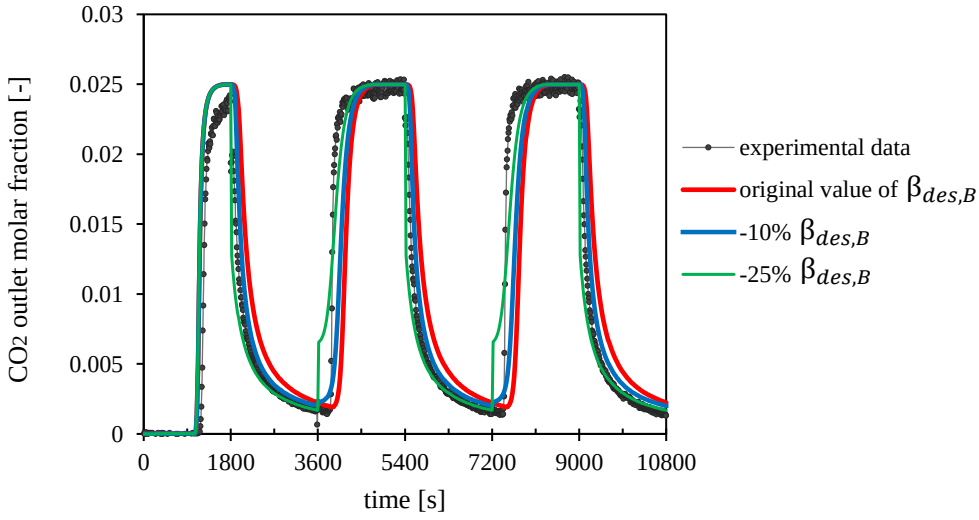

Figure 3.18 *Selected results of the sensitivity analysis on* $\beta_{des,B}$

Hence, it appeared clear that reducing the desorption rate is not enough for fitting the experimental data with enough accuracy: the sorption capacity has to be increased as well, especially at low p_{CO_2}. For this reason, a sensitivity analysis was carried out also on the parameters of the Freundlich isotherm for site B (Equation 2.12): $n_{f,B}$ and $k_{f,B}$. In Figure 3.19 the equilibrium carbonate mass fraction profiles for Site B calculated with Equation 2.12 are reported for different values of $n_{f,B}$ (left graph) and $k_{f,B}$ (right graph).

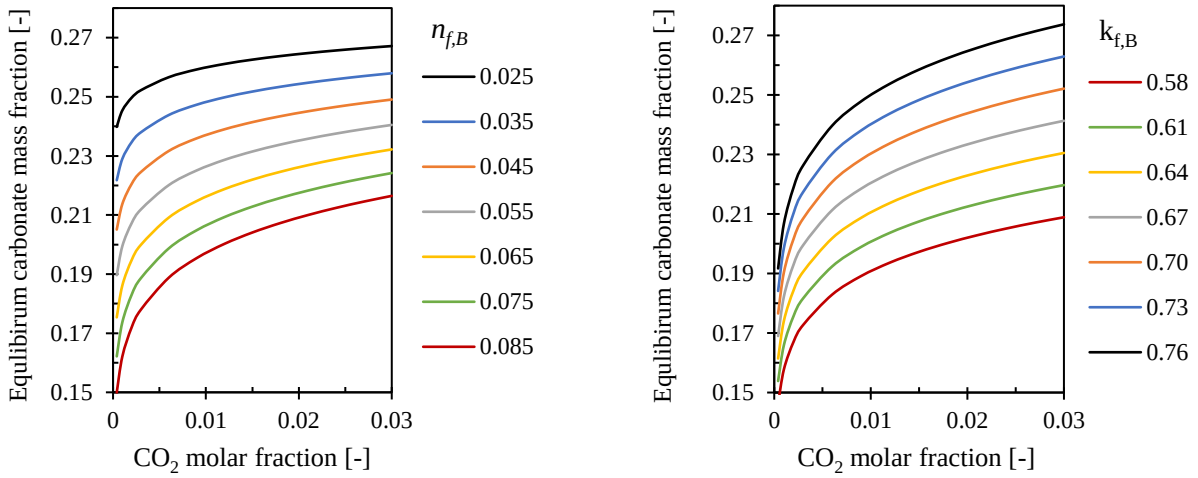

Figure 3.19 *Sensitivity analysis on the equilibrium mass fraction of carbonate in Site B. Left: sensitivity on Equation 2.12 exponent. Right: sensitivity on Equation 2.12 pre-exponential factor*

When $n_{f,B}$ is reduced and when $k_{f,B}$ increases, w_{carB}^{eq} becomes higher, as it is desired for eliminating the step at the beginning of the second adsorption step. Increasing $k_{f,B}$, w_{carB}^{eq} has an increase of about the same amount for every partial pressure of CO_2. Instead, a $n_{f,B}$ reduction leads to a higher increase of w_{carB}^{eq} at low pressures, with respect than to higher pressures. Since the problem of the step at the beginning of the second adsorption step is due to a too small w_{carB}^{eq} for low p_{CO2}, acting on $n_{f,B}$ to shift the equilibrium seems the best option. Hence, from now on $k_{f,B}$ will be kept at the original value of 0.6063 [mol kg^{-1}] and only $n_{f,B}$ will be changed to better fit experimental data. This way, to eliminate the problem at the beginning of the adsorption steps it will not be necessary to modify too much the equilibrium value at higher pressures of CO_2. Simulations carried out for different values of $n_{f,B}$ proved that reducing $n_{f,B}$ the step that appears at reduced desorption rate can be eliminated, improving the fitting of experimental data significantly. Selected results of the sensitivity analysis on $n_{f,B}$ are reported in Figure 3.20. In the simulation the desorption rate was reduced of 80% with respect to the original model, to assess if the new values for $n_{f,B}$ were actually able to eliminate the step problem. Not all the simulations performed on $n_{f,B}$ are reported in Figure 3.20, but the results showed that the curves for $n_{f,B}$ lower than 0.06 do not present the steps at the

beginning of the adsorption steps. However, when $n_{f,B}$ is further reduced the experimental data are reproduced even better, as far as the second and the third peaks are concerned. Actually, the simulated second and third adsorption breakthroughs occur a little bit slower than how was shown by experiments, and lower values of $n_{f,B}$ reduce the problem. This error can also be decreased by increasing $k^0_{ads,B}$, so also the effect of this parameter was studied with a sensitivity analysis.

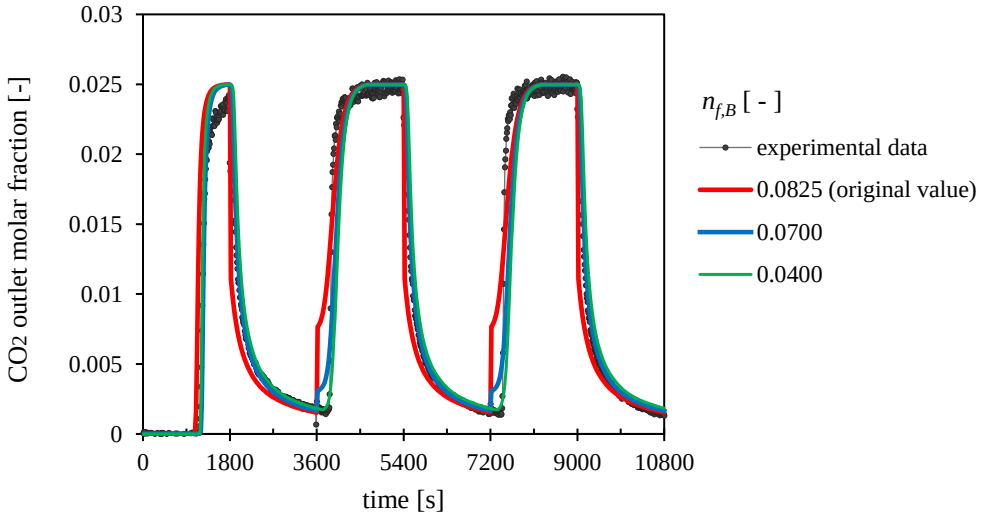

Figure 3.20 *Selected results of the sensitivity analysis on* $n_{f,B}$

Finally, sensitivity analysis were carried out on bulk adsorption and desorption rates, acting on $k^0_{bulk\ ads,B}$ and $k^0_{bulk\ des,B}$. Selected results of the performed simulations are reported in Figure 3.21. As expected, these parameters mainly affect the shape of the peaks and the CO_2 outlet concentration after the breakthrough. Fine-tuning both the bulk adsorption and desorption kinetic constants allowed to fit experimental data within an acceptable accuracy.

Several simulations were performed varying all the parameters whose effect has been presented so far. It was possible to conclude that the original model (Paragraph §2.1) fails to accurately describe the experimental data because:

- Internal mass transfer is neglected;
- The number of available sites is underpredicted, especially at low p_{CO2};
- Desorption kinetics are overpredicted;
- Bulk carbonates are not accurately implemented.

Based on the previous considerations, in Table 3.5 the final proposed values for the studied parameters are presented. The results of the simulation with the final proposed parameters are presented in Figure 3.22. The improvement with respect to the simulations obtained with the

original model is obvious (Figure 3.12), but also with respect to the simulations of Figure 3.16, where only the bulk adsorption rate was modified and the internal mass transfer limitations were introduced.

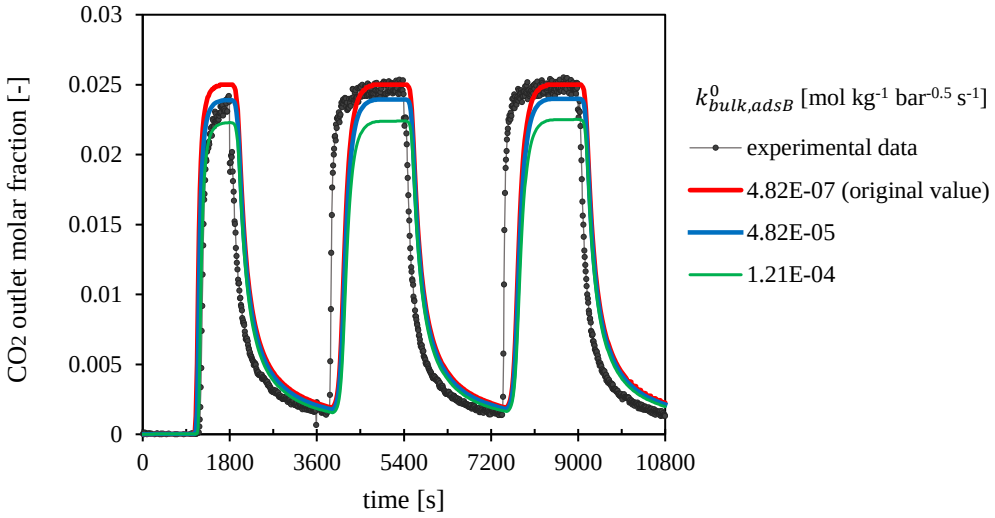

Figure 3.21 *Selected results of the sensitivity analysis on bulk carbonation reaction rate*

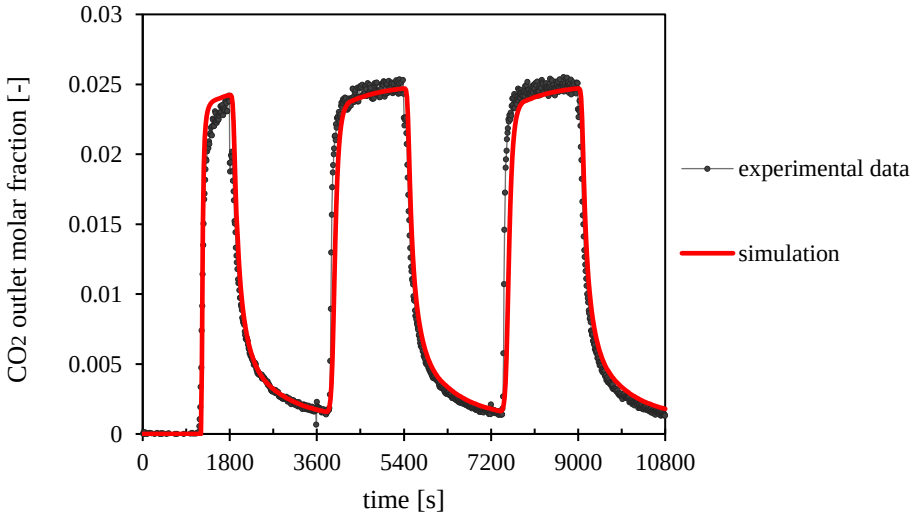

Figure 3.22 *Simulation with the optimized parameters for Site B*

The main remaining model-data mismatch is in the first breakthrough peak: the outlet CO_2 concentration is overpredicted by the model, while the following peaks are reproduced with more accuracy. Actually, Step 1 cannot be correctly reproduced without considering CO_2 adsorption in Site C, that has been neglected so far, while Site C reactions have no effect on Steps 2-6. As a matter of fact, C sites are available for CO_2 adsorption only during the first step after the pre-treatment: they could be regenerated only with steam, but pure nitrogen is exploited for the

desorption step in Steps 1-6. When also the reactions of Site C were implemented in the model, the fitting of experimental data became even more accurate in reproducing Step 1, as expected (Figure 3.23). The original equations proposed for Site C reaction rates were used (Paragraph §2.1), while the new proposed optimized parameters were exploited for Site B equations. The value of the initial concentration of carbonates in Site B after the pretreatment necessary to match the breakthrough time in the final performed simulation (with the optimized parameters for Site B and considering also Site C reactions) is 16.1%w.

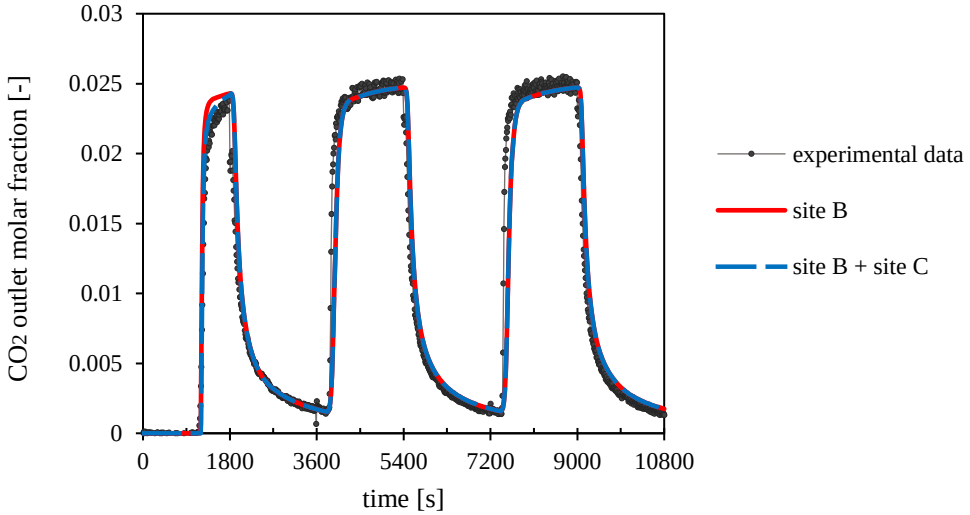

Figure 3.23 *Simulations with and without considering Site C reactions. Site B reactions are instead implemented in both of the cases*

3.4 H_2O sorption model

Steam adsorption and desorption in hydrotalcites is of secondary importance if compared to CO_2 sorption for DAC processes. Nevertheless, regeneration of adsorbed CO_2 with steam may lead to an improved cyclic working capacity, since also carbonates in Site C may be desorbed. For this reason, also the part of the kinetic model presented in Paragraph §2.1 involving steam sorption will be validated and optimized. Dataset 2 (Paragraph §3.1) was used for this purpose. First, only Site A reactions were considered, since this site has higher capacity with respect to Site C, and it can be regenerated with nitrogen, as is done in the experiments of Dataset 2. The simulated breakthrough curves obtained with the original kinetic model match with quite a good approximation experimental results (Figure 3.24). However, there are some deviations between simulations and experimental data. Profiles are too steep and breakthrough time is overpredicted for the second adsorption step, because too much H_2O is desorbed during the regeneration step in the simulations. The steepness problem for CO_2 sorption was initially solved by tuning bulk

reactions parameters. However, according to the previous studies on the kinetic model (Coenen *et al.*, 2018d), the formation of bulk hydrates is negligible.

As shown in Paragraph 3.2, the particle model predicts that internal mass transfer limitations play a role also in the adsorption of H_2O. Hence, to reduce the steepness of the curves, effectiveness factors for H_2O adsorption and desorption reactions (Equation 3.7 and Equation 3.8) on Site A were implemented in the model. The results of the simulations carried out including the intra-particle mass transfer are reported in Figure 3.25. The effectiveness factor has little to no effect on the breakthrough curves during the adsorption steps: despite being slowed down by the effectiveness factor, the adsorption kinetics are so fast that the H_2O outlet molar fraction suddenly goes from 0 to 0.10 at the breakthrough. The problem is more evident in the first peak, while the error in the second and third peaks is smaller. Actually, as for CO_2 adsorption (Paragraph §3.3), in the first adsorption step also Site C is saturated, but this is not accounted for in these simulations. In any case, the implementation of the effectiveness factor for H_2O adsorption reaction doesn't appear to be much significant compared to the added computational effort, so Equation 3.7 was not used in any other simulation. For the reduction step, instead, the use of Equation 3.8 has a clear effect on the results of the simulation, as shown in Figure 3.26. However, it was observed in Paragraph §3.2 that H_2O desorption is not mass transfer limited. Indeed, the deviation between model and experiments in the desorption step could be due to an overestimation of desorption kinetics, which was the case for CO_2. As a matter of fact, the same result can be achieved by reducing the desorption rate. In particular, if k^0_{desA} = 56.4 [s^{-1}] instead than 564 [s^{-1}] as in the original model, the same profiles obtained in Figure 3.25 using the effectiveness factor for the steam desorption reaction are obtained. Therefore, from observation made in Paragraph 3.2 and above, it can be supposed that also the mass transfer for Site A regeneration is efficient, and, consequently, it is not necessary to implement Equations 3.7 and 3.8.

Looking at Figure 3.25, it is possible to notice that a step in the H2O outlet molar fraction appears at the beginning of the second and the third adsorption steps. The reason for the step is that at the beginning of the adsorption cycles (but for the first) the hydrates concentration is higher than the value of equilibrium, so the adsorption reaction does not occur. The same problem of underestimation of the sorption capacity at low pressures was found for CO_2 in §3.3. The solution for eliminating the step, as for CO_2 sorption, was found to be increasing the adsorption capacity for H_2O. Hence, a sensitivity analysis was performed, acting on $n_{f,A}$ and $k_{f,A}$.

At the end, the only changes proposed to the original model for Site A presented in Paragraph §2.1 are:

- k^0_{desA} = 56.4 [s^{-1}] instead than 564 [s^{-1}]
- using $n_{f,A}$ = 0.05 instead of 0.124

In Figure 3.26 simulations with the original model and with the new proposed changes are compared with experimental data. Site C reactions are also included, so the first peak is reproduced better than in Figure 3.24 and Figure 3.25.

The simple proposed improvements lead to results that are much better than with the original model, therefore the new values proposed for $k^0_{des,A}$ and $n_{f,A}$ will be used from now on. The initial hydrates mass fraction in Site A necessary to match the experimental breakthrough time was assessed to be 38% in the final simulation.

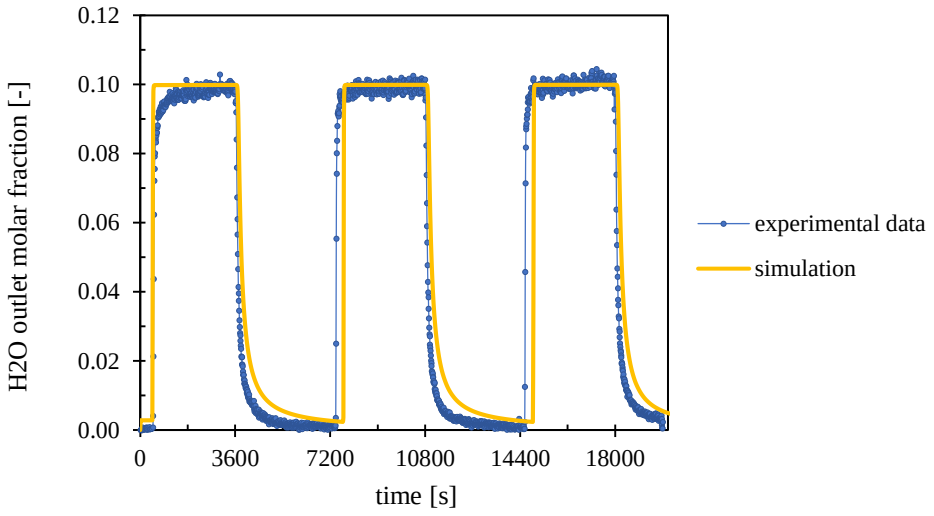

Figure 3.24 *Steam sorption experimental breakthrough curves compared with the results of simulations using the original model for Site A*

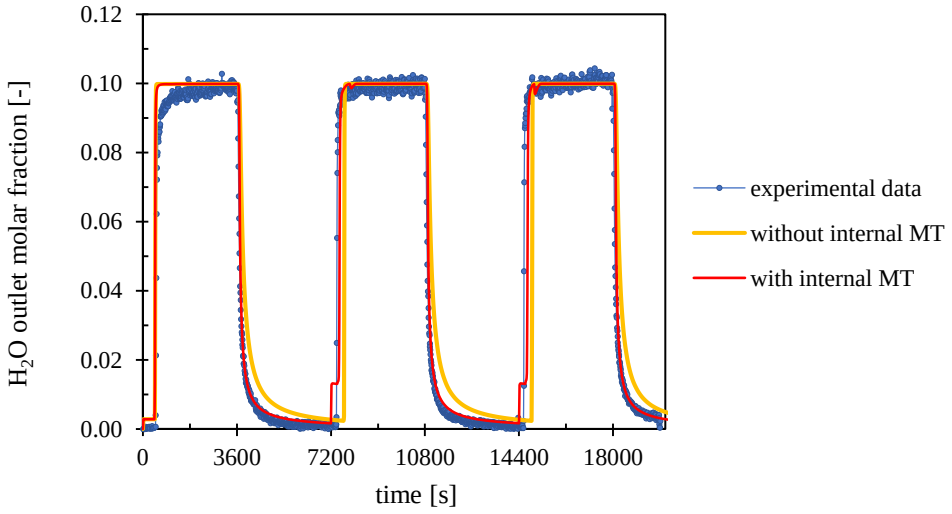

Figure 3.25 *Steam sorption experimental breakthrough curves compared with the results of simulations either considering and not considering the intra-particle mass transfer limitations. The original kinetic model is used in both of the cases*

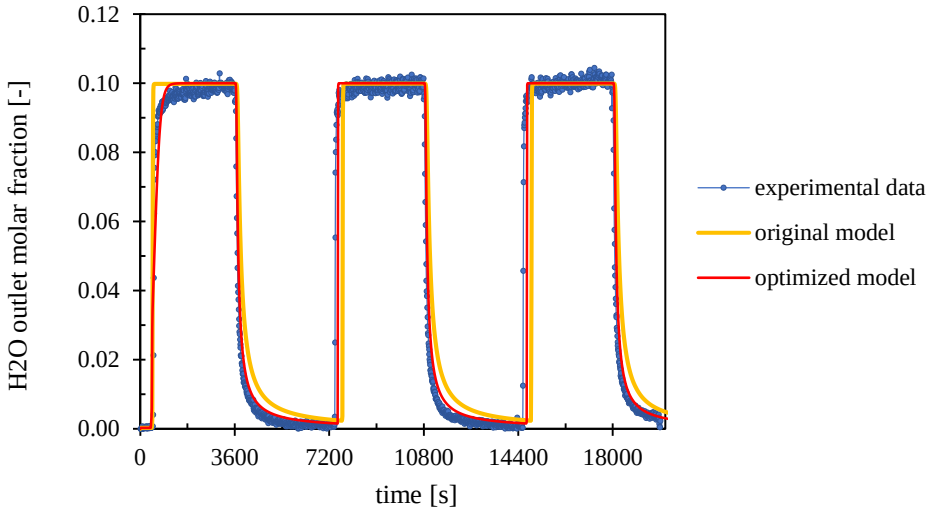

Figure 3.26 *Steam sorption experimental breakthrough curves compared with the results of simulations with the original model and with the proposed changes. In the simulation with the optimized model also Site C reactions were computed, while the original model simulation only considers Site A reactions*

3.5 Effect of steam on CO_2 sorption

Once that the part of the model describing the single species sorption of CO_2 and H_2O was completed, focus was given to the validation of the equations taking into account the simultaneous presence of CO_2 and H_2O. In Steps 1-6 of Dataset 1 (Table 3.2), already used for validation in Paragraph §3.3, only CO_2/N_2 mixtures are used. Steps 7-33 of the same dataset are instead useful for this new analysis, because they contain data involving experiments in which CO_2 and H_2O are fed simultaneously. An initial simulation was carried out with the original proposed model for Site C and the optimized values (Paragraph §3.3 and Paragraph §3.4) of the parameters for Site A and Site B. The implemented reactor properties are the same of the one used for the experiments (Table 3.1). The initial mass solid composition was set to be 16% of Site B carbonates and 38% of Site A hydrates, as found out to be for KMG30 after the initial pretreatment from results of Paragraphs §3.3 and §3.4. The other 46% of the solid was set to be free adsorbent, since all species adsorbed in Site C are desorbed during the pretreatment at 600°C (Coenen *et al.*, 2018d). The resulting outlet profiles of CO_2 and H_2O molar fractions are respectively reported in Figure 3.27 and Figure 3.28 for Steps 1-20.

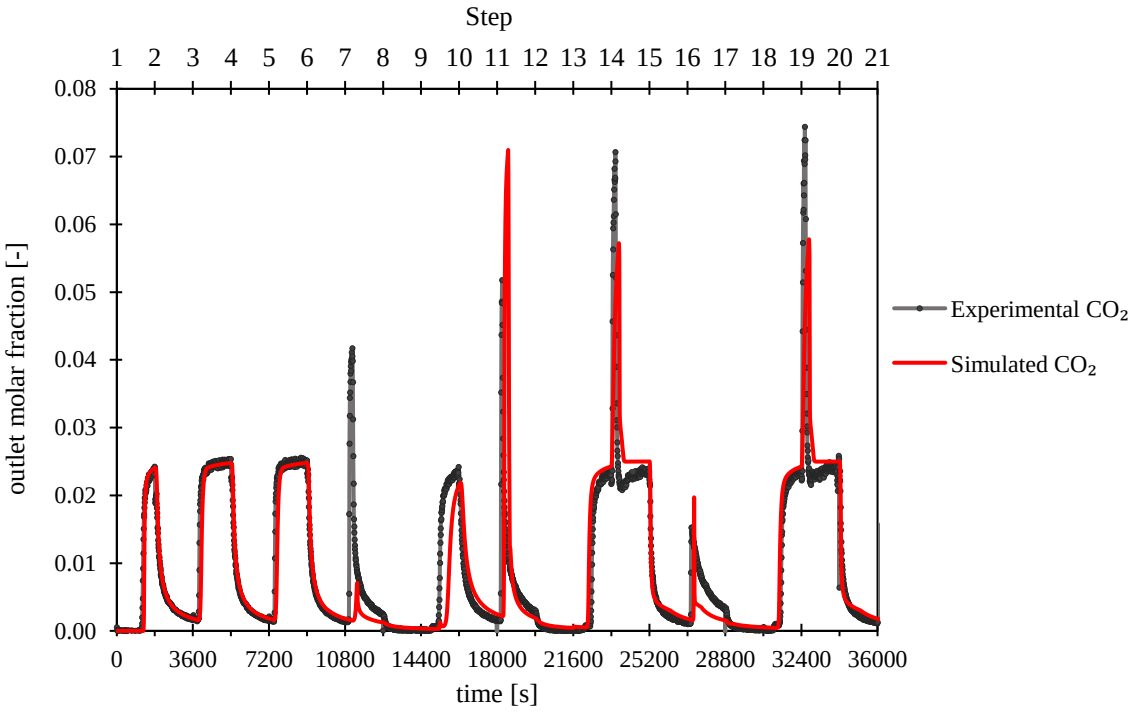

Figure 3.27 *CO_2 reactor outlet molar fractions profiles: Dataset 1 Steps 1-20 are compared with the results of the simulations carried out using the original model for Site C and the one optimized in the previous paragraph for Sites A and B*

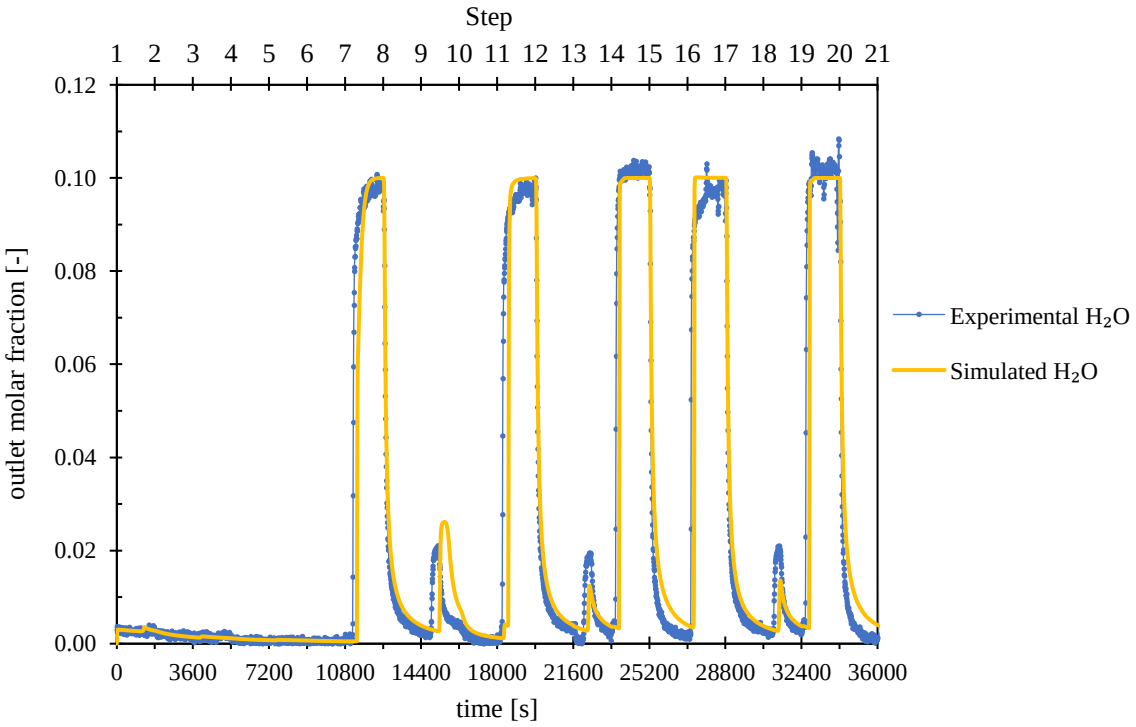

Figure 3.28 *H_2O reactor outlet molar fractions profiles: Dataset 1 Steps 1-20 are compared with the results of the simulations carried out using the original model for Site C and the one optimized in the previous paragraph for Sites A and B*

The simulations of the first six steps perfectly fit CO_2 experimental data, because they are the experiments for which the model was optimized in Paragraph §3.3. The outlet fraction of steam in these first six steps is only due to the desorption of hydrates from the sorbent, because no H_2O is fed to the reactor. Simulated values are consistent with experimental data, bringing an additional validation to the initial concentration of hydrates adsorbed in Site A, that was obtained exploiting Dataset 2 in Paragraph §3.4. Some deviations are instead found in the following steps, the ones not considered so far (Table 3.2, Figure 3.27, Figure 3.28 and Figure 3.29 are useful to better understand the following considerations):

1. The CO_2 adsorption capacity in Site C, expressed in Equation 2.19 as $k_{c1}p_{CO_2}\rho_s$, is underestimated. Site C is filled with carbonates for the first time during Steps 1-6 through the reaction reported in Equation 2.16. In Step 7, when a H_2O/N_2 mixture is for the first time fed to the reactor, the CO_2 previously adsorbed is released from Site C through the hydrates/carbonates exchange reaction (Equation 2.20). The calculated outlet peak of CO_2 is much lower than experimental data, meaning that the adsorption capacity for CO_2 in Site C is underestimated. This causes a model-experiments deviation only the first time that steam enters the reactor;

2. The H_2O adsorption capacity in Site C is overestimated, leading to deviations also in the estimation of CO_2 sorption in Site C. This problem is the most important, because it causes errors every time that the carbonated Site C is regenerated with steam, so the calculated cyclic working capacity obtained exploiting steam for regeneration would be wrong:
    - In Steps 1-6 no steam enters the reactor, so no hydrates are formed in Site C. The axial profiles of carbonates and hydrates in Site C at the end of Step 6 is reported in Figure 3.29: less than 1%w of the solid is composed by carbonates in Site C, which were formed by direct adsorption through the reaction expressed by Equation 2.16. A small negligible amount of hydrates is also present in Site C, formed upon the adsorption of the steam desorbed from Site A during Steps 1-6;
    - A significant amount of steam adsorbs for the first time in Site C during Step 7 (feed = H_2O/N_2 mixture) through the direct adsorption reaction (Equation 2.15) and the exchange with the carbonates (Equation 2.20) already adsorbed in Site C during the previous steps. At the end of the step, there are no more carbonates in Site C. About 8%w of the solid is now composed by hydrates adsorbed in Site C (Figure 3.29). Hence, the capacity of Site C increased about eight times compared to the previous steps, due to the use of steam;

- During Step 8, regeneration is made with pure nitrogen, with no effect on Site C adsorbed species;
- In Step 9 a CO_2/N_2 mixture is fed to the reactor, leading to the exchange of hydrates with carbonates in Site C (exchange reaction, Equation 2.20). At the end of Step 9, almost all of the hydrates that were present in Site C at the end of Step 7 have been exchanged with carbonates (Figure 3.29). By comparison with the situation at the end of Step 6, it is possible to notice that the amount of carbonates adsorbed in the Site C is now much more significant. However, the model predicts a greater emission of H_2O during Step 9, compared to the experimental results (Figure 3.27). Hence during Step 7 too many steam had been adsorbed according to the model and, because of the substitution, the model accounts now for too much considerable amount of CO_2 adsorbed in Site C. As a consequence, the breakthrough of CO_2 during Step 9 is delayed as well. This result is not in contrast with the underestimation of the adsorption capacity of CO_2 earlier described. In Step 9 too much CO_2 is adsorbed due to the exchange reaction (Equation 2.20) with the hydrates, which are more than expected, and not to the single species adsorption (Equation 2.15), where the capacity is underpredicted (Equation 2.19).
- During Step 10, only nitrogen enters the reactor; it does not affect Site C;
- As a result, during Step 11 (feed = H_2O/N_2 mixture) the calculated outlet concentration of CO_2, which is due only to the hydrates/carbonates exchange in Site C, is overestimated.

In any case, an important consequence of the presented analysis of the solid species axial profiles over time is that the adsorption capacity of CO_2 in Site C can be increased by regeneration with steam, though the original model commits some slight overestimations and adjustments are necessary;

3. The model is less performing when both the adsorbing gases are fed to the reactor. After both CO_2 and H_2O are fed (Steps 14 and 18), accuracy is lower, also in the following regeneration steps.

For the purposes of DAC, the only interest towards steam is the possibility to exploit it to enhance the regeneration of Site C from CO_2 and to increase the adsorption capacity of the sorbent through the exchange of hydrates with carbonates, as previously discussed and shown in Figure 3.29. Not much effort has to be spent in validating and optimizing the model to correctly reproduce experiments in which both CO_2 and H_2O are simultaneously fed to the reactor. Hence, point 3 was

not further analyzed and only Steps 1-12 have been used for improving the model performance with respect to point 1 and 2.

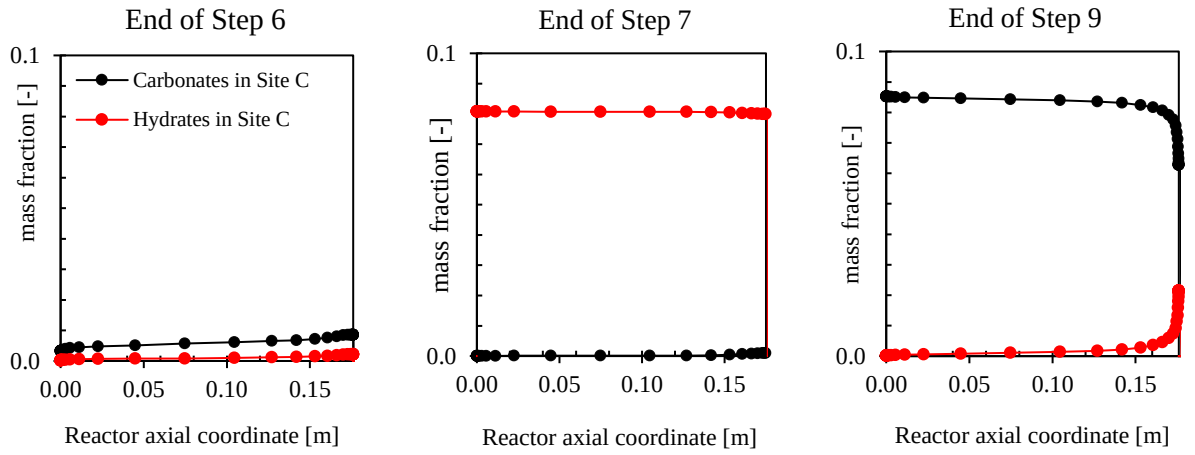

Figure 3.29 *Simulated mass fraction axial profiles for carbonates and hydrates adsorbed in Site C. The original kinetic model for Site C was used, while the optimized parameters for Sites A and B are employed. Left: situation at the end of Step 6. Middle: situation at the end of Step 7. Right: situation at the end of Step 9.*

The underestimated capacity of CO_2 adsorption in Site C in the absence of steam and hydrates (calculated according to Equation 3.19 as $k_{C1}p_{CO_2}\rho_s$) was improved carrying out a sensitivity analysis on the parameter k_{C1} (from Table 2.2). It was decided to assess the best value for the parameters by comparing the experimental amount of CO_2 desorbed in Step 7 with the simulated one, for the different cases of the sensitivity. It was found that a value of the parameter equal to 2.62 instead of 0.156 [mol kg^{-1} bar^{-1}] leads to a better approximation of the actual release of CO_2 from Site C during Step 7. Actually, using the trapeze integration method on the experimental and simulated breakthrough curves, it was determined that during the experiments 124.7 NmL of CO_2 are released in step 7, while simulations with the new value estimate a release of 86.2 NmL of CO_2 (relative error of 30%). The improvement is considerable, because with the initial value of the parameter k_{C1} the release was only of 23.7 NmL of CO_2 (relative error of more than 80%). The model-experiments mismatch could have been reduced by increasing k_{C1} even more, however even with the proposed change the accuracy was decreased in the fitting of the already optimized Steps 1-6. The new emerged problem was solved increasing the Site C adsorption kinetic constant parameter $k_{C,ads}$ of Equation 2.17 from 0.1 to 1 s^{-1}. If the value of k_{C1} was increased more, the accuracy in Steps 1-6 could not be recovered increasing $k_{C,ads}$ anymore. In order to avoid introducing other changes that could reduce the accuracy of the simulations of Steps 1-6, it was decided to accept an error of 30% in Step 7 released CO_2 amount, since the fitting of this step is less important compared to the other ones. As a matter of fact, the error of Step 7 occurs only once (the first time that steam is fed to the reactor) and is not related to the cyclic working capacity (the

most important variable to be optimized), while Steps 1-6 are related to the cyclic working capacity in dry conditions.

On the other hand, improving the accuracy of the simulated capacity of Site C for hydrates is very important, because it is a fundamental parameter for calculating the cyclic working capacity obtained using steam for regeneration. According to Equation 2.19, the capacity for steam adsorption is $k_{C2}p_{H_2O}^{n_C}\rho_s$. A sensitivity analysis on k_{C2} was performed. As expected, it was observed that k_{C2} has no effect on the breakthrough curve of CO_2 in steps 1-6: this parameter affects only the adsorption capacity of steam in Site C, but no steam is fed to the reactor during these cycles. The chosen criteria for deciding which value of k_{C2} to adopt is the minimization of the error between the simulated and experimental amount of CO_2 released from Site C during Step 11, calculated with the trapeze method from the outlet molar fraction profiles of CO_2. Selected results of the sensitivity analysis are reported in Table 3.6, compared with the amount of released CO_2 calculated from the experimental data (126.3 NmL). The final selected value of the parameter is k_{C2} = 0.518 [mol kg^{-1} bar$^{-0.591}$], that leads to an underestimation of the cyclic working capacity of CO_2 in Site C of only 0.55% compared to the experimental results.

The outlet molar fractions of CO_2 obtained with the final simulation using the new values of the parameters for Site C is reported in Figure 3.30. The optimized values for the parameters of Site A and B are used as well. It is possible to notice that, with respect to the results previous to the optimization of Site C model, also reported in Figure 3.30, the prediction of the amount of CO_2 released during the regeneration of the exchange site is much more accurate, without any loss of precision in the description of the reactions of Sites A and B (Steps 1-6, from 0 to 10800 seconds). In particular, the error on the cyclic working capacity of Site C is only 0.55%. The final model will therefore be useful for simulating the behaviour of packed bed reactors in the proximity of 400°C.

Table 3.6 *Selected results of the sensitivity analysis on k_{C2}, the parameter directly proportional to the adsorption capacity of steam in Site C*

k_{C2}[mol kg^{-1} bar$^{-0.591}$]	CO_2 released in Step 11 [NmL]	Relative error with experimental value [%]
0.311	68.6	-45.68
0.346	82.5	-34.68
0.415	104.6	-17.18
0.449	108.2	-14.33
0.484	111.2	-11.96
0.518	125.6	-0.55
0.553	135.5	7.28
0.691	168.5	33.41

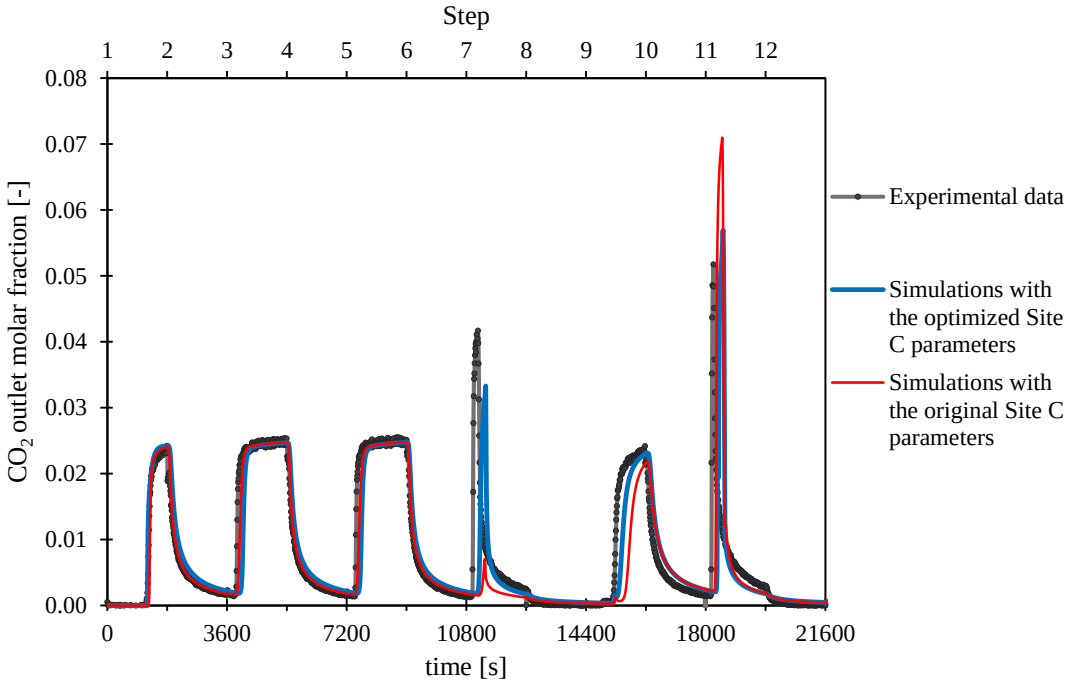

Figure 3.30 *CO_2 reactor outlet molar fractions profiles: Dataset 1 Steps 1-12 are compared with the results of the simulation carried out using the final optimized model for all the sorption sites. Also the results of the simulations with the original values of the parameters for Site C are reported*

Considering the changes introduced in Site C capacity, adjustments had to be done in the initial composition of the solid after the pretreatment to match the first breakthrough curve. In particular, it was found out that 18.6%w is composed by carbonates in Site B, 38%w by hydrates in Site A, the remaining 56.6%w being unoccupied sites (distributed approximately as 15% Site A, 15-20% Site B and 15-20% Site C).

Chapter 4

DAC with KMG30: analysis and optimization

The sorption model presented and optimized in Chapter 3 will be used in this chapter for analyzing and assessing the optimal conditions for the DAC process. The possibility to use a TSA approach will be evaluated, exploiting the results of experiments at low temperature.

4.1 Preliminary considerations

First, the range of operative conditions in which the model of Chapter 3 is valid will be analyzed. As far as pressure is concerned, special attention was given in Chapter 3 at validating the model for low p_{CO_2}. The available experimental data for validation had p_{CO_2} in the outlet of the reactor that ranged from 0.0015 to 0.025 bar. These data allowed to obtain the optimal values of the parameters of the Freundlich Equation for the equilibrium concentration of carbonates in Site B (Equation 2.12, Figure 3.19). This is the equation of the model which is most affected by p_{CO_2}: direct sorption reaction of CO_2 in Site C (Equation 2.16) is negligible for DAC. Extrapolating the equilibrium concentration at 400 ppm of CO_2 seems fair, because the adsorption isotherm is only one for a given temperature, and the one obtained at 400°C proved to be effective in a wide range of pressures. In addition, even if experimental concentrations inside the rectors are not available, as clearly shown by simulations, the CO_2 concentration inside the reactor is even lower than 400 ppm during some phases of the process. For example, in the first parts of the bed during the desorption step (Figure 4.1) CO_2 concentrations can be very low, despite in the outlet they are higher. Even during the adsorption step, CO_2 concentrations are low in the advancing adsorption front (Figure 4.1). Hence, Equation 2.12 can be considered validated even at 400 ppm: the calculated carbonate concentration in Site B at the equilibrium is 0.464 mol/kg (against 0.535 mol/kg for p_{CO2} = 0.025 bar). As far as the steam pressure is concerned, more problems arise, this time for high pressures. In both the datasets used for validation, the maximum steam pressure fed to the reactor is 0.10 bar. In the experiments used for the kinetic model regression, steam pressures up to 0.34 bar were used.

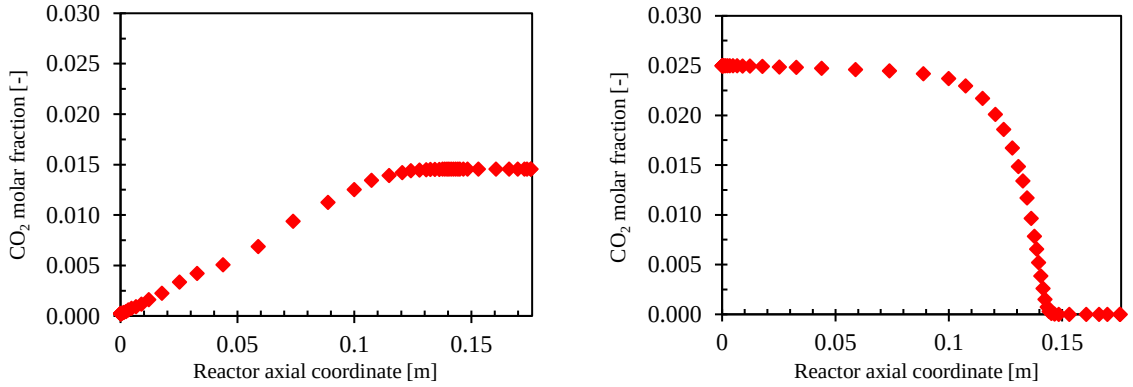

Figure 4.1 *Simulated CO_2 axial profiles inside the bed for t =2000 s (left, desorption step) and t = 1000 s (right, adsorption step) in the conditions of Dataset 1. In different points the concentration of CO_2 is of some ppm*

However, pure steam (at normal pressure) is expected to be used for DAC: if N_2 were present in the regeneration feed, it would be necessary to separate the captured CO_2 from N_2 to obtain the desired product of the process. On the other hand, steam can be simply separated from CO_2 by condensation. Even if the captured CO_2 was meant to be used in a process in which the presence of N_2 was not a problem, regeneration with steam is more convenient since it increases very much the adsorption capacity of hydrotalcites, as discussed in Chapter 3. The sorption capacity of Site A and Site C must therefore be evaluated by extrapolation, using the due precautions, respectively from Equations 2.16 and 2.19. It is necessary to keep in mind that the equations represent the equilibrium isotherms at 400°C and, even if they are based on experimental data up to p_{H_2O} = 0.33 bar, the isotherms should be the same for all the pressures, fixed the temperature. Different values of adsorption capacity for H_2O will be considered when calculating the wet Cyclic Working Capacity (CWC), to see how the performance would change if Equations 2.16 and 2.19 were not much accurate for p_{H_2O} = 1 bar. In any case, no advantage would be obtained in operating the process at higher pressure: the increase of sorption capacity would be negligible, while the cost for compressing a large amount of air would be too much consistent.

Focusing on the optimal temperature conditions for the process, it is important to remember that the model was obtained from data collected in the temperature range 300-500°C (Coenen *et al.*, 2018d), while the validation was performed at 400°C. Hence, its validity cannot be assumed in wider ranges of temperatures and sensitivity analysis cannot be performed at low temperatures prior to the eventual introduction of some changes.

The model is, however, very useful to simulate the desorption step, the one which affects mostly the CWC: the activation energies for the desorption reactions are present in the model, so the kinetic constants for the desorption reactions can be evaluated properly even for temperatures above 250°C. The regeneration of chemisorbed CO_2 does not actually occur below 250-300°C, where

kinetics are too slow. As far as finding the optimal temperature conditions for DAC is concerned, the following approach will be followed:

- In a first moment, the isothermal process at 400°C will be analyzed through the model. Though it is not probably convenient to heat the reactor during the adsorption step, with this study it will be possible to understand better the physical dynamics of the process, since the model is perfectly validated for this situation. Regeneration with both N_2 and steam will be analyzed, to understand better the contribution of the different sorption sites to the CWC;
- The possibility to exploit a TSA approach will be considered. Experimental results will be used to evaluate the adsorption capacity for CO_2 at room temperature and to attempt to extend the validity of the kinetic model to these conditions. Process simulation will then be performed to evaluate the CWC of DAC in TSA conditions.

4.2 Isothermal high temperature process: analysis and CWC

In this paragraph, the isothermal, high temperature DAC process based on KMG30 will be studied exploiting the sorption model presented and optimized in Chapter 3. A temperature of 400°C has been chosen since the sorption capacity for Site B is higher at 400°C than at 300°C and at 500°C. The reactor can be kept at 400°C during both the adsorption and the desorption steps by pre-heating the feed and heating the walls at that temperature. Before to proceed, it was verified with simulations that by this way it is possible to keep the temperature constant, even considering the enthalpies of the reactions. Simulations were carried out to assess the performance of DAC in this situation, with a reactor of the same characteristics as in Table 3.1. An inlet flowrate of 1000 NmL/min of air was used during adsorption step, while pure nitrogen at the same flowrate was exploited for the regeneration. Initially, the attention was focused on Site B in order to calculate the dry CWC. The initial concentration of carbonates was set to be 18.6%w, as found at the end of Chapter 3 for KMG30 after the pre-treatment. Three different simulations were performed, with the desorption step lasting respectively 1800 s (Case A), 3000 s (Case B) and 6000 s (Case C). In all the simulations, the first adsorption cycle lasted 30000 s, to fill the sites of regenerated materials. All the following adsorption cycles, instead, lasted 10000 s, which demonstrated to be enough to saturate the bed. Five adsorption/desorption cycles were carried out for each case of different desorption duration. The amount of CO_2 adsorbed in each adsorption step and released during the desorption steps were calculated based on the data obtained from the simulations and are reported in Table 4.1. The amounts of CO_2 released in the first six steps of Dataset 1 are reported as well, for comparison.

Table 4.1 *Amounts of CO_2, expressed in NmL_{CO2}, adsorbed or released from Site B in simulations with different regeneration duration (Case A: 1800 s, Case B: 3000s, Case C: 6000 s). The same data are reported for the first three steps of Dataset 1 (Paragraph 3.1)*

	ADS1	DES1	ADS2	DES2	ADS3	DES3	ADS4	DES4	ADS5	DES5
Case A	119.071	11.866	12.534	11.903	12.230	11.950	12.174	11.949	12.240	11.969
Case B	119.120	18.624	19.034	18.701	18.827	18.800	18.856	18.794	18.853	18.8
Case C	118.995	31.396	32.158	31.395	31.725	31.318	31.454	31.233	31.370	31.284
Dataset 1	151.897	78.888	75.403	80.441	75.426	84.258	X	X	X	X

In the first adsorption step the amount of adsorbed CO_2 is obviously the same for each of the three DAC simulations (about 120 NmL_{CO2}). In the first adsorption step of Dataset 1, a slightly higher amount of CO_2 was adsorbed (about 150 NmL_{CO2}), because the adsorption capacity was greater in those experiments due to the higher concentration of CO_2 in the inlet (2.5% against 0.04% in air). The CWC in cycles 2-5 is about the same for a fixed regeneration duration: in every adsorption step about the same amount of CO_2 that was released during the previous desorption step is adsorbed again. When the duration of the desorption step increases, the CWC increases as well. Actually, as already discussed, the slowest step in the process is the regeneration. The CWC was calculated converting the NmL of CO_2 in moles, and dividing the result by the total mass of sorbent in the reactor (0.0536 kg), to obtain the value in mol/kg. In Case A the calculated CWC is 0.0091 mol/kg, which is very low compared to the experiments of Dataset 1, in which the CWC was 0.0563 mol/kg and the regeneration duration was the same. The reason is that in DAC the regeneration occurs more slowly: the desorption rate (Equation 2.11) is directly proportional to the concentration of carbonates, and as a matter of fact, in DAC the equilibrium value of carbonates is slower than in the experiments of Dataset 1, due to the bigger dilution of CO_2. Longer regeneration times allowed to obtain better results: for Case B (regeneration 3000 s) the dry CWC is 0.0139 mol/kg, while for Case C (regeneration 6000 s) it is 0.0233 mol/kg.

To better understand what is actually happening during the process inside the air contactor, the phenomenological model was exploited to build the axial profiles of solid and gaseous species at selected moments. The analysis was carried out for Case C, for the same conditions described above. A final desorption step lasting 50000s was simulated, to assess the regeneration behavior in long times. The outlet molar fraction profile resulted from the simulation is reported in Figure 4.2. It is possible to notice that the profiles from the first desorption step to the fifth adsorption steps are exactly the same: a cyclic steady-state is achieved. In the last desorption step, about 72.3 NmL

of CO_2 are released. This value is close to the CWC of the experiments of Dataset 1, so for DAC in these conditions a regeneration of 50000 s would be needed to get about the same performance obtained with a feed of 2.5% CO_2.

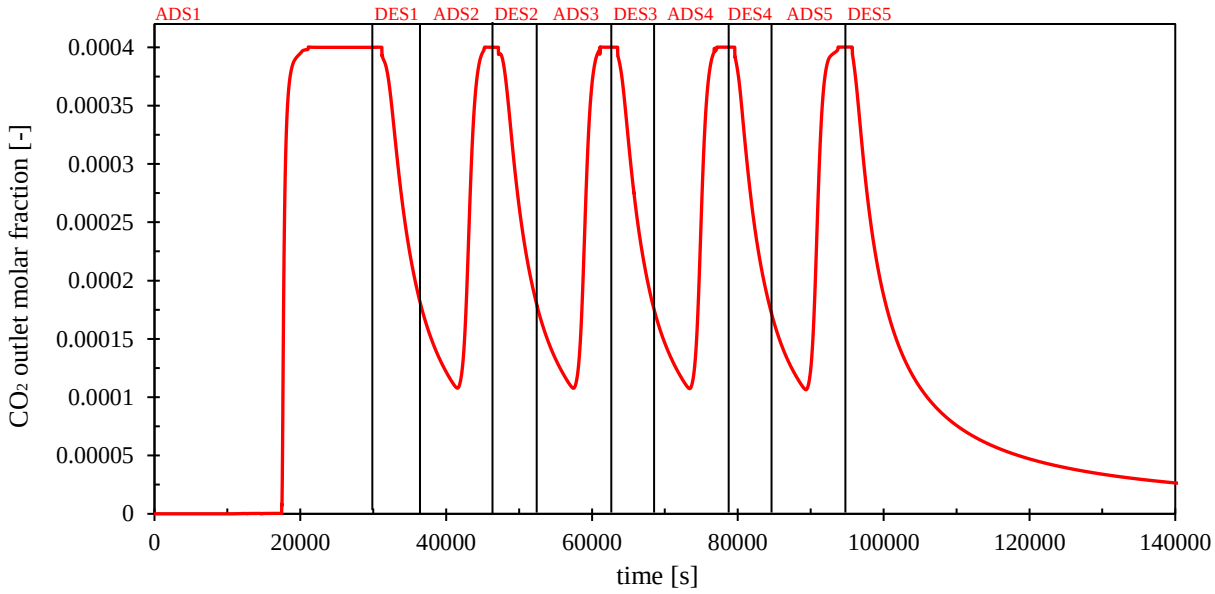

Figure 4.2 *Outlet molar fraction of CO_2 from a DAC simulation at 400°C*

The internal profiles of carbonates and of CO_2 for different times during the first adsorption step are reported in Figure 4.3. As the front of CO_2 enters the reactor, the mass fraction of carbonates increases, reaching the equilibrium value w_{carB}^{eq} = 0.2248 in the regions of the reactor where y_{CO_2} = 0.0004 and intermediate values between the initial mass fraction and the equilibrium value in the zone where CO_2 is penetrating. After about 20000 s, the concentration of CO_2 is 400 ppm everywhere and the equilibrium value of carbonates has been reached in all the reactor. The same situation is found at the end of all the other adsorption steps.

Adsorption and desorption reactions rates were calculated for selected moments, in order to understand better what happens inside the reactor during the steps of the process. In the middle of all the adsorption steps (excluded the first one), the axial profiles are as reported in Figure 4.4. The desorption rate is null in all the reactor, while the adsorption reaction has a maximum in the point of the bed where CO_2 is advancing: the adsorption rate peak moves with CO_2 while it proceeds in further regions of the reactor. In any case, the driving force for the adsorption reaction ($w_{carB}^{eq} - w_{carB}$) is quite low, both because the CO_2 concentration is low (and so w_{carB}^{eq} is low) and because the desorption reaction is slow. Hence, the adsorption reaction rate is always below 0.50 mol m^{-3} s^{-1}.

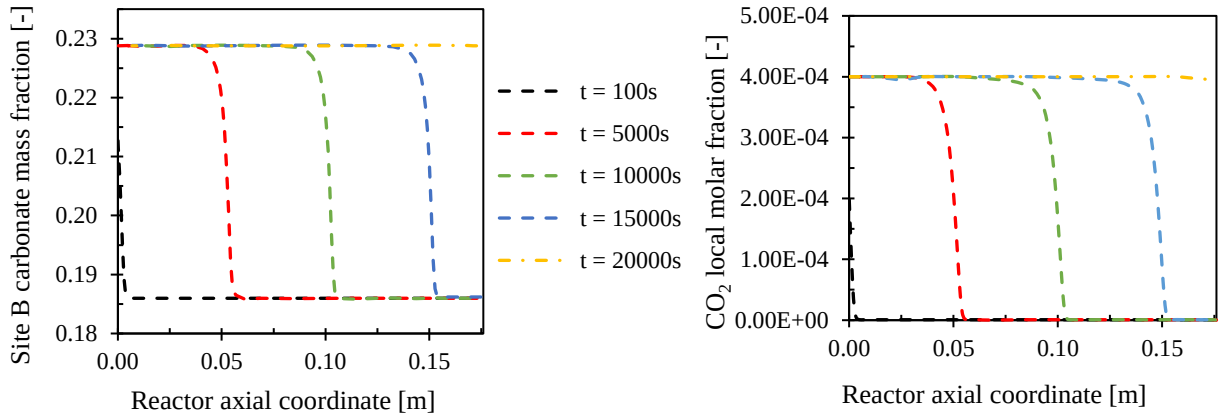

Figure 4.3 *Carbonates (left) and CO_2 (right) internal profiles during the first adsorption step*

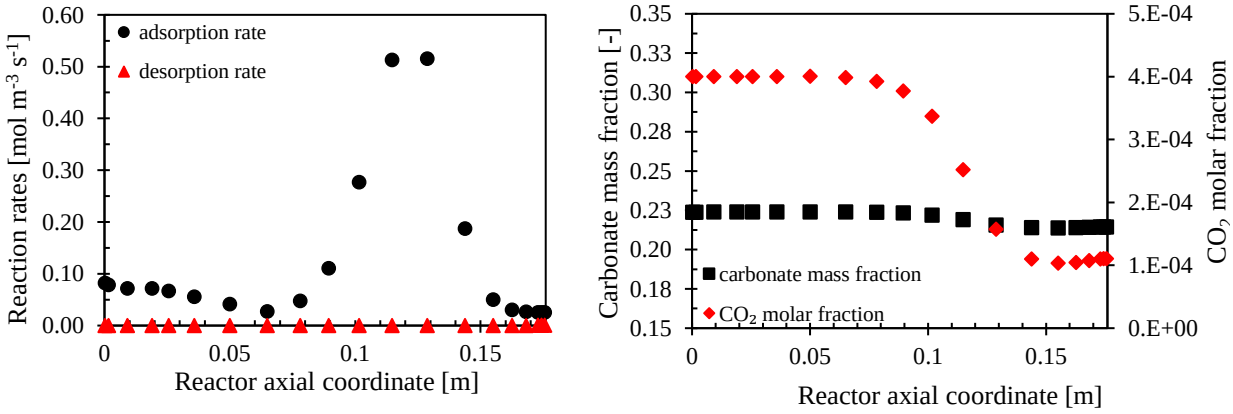

Figure 4.4 *Axial profiles of adsorption and desorption reaction rates (left) and of CO_2 and carbonate concentrations (right) in DAC simulation in the middle of the cyclic adsorption steps*

As far as the desorption step is concerned, interesting results can be obtained by analyzing the axial profiles within the bed. Reaction rates and CO_2 and carbonate concentrations axial profiles are reported in Figure 4.5 and Figure 4.6 for the bed respectively after 1000 s and 6000 s after the beginning of the regeneration steps. The carbonate equilibrium mass fraction is reported as well.
The first important result is that both after 1000 s and 6000 s from the beginning of the regeneration the adsorption rate is null in axial position. This means that none of the CO_2 released from the first part of the bed is adsorbed in the last part. The desorption rate during the regeneration is slower than the adsorption rate during the adsorption (the average rate during regeneration is 0.010 against 0.1 mol m^{-3} s^{-1} for the adsorption). As it is possible to see from Figure 4.5 and Figure 4.6, the desorption rate decreases with the passing of time, because it is proportional to the carbonate concentration, hence when CO_2 is released the rate is reduced.

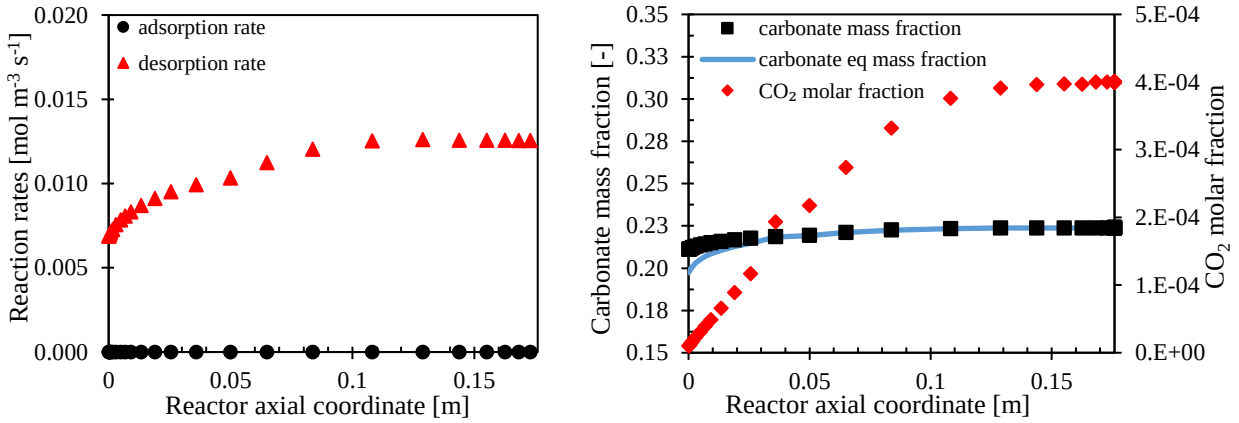

Figure 4.5 *Axial profiles of adsorption and desorption reaction rates (left) and of CO_2, carbonate and equilibrium carbonate concentrations (right) in DAC simulation after 1000 s from the beginning of a desorption step*

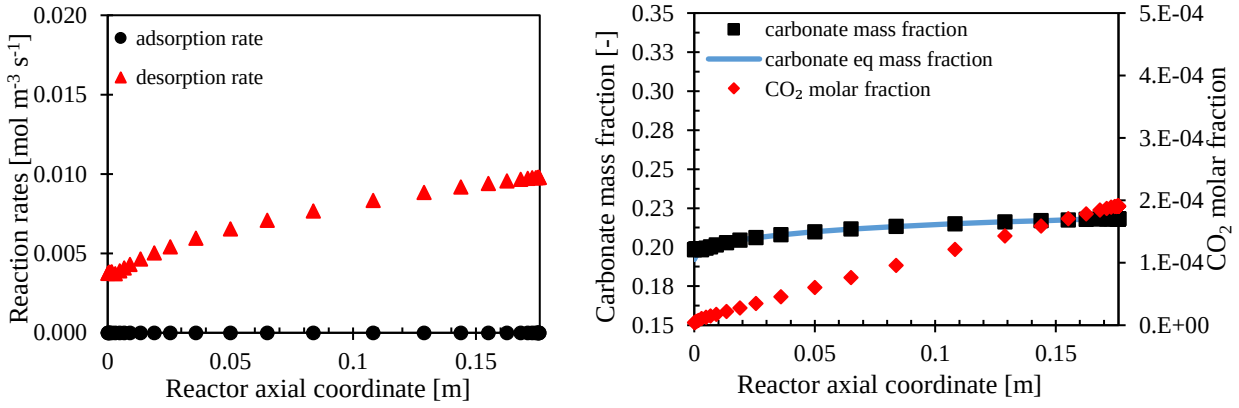

Figure 4.6 *Axial profiles of adsorption and desorption reaction rates (left) and of CO_2, carbonate and equilibrium carbonate concentrations (right) in DAC simulation after 6000 s from the beginning of a desorption step*

At both of the analyzed moments, it is possible to see that the desorption rate is lower at the beginning of the bed and it increases moving along the axial coordinate, reaching the maximum at the end. However, the same figures also show that the lowest concentration of carbonates at the end of the regeneration is at the beginning of the bed, and that at the end of the air contactor the concentration of carbonates reaches the highest value. The explanation of this apparent contradiction is that the Langeren model used to describe the reactions (Equation 2.11) allows desorption to occur only when the carbonate mass fraction is lower than the equilibrium value (calculated with Equation 2.12). Hence, despite the desorption rate are greater than zero, the carbonate concentration cannot locally go below the equilibrium value, represented in Figure 4.5 and Figure 4.6 by the blue line. For these reasons, a homogeneous regeneration cannot be obtained: the regeneration proceeds faster at the beginning of the bed, where there is little CO_2, and the equilibrium concentration is inferior. After 1000 s, in one third of the bed the concentration of CO_2

is 400 ppm, as in the adsorption step, so the regeneration cannot occur there. As the process goes on, less CO_2 is released from the first part of the contactor and the regeneration of additional parts of the bed can begin. After 6000 s, the mass fraction of carbonate at the inlet is 0.20, but at the outlet it is 0.218, much closer to the equilibrium value at 400 ppm of CO_2 (0.2248).

So far, only the dry CWC has been considered. However, since as already discussed the regeneration should be fulfilled with steam, some considerations have to be made about the wet CWC. First, axial profiles during wet regeneration have been analyzed, to better understand what happens inside the reactor. In Figure 4.7 axial profiles of molar fraction of CO_2 and of mass fraction of carbonates in Site B and Site C are reported for a regeneration step performed with steam. The profiles refer to the simulation of Step 11 of Dataset 1 (outlet profiles are reported in Figure 3.30). In particular, the profiles are reported for the initial moment (t = 18000 s) and for 100 s after the beginning of the regeneration (t = 18100 s). At the beginning, about 5%w of the solid in all the points of the bed is composed by carbonate in Site C. After 100 s, all the CO_2 in Site C has been released (except in the very last part). On the other hand, the mass fraction of carbonates in Site B has increased: the CO_2 desorbed from Site C when steam arrives in a certain point of the reactor is quickly adsorbed in Site B in the following regions. Hence, there is a peak of CO_2 which moves with the advancing front of steam in the air contactor. When steam arrives at the end of the bed, the CO_2 peak exits the reactor. The peak of CO_2 reported in Figure 4.7 for t = 18100 s actually corresponds to the peak in Step 11 in Figure 3.30. After that moment, desorption occurs only in Site B, where it is much slower, so the outlet CO_2 concentration starts to decrease.

The adsorption capacity of Site C will be now discussed. According to Equation 2.19, the capacity of Site C with a feed of pure steam at 400°C is 0.518 mol/kg, corresponding to about 23.6%w. This means that after a regeneration made with pure steam, 0.518 moles of CO_2 could be adsorbed in a kilo of sorbent in the following adsorption cycle. Hence, the wet CWC would be extremely higher than the dry one, that was only about 0.02 mol/kg with a 6000 s desorption step. Even if the extrapolation of the capacity of Site C with pure steam was not accepted, keeping the capacity value for p_{H2O} = 0.10 bar in nitrogen (inside the validated range), the capacity of Site C is equal to 0.1328 mol/kg, which is a significant contribution, compared to Site B. In any case, Coenen *et al.* (2018d) experimentally found that at 400°C, total pressure 1 bar and feeds composed only by steam and CO_2, the capacity of Site C reaches values above 0.400 mol/kg. No experiments are available with pure steam, however from the results of this work it seems that Site C is the main contributor to the CWC for DAC at 400°C, when pure steam is used for regeneration. Actually, at these low concentrations of CO_2 the adsorption in Site B is performing in a worst fashion than for more CO_2-concentrated streams. Exploiting pure steam to activate Site C and then substituting the hydrates

with carbonates appears to be the most promising strategy. An experimental validation should anyway be performed to confirm the high capacity of Site C when pure steam is fed.

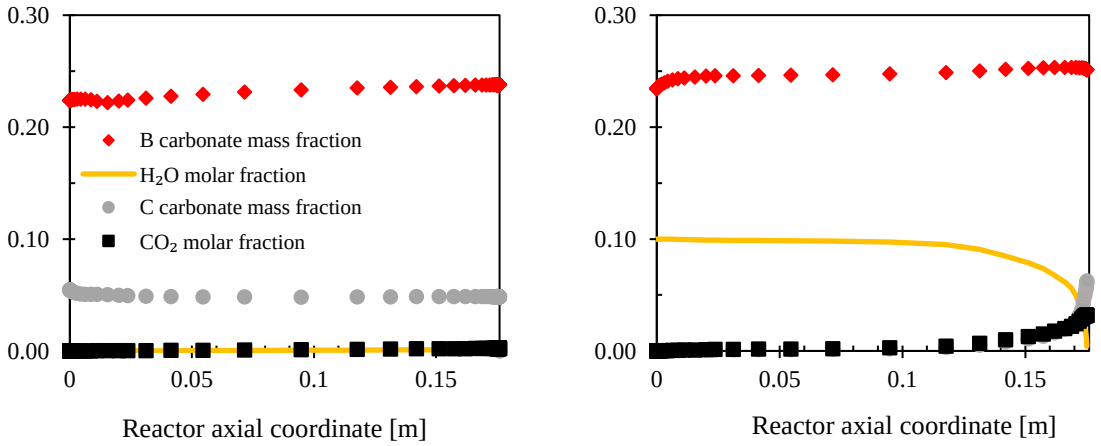

Figure 4.7 *Axial profiles of CO_2 molar fraction and of the mass fractions of carbonates in Site B and Site C during two moments of a regeneration step performed with steam. The axial profiles refer to the simulation of Dataset 1, Step 11 (outlet profiles are in Figure 3.30). Left: t = 18000 s. Right: t = 18100 s.*

4.3 DAC through a TSA process

4.3.1 Experimental results for DAC at low temperature

Breakthrough experiments were carried out at room temperature in order to collect data for extending the kinetic model presented in Chapter 3 to low temperature conditions. The results of the experimental procedure described in Paragraph §2.4 are further presented.

The KMG30 pellets (a picture of the cylindric pellets is reported in Figure 4.8) were analyzed after the promotion with K_2CO_3 through XRD techniques. The resulting spectra are reported in Figure 4.9. It is possible to notice that both the promoted and unpromoted samples present peaks for $2\gamma \approx 35°$, 45° and 60°, but the peak at 35° is higher in the promoted hydrotalcite. According to literature (Jang *et al.*, 2014, Walspurger *et al.*, 2008, Lee *et al.*, 2010) and to the XRD analysis on the KMG30 used in previous works on the kinetic model (Coenen *et al.*, 2016), the main K_2CO_3 peaks are actually for 2γ between 25° and 35°. The spectrum of KMG30 presents a peak at 25°, too, as expected. Hence, it was concluded that the promotion procedure had been completed successfully. The particles were then grinded. After the crushing, the mean particle diameter was verified to be one order of magnitude smaller than the reactor one. Hence, the bed was filled with the sorbent and breakthrough experiments were performed. The amount of sorbent particles put in the reactor is 2.5 grams.

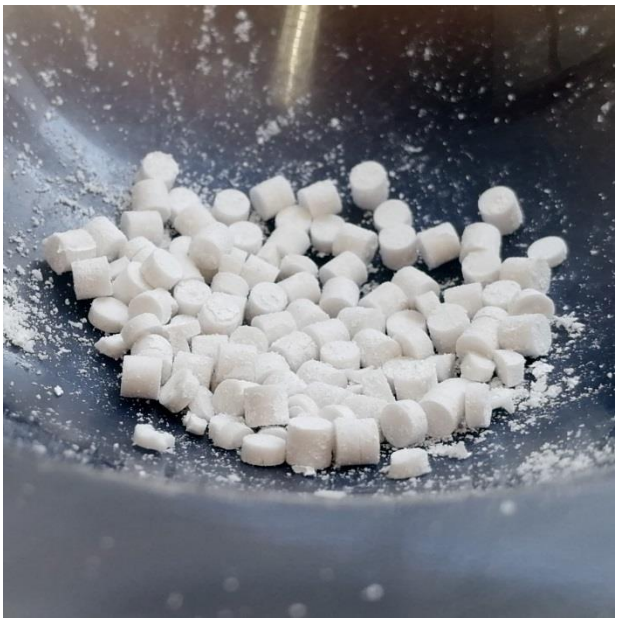

Figure 4.8 *Picture of KMG30 cylindric pellets prior of the crushing*

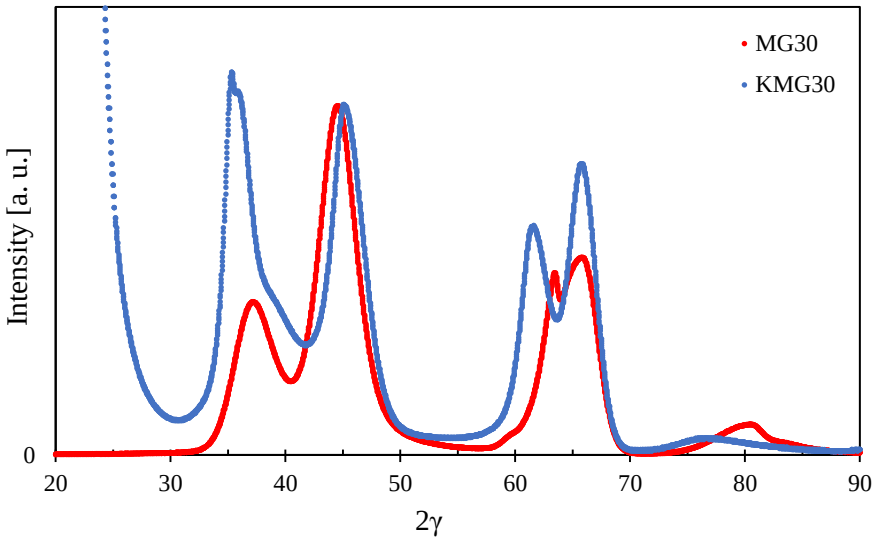

Figure 4.9 *XRD spectra for MG30 pellets before and after impregnation with K_2CO_3*

It was decided to execute a first breakthrough experiment at 25°C, to evaluate the adsorption capacity of KMG30 at room temperature and to try to fit the experimental data with the model by conveniently adjusting the main parameters. The characteristics of the experimental setup are described in Paragraph §2.4. After a pre-treatment of 4h at 600°C with N_2, a feed of 1 Nl/min of air was sent to the reactor, until the outlet concentration stabilized to 400 ppm, proving that the bed had been saturated. The measured CO_2 outlet concentrations are reported in Figure 4.10. Contrary

to the breakthrough experiments of Dataset 1, some CO_2 escapes from the reactor just a few minutes after that the experiment has started. At the beginning, only a few ppm are measured, and with the passing of time the concentration increases. After about 13 h, the outlet concentration reaches 400 ppm, which is the concentration of CO_2 in air, hence the bed is completely filled. The fact that some CO_2 exits from the reactor a few minutes from the beginning of the process means that there is not enough sorbent to capture all the CO_2 fed to the air contactor. As a matter of fact, the reactor is quite small (diameter = 7 mm, length = 11 cm), so this phenomenon is normal, also considering that some mass transfer limitations may play a role in reducing the adsorption rate and letting some CO_2 escape. The collected data are however useful to determine the adsorption capacity at 25°C. The trapeze method showed that 1.698 moles of CO_2 were adsorbed per kg of sorbent upon saturation of the bed. Since no steam had ever been fed to the material, Site C was not activated and only Site B was responsible for the chemisorption. As expected, physisorption contribution to the total adsorbed CO_2 is significant. Actually, if all the CO_2 had been chemically sorbed forming carbonates, 1.698 moles of carbonates would have been formed per kg of sorbent. This value, once transformed through the molecular weight in mass fraction, would lead to $w_{carB} = 0.818$, which is impossible, because it means that almost no hydrates could be formed and that almost no species could be adsorbed in Site C. Chapter 3 analysis showed that at 400°C about 50-55%%w of the sorbent is composed by Site A, 25-30%w by Site B and 15-20%w by Site C. The capacity may change with temperature, but in any case a maximum value of 40%w Site B can be assumed even at 25°C. Hence, a big amount of the adsorbed 1.698 mol/kg must be due to physisorption. To understand how much CO_2 is physisorbed, it is necessary to perform experiments at higher temperature, where the contribution of physisorption is smaller. According to the studies of Moreira et al. (2006) on hydrotalcites, physisorption occurs for temperatures below 150°C (Figure 1.9). Hence, at 100°C the phenomenon is present, but much less than at 25°C. On the other hand, the chemisorption capacity at 100°C is probably very close to the one at 25°C. At 200°C no physisorption occurs, while chemisorption capacity should be slightly inferior than at 100°C. Therefore, it was decided to exploit data on the adsorption capacity at 100°C and at 200°C to assess the contribution of physisorption to the total capacity at room temperature. For this purpose, breakthrough experiments could have been performed with the setup described in Paragraph §2.4, however it was decided to use information from available TGA experiments with KMG30. By this way, it is possible to get more reliable data, because TGA experiments are neither limited by mass transfer nor vulnerable to other problems which could alter the data collected with a PBR (bypassing phenomena, inhomogeneous distribution of sorbent particles, …). Breakthrough curves would have represented an advantage with respect to TGA to try to extend and validate the model developed for high temperatures to low temperatures. A powerful tool would have been obtained

for simulating actual DAC processes in a reactor, however, the analysis of the experiment reported in Figure 4.10 showed that this is not possible: the model is not capable of accounting for a so significant contribution of physisorption. Breakthrough curves at low temperature cannot be fitted by the model, unless physisorption was modelled, but this lies outside the objectives of this work. Determining the contribution of physisorption and chemisorption to the total amount of captured CO_2 makes possible to at least calculate the CWC in different conditions, and as discussed above TGA is the preferred method to obtain reliable data on the capacities.

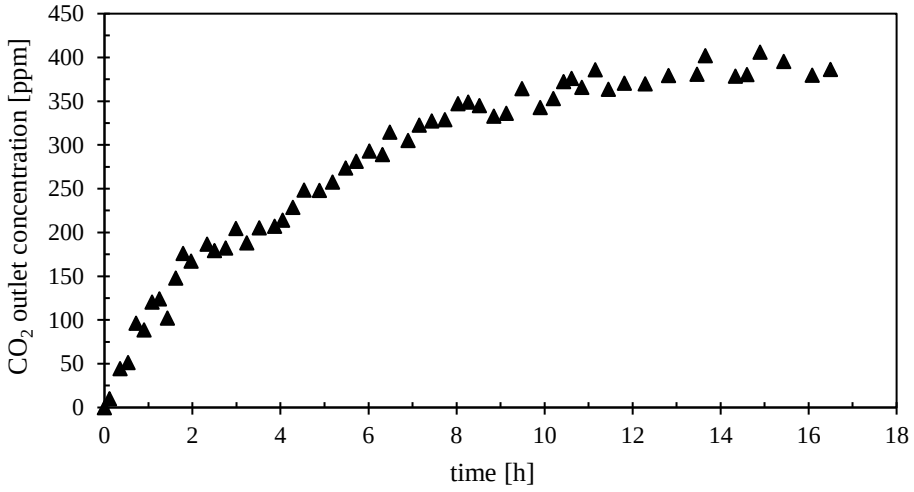

Figure 4.10 *Outlet CO_2 concentration of the executed breakthrough profile*

In a TGA experiment a certain amount of sorbent is placed on a balance, and desired gas streams are sent towards the sample. The changes of weight of the initial sorbent mass are then measured, and from the increase of mass it is possible to understand how much gas species have been sorbed. The results of the experiment are reported in Figure 4.11, which shows the changes in the mass of the sorbent while it undergoes treatments with different feeds (summarized in Table 4.2). As it is possible to see from Figure 4.11, the initial amount of sorbent is 48.9 mg. The most important steps for calculating the capacities at 25°C, 100°C and 200°C are respectively Step 8, 9 and 4. Elaborating the data relative to Step 8, the adsorption capacity of KMG30 in DAC conditions at 25°C is 2.80 mol/kg. This result is higher than the one obtained with the breakthrough experiment (1.988 mol/kg), probably because, as already discussed, the breakthrough experiment was limited by mass transfer. At 100°C and at 200°C, desorption of chemisorbed CO_2 is negligible, because the reaction is very slow. Hence, the CO_2 released during Steps 9 and 4 was the physisorbed one and the value reached at the end of Step 4 corresponds to the CO_2 which was chemisorbed during Step 2. At the end of Step 9 (regeneration at 100°C), 1.391 moles of CO_2 were adsorbed per kg of sorbent. At this temperature, a big percentage of the physisorbed CO_2 was desorbed, though not all

of it, and results at 200°C are more reliable to account for the actual amount of physisorbed CO_2. A plateau is reached at the end of Step 4 (regeneration at 200°C), and from the change of mass with respect to the initial weight of the sample it is possible to calculate an adsorbed CO_2 concentration of 0.783 mol/kg. Above 150°C, at the equilibrium, no physisorbed CO_2 is present, so all of this adsorbed CO_2 is chemically bonded to the sorbent. The corresponding mass fraction is w_{carB} = 0.378. Even assuming that some chemical desorption had occurred at 200°C, the maximum equilibrium value for the conditions of Step 2 is w_{carB} = 0.40. The feed of Step 2 contained 2% CO_2, so a higher concentration that in DAC conditions. However, as seen in Paragraph §5.1 and using Equation 2.12, switching from 2% CO_2 to 400 ppm leads to a loss of chemisorbed equilibrium mass fraction of maximum 0.05.

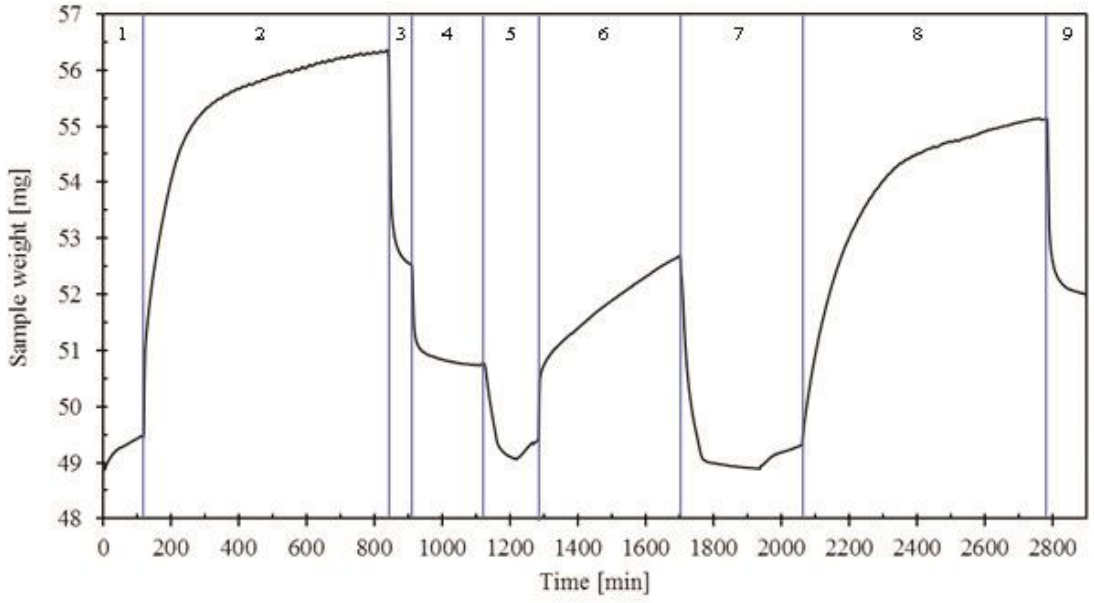

Figure 4.11 *TGA experiment on KMG30. The trend of the sample weight against time is reported for nine steps, whose feed conditions are as in Table 4.2. The sample was previously pre-treated in N_2 at 600°C for 4 h*

As a result, it is possible to conclude that at 25°C in DAC conditions the equilibrium value of the chemisorbed CO_2 is between 0.72 and 0.83 mol/kg, corresponding to a mass fraction of sorbent between 0.35 and 0.40. On the other hand, the physisorbed CO_2 at 25°C should be about 2 mol/kg, subtracting the chemisorbed CO_2 from the total capacity obtained from the TGA experiment.
As seen comparing the results of the TGA and of the breakthrough experiment at 25°C, in an actual reactor the sorption capacity may be smaller, especially if the air contactor is not perfectly designed to avoid mass transfer limitations and other problems which may reduce the efficiency. In any case, the proportion between chemisorbed and physisorbed CO_2 should be the same. Another possible reason for the higher capacity measured in the TGA experiments could be the adsorption of O_2 or

N_2 in the sorbent, which was never found to occur in literature, but additional experiments should be carried out to confirm these results. In any case, both the breakthrough and the TGA experiments showed that the contribution of physisorption is much greater than the one of the chemisorption for DAC in KMG30 at 25°C.

Table 4.2 *Conditions for the nine steps of the TGA experiment*

Step	Conditions
1	Cooling at 25°C with N_2
2	Adsorption at 25°C with 470 Nml/min air + 10 ml/min CO_2
3	Desorption at 100°C with N_2
4	Desorption at 200°C with N_2
5	Regeneration at 600 °C with N_2 and cooling at 25°C
6	Adsorption at 25°C with 470 Nml/min N_2 + 10 Nml/min CO_2
7	Regeneration at 600 °C with N_2 and cooling at 25°C
8	Adsorption at 25°C with 480 Nml/min air
9	Desorption at 100°C with N_2

4.3.2 TSA process: analysis and CWC

Based on the results of the previous paragraphs and chapters, the dry and wet CWC for DAC with a TSA process will be further estimated.

It was decided to operate with a reactor as in Table 3.1, the same used for the experiments of Dataset 1 and for calculating the CWC for the isothermal process (Paragraph §5.2), in order to compare the results. In Paragraph §4.3.1 it was demonstrated that after an adsorption cycle at 25°C with air as feed, chemisorbed CO_2 in Site B is between 35%w and 40%w of the sorbent particles. Simulations were carried out using the model developed in Chapter 3 to assess the performance of the regeneration of the chemisorbed CO_2 with a steam feed of 1 Nl/min. This way, the CWC for Site B can be estimated. The simulations were performed for three different values of initial mass fraction of carbonate in Site B (30%w, 35%w and 40%w): since the precise value is not known, it was decided to understand the effect of this uncertainty. As far as temperature is concerned, all the bed was at 25°C in the initial moment of the simulations. All the energy necessary to heat up the reactor to the regeneration temperature was provided by the steam feed, set to a temperature of 400°C. The reactor was considered adiabatic and the enthalpy of the CO_2 desorption reaction (Equation 2.10) was included in the computation. Simulations showed that a few minutes were needed to reach a homogeneous temperature of 400°C in all the reactor. When increasing w_{carB}^0, more time is needed to heat the reactor, because the endothermic reaction consumes more heat.

However, even with w^0_{carB} = 0.40 only five minutes are needed to reach 400°C in all the air contactor, which is a small amount of time compared to the duration of the regeneration step. In the first moments of the process, desorption occurs only at the inlet of the reactor, which is heated almost immediately. Then, the reaction proceeds also in further regions of the bed, as soon as the temperature goes above 250°C. The results of the simulations are reported in Figure 4.12. For all the three initial mass fractions of carbonates in Site B, most of the regeneration occurs in the first 1000-1500 s, and then the reaction proceeds more slowly. The bigger the initial concentration, the faster the desorption. Infinite time would be needed to completely regenerate the sites, and after 15000 s, which is quite a long time, about 0.33 mol/kg are regenerated if w^0_{carB} = 0.40, while **Figure 4.10**only 0.25 mol/kg are desorbed if w^0_{carB} = 0.35. From the considerations of Paragraph §4.3.1, w^0_{carB} should be close to 0.40. Hence, the CWC for Site B can be assumed with good approximation to be between 0.27 and 0.30 mol/kg with a regeneration of 6000 s. This value is significantly higher than the one obtained for the CWC of Site B working with the isothermal process at 400°C for a regeneration of the same duration (about 0.02 mol/kg, Paragraph §4.2).

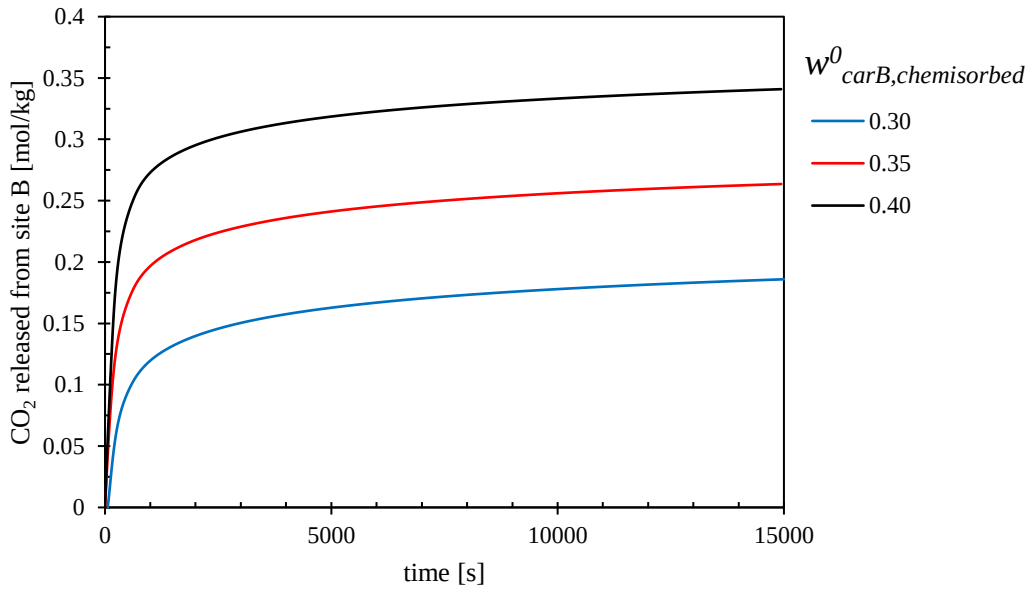

Figure 4.12 *CO_2 released upon regeneration of Site B with steam at 400°C, expressed in moles per kg of sorbent. Data were obtained with simulations for different initial values of carbonates (30%w, 35%w, 40%w)*

Site C CWC can be estimated with less accuracy, because no data at room temperature are available, and the problem introduced in the previous paragraphs about the accuracy of the estimation of the capacity of Site C for p_{H2O} = 1 bar is still present. In Paragraph §4.2 it was concluded that the adsorption capacity of H_2O in Site C at 400°C is at least 0.13 mol/kg, but more probably at least 0.30-0.35 mol/kg, with some estimations above 0.40 mol/kg. This means that after

a regeneration cycle, this amount of hydrates would be present in Site C. If the exchange reaction between carbonates and hydrates (Equation 2.20) occurred also at room temperature, an additional contribution to the CWC for the TSA process should be accounted for. According to the kinetic model developed by Coenen et al. (2018d; §2.1), the reaction of substitution of hydrates with carbonates proceeds faster at lower temperatures than at high temperatures, at least in the validated range (between 300°C and 500°C). A negative activation energy is actually proposed in literature for this reaction. Experiments should be carried out to verify that the exchange reaction actually occurs also at room temperature, but Site C should probably bring an additional contribution to the CWC, of at least 0.10 mol/kg up to 0.50 mol/kg.

On the other hand, the CWC due to physisorption seems to be much greater. In Paragraph §4.3.1 it was assessed that 2 moles of CO_2 are physisorbed per kg of sorbent at room temperature after the pre-treatment. This value was calculated in a conservative way, assuming that some chemical desorption occurred at 100°C and 200°C, though previous studies and considerations showed that this should not happen. Most of the physisorbed CO_2 can be quickly desorbed upon thermal treatment at 150-200°C: in Steps 9 and 4 in Figure 4.11, as soon as the temperature is increased, a lot of CO_2 is desorbed, while another smaller amount is desorbed keeping the sorbent in temperature. From the data reported in Figure 4.11, upon regeneration of 10000 s at 200°C, a CWC due to physisorption of about 2 mol/kg is reached, which corresponds to the previously estimated physisorption capacity. However, a high CWC due to physisorption could be obtained even with a shorter thermal treatment: summing up the CO_2 instantaneously released after that the temperature is increased at 100°C and after the increase of temperature at 200°C, the result is that 1.50 moles of CO_2 are almost instantaneously desorbed per kg of sorbent when it is heated up to 200°C. Even if these capacities were slightly overestimated for errors in the TGA experiments, they are much greater than the maximum CWC for chemisorption, which as previously demonstrated should not exceed 0.85 mol/kg. In addition, it is probable that even at 200°C Site C exchange reactions occur, though at reduced adsorption capacity, bringing an additional contribution to the CWC obtained operating the regeneration at 200°C.

4.4 Major findings

The main results of the process analysis and optimization are further summarized:

1. The breakthrough and the TGA experiments led to obtain different values for the CO_2 adsorption capacity of KMG30 at room temperature, respectively 1.70 and 2.80 mol/kg. Probably, mass transfer and channeling phenomena decreased the sorption capacity in the

breakthrough experiment. Anyway, this result is important, because it accounts for what happens in an actual reactor. Experiments could be repeated in a reactor with optimized design, to assess if the new measured capacity is closer to the one measured with the TGA. On the other hand, the TGA experiments could slightly overestimate the capacity, since the increase of weight of the sorbent attributed to CO_2 sorption may be partially due to physisorption of N_2 or O_2. Though no reference to this phenomenon was found in literature, it cannot be excluded *a priori* and additional experiments should be carried out to verify this possibility;

2. The measured adsorption capacities of KMG30 at room temperature are in both experiments too high to be due only to chemisorption: a significant amount of CO_2 must be physisorbed. Hence, the model developed in Chapter 3 cannot describe DAC in KMG30 at low temperature, unless some new features are implemented. As a matter of fact, modelling physisorption would be the only way to accurately describe the DAC process in TSA. A black box model could be exploited, since a phenomenological description of the physisorption reactions would probably be too much complicated;
3. As a first approximation, the CWC was calculated for different process conditions, exploiting both the model and the experimental data, to assess the most performing solution. In every situation, steam at atmospheric pressure is the best regeneration approach. Different situations were analyzed:
    - In an isothermal process at 400°C, the CWC of Site B was found to be very poor (only 0.02 mol/kg), while Site C CWC was estimated to be between 0.15 and 0.50 mol/kg;
    - A TSA process was studied, with the adsorption step at room temperature and the regeneration at higher temperature. TGA experiments showed that the 2.80 moles of CO_2 adsorbed at 25°C are 30% chemisorbed (0.80 mol/kg) and 70% physisorbed (2 mol/kg).

      Hence, a CWC due to physisorption of 2 mol/kg should be achieved by carrying out the regeneration at 200°C. At this temperature, no chemical desorption in Site B occurs, but it is reported in literature that Site C reactions could further increase the CWC. This information should be quantitatively assessed experimentally.

      Performing the regeneration at 400°C would allow to desorb CO_2 from Site B, but the increase of the CWC would be of only 0.25-0.35 mol/kg (according to the simulations carried out with the model). At this temperature, Site C CWC should be between 0.15 and 0.50 mol/kg;

4. Accurate values of the CWC can be obtained only with the results of the proposed additional experiments, while an actual process simulation could be performed only with a model for the physisorption. However, the performed analysis is enough to draw preliminary conclusions on the optimal conditions for the process. The TSA approach is the most convenient solution, probably with the regeneration at 200°C. A cost analysis should be performed to assess if using more expensive steam at 400°C for regenerating chemisorbed CO_2 could be economically advantageous.

Conclusions and considerations for future work

The kinetic model developed by Coenen *et al.* (2018d) for sorption of CO_2 and H_2O in hydrotalcites between 300°C and 500°C has been successfully implemented in a 1-D PBR model. A verification study has been performed to prove that the model actually solves the implemented balances and is able to correctly simulate an adsorption process. A first validation of the model with breakthrough experimental data showed that it was not enough accurate to describe experiments at low CO_2 concentrations. The parameters of the kinetic model had actually been regressed to describe the reactions in wide concentration ranges of CO_2 and H_2O, for simulating SEWGS processes.

The model was improved to increase the accuracy in the particular conditions of DAC. First, the intra-particle mass transfer was studied through a particle model. It was demonstrated that CO_2 adsorption and desorption reactions in Site B (CO_2 sorption site) are limited by mass transfer at high temperature, and a relation between conversion and effectiveness factor for these reactions was obtained. Site A and Site C reactions (were also steam sorption is involved) were found not to be limited by mass transfer. After the implementation of the mass transfer limitations equations, the accuracy of the model in reproducing experimental data improved, but still not enough.

A sensitivity analysis on the most important parameters of the kinetic model was carried out, in order to increase the accuracy. As far as Site B is concerned, it was found that, in addition to neglecting the internal mass transfer, the original kinetic model underestimated the adsorption capacity, especially at low p_{CO_2}. At the same time, desorption kinetics were overpredicted and bulk carbonation reactions were not accurately implemented. New values for the parameters related to these problems were proposed, with a significant improvement of accuracy in the reproduction of experimental data. Focus was then given to validate the part of the model which describes the adsorption of CO_2 in presence of H_2O. Particular attention was dedicated to this purpose, since previous studies had demonstrated that in these conditions the adsorption capacity of CO_2 is enhanced. Also in this case, the accuracy of the original kinetic model was not satisfying and a parametric study was performed. It was proven that for Site A (where only H_2O adsorbs) the model was validated only once that the desorption rate was decreased (about one order of magnitude) and by increasing the adsorption capacity, especially at low p_{H_2O}. The study on Site C kinetics was more complicated, because it involved simultaneous sorption reactions of CO_2 and H_2O, and interactions had to be accounted for. It was discovered that, with respect to the original model, the capacity for CO_2 adsorption had to be increased, while the steam one had to be reduced, in order

to reproduce experimental data with acceptable accuracy. After the introduction of the proposed changes to the parameters, the model was validated by experimental data, proving that it could be used to obtain reliable data for both dry and wet CWC in DAC feed conditions at temperatures close to 400°C.

Exploiting the obtained model, the isothermal DAC process at 400°C was analyzed. The internal phenomena occurring inside the air contactor during the experiments used for validation were simulated, in order to understand better the process. An important obtained result is that, during the regeneration step, the CO_2 released from Site B at the beginning of the bed is not adsorbed again in other sites, while the CO_2 released from Site C during a wet regeneration is partially adsorbed again in Site B.

Based on the previous results, the optimal conditions for DAC with KMG30 were investigated. In the simulations and in the calculations, it was considered to use a reactor as the one used to perform the experiments used for validation. It was assessed that compressing the air feed is a worthless expense, since it brings almost no increase of adsorption capacity. As far as the regeneration step is concerned, desorption with steam is the best option, compared to nitrogen, because it allows an easy separation from CO_2 and it increases the CWC. The assessment of the optimal temperature for the process is a more complicated issue. Since the model is perfectly validated at 400°C, the CWC was calculated for an isothermal process at this temperature to have a first reference value. The result is that the dry CWC is only 0.02 mol/kg with a regeneration of 6000 s. The wet CWC was instead estimated to be between 0.15 (very conservative value) and 0.55 mol/kg. The uncertainty is due to the unavailability of data for the sorption capacity of steam in Site C for p_{H2O} = 1 bar, as in the regeneration step, however from the data at smaller pressures it may be deduced that there is a high probability that the wet CWC for p_{H2O} = 1 bar is of at least 0.40 mol/kg. In any case, Site C is the main contributor to the CWC in the isothermal process at 400°C.

Since results from literature showed that the adsorption capacity for CO_2 in hydrotalcites is higher at low temperatures, the opportunity to use a TSA approach for DAC was approached. Operating the adsorption step at room temperature and regenerating the saturated sorbent at high temperature allows to save energy costs during the adsorption step, too. Results of TGA experiments at 25°C, 100°C and 200°C allowed to estimate that the adsorption capacity of KMG30 at room temperature is of about 2.80 mol/kg, divided in physisorbed CO_2 (about 2.00 mol/kg) and chemisorbed CO_2 (about 0.80 mol/kg). Breakthrough experiments showed that in an air contactor the adsorption capacity may be smaller than in a TGA (up to 30-40%), probably due to mass transfer limitations and to bypassing problems. Another possibility for the difference of the results may be that in the TGA experiment some increase of weight of the sample was due to adsorption of N_2 and O_2. Though this phenomenon is not documented in literature, additional experiments should be

performed to verify this possibility. The CWC of the TSA process was calculated considering to operate the adsorption step at 25°C, while the possibilities to regenerate at 150-200°C and 400°C were both evaluated.

The analysis showed that it is convenient for DAC with KMG30 to use a TSA approach instead of operating isothermally at high temperature. Probably, the best configuration is with the adsorption step at room temperature, exploiting steam at 150-200°C for the regeneration. By this way, only physisorbed CO_2 would be desorbed, but with a regeneration of just half an hour a CWC of about 1.5 mol/kg should be reached, while even 2 mol/kg could be achieved with a regeneration of 10000-12000 s. Even if these capacities were slightly overestimated because of eventual errors in the TGA experiments, this solution seems to be the best option. This values of capacities are close to the best performing adsorbents for DAC (Figure 1.4), though KMG30 is generally cheaper. In addition, Site C sorption should bring an additional contribution to the CWC achieved with the regeneration at 150-200°C, though more experiments should be carried out to validate Site C kinetics between 25°C and 200°C. Using steam at 400°C for the regeneration would allow to desorb also the chemisorbed CO_2, with an additional CWC of maximum 0.85 mol/kg (probably of about 0.50-0-60 mol/kg), but at a higher steam cost.

Experiments should be carried to understand the adsorption capacity of Site C for steam both at 200°C and at 400°C, and to confirm that the reaction of substitution of hydrates with carbonates proceeds also at room temperature. Modelling physisorption or performing other experiments to confirm the estimated physisorption capacity is another task which should be carried out, to have more accurate estimations of the CWC.

In any case, this study demonstrated that it is convenient to perform DAC with KMG30 in TSA, with adsorption at room temperature and regenerating with steam, probably at 150-200°C. A cost assessment should be performed, to evaluate if it is convenient to use more expensive steam at 400°C to regenerate also the chemisorbed CO_2.

Appendix A - Reactor model verification

After implementing the kinetics for all the three sorption sites in the simulation code of the pseudo-homogeneous reactor model (Paragraph §3.3), the numerical solution of a simplified version of the model was compared with the analytical solution for verifying that the correct equations are solved. All equations and methods are as described in Paragraph §3.3, but for some introduced simplifying assumptions:

- no dispersion occurs within the reactor;
- the adsorption kinetics is: $rate = k_g\, a_s \left(q_{CO_2} - q_{car}\, K_e^{-1}\right) [mol\, m^{-3}]$, where k_g is the mass transfer coefficient between the gas and the solid phase, a_s is the specific surface of the catalyst particles and K_e is the adsorption equilibrium constant;
- no pressure drops within the reactor.

In Table A.1 the conditions of the simulation performed and compared with the analytical solution are reported.

Table A.1 *Conditions of the simulations carried out with the simplified version of the model for comparying the numerical solution with the analytical one*

Gas phase components:	N_2, CO_2
Solid phase components	Inert, free adsorbent ($Mg_6Al_2K_2O_{10}$), carbonate ($Mg_6Al_2K_2O_9CO_3$)
Initial conditions	Gas phase: N_2 100%, 673 K Solid phase: 25% free adsorbent, 75% inert, 673 K
Feed	2.5% CO_2, 97.5% N_2, 500 NmL/min, 1 bar, 673 K
Parameters values	k_g = 0.01 m/s K_e = 100 ϵ_g = 0.40 Bed length = 0.176 m Bed diameter = 0.027 m Spherical catalyst particles diameters = 0.0025 mm Residence time = 2 s
Space discretization	500 grid points
Time discretization	Maximum time step 0.1 s

The analytical solution of the problem was taken from Deen et al. (2016) and it is reported in terms of adimensional variables as the black part of the graph of Figure A.1. The analytical solution corresponding to the parameters and the conditions presented above is the curve plotted for the thickness modulus aZ = 0.117. The obtained numerical solution is plotted in blue and perfectly overlaps the analytical solution.

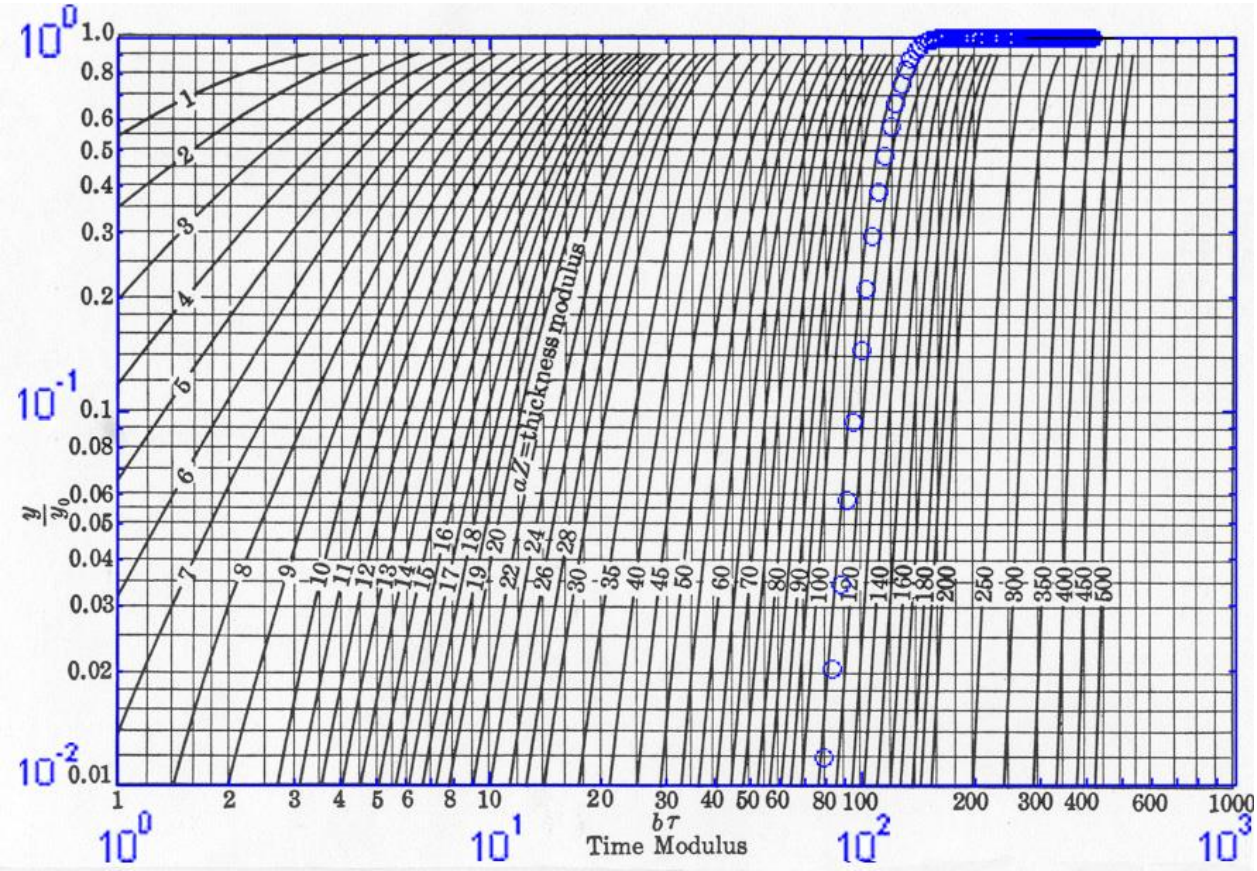

Figure A.1 *The numerical solution (blue) of a simplified adsorption problem solved with the developed code is compared to the analytical solution (black curve for aZ = 0.117)*

This study proved that the code solves the actual equations that it is supposed to and that it is a powerful tool for studying sorption reactions in a PBR.

Nomenclature

Abbreviations

CCS	Carbon Capture and Storage
DAC	Direct Air Capture
GHG	Greenhouse gas
IPCC	Intergovernmental Panel on Climate Change
MOFs	Metal-Organic Frameworks
MW	Molecular Weight
PBR	Packed Bed Reactor
PFD	Process Flow Diagram
SEWGS	Sorbent Enhanced Water Gas Shift
SSE	Sum of Squared Errors
TSA	Temperature Swing Adsorption
XRD	X-rays Diffraction

Greek letters

α	Heat transfer coefficient between the reactor and the environment [W m^{-2} K^{-1}]
$\beta_{rxn,site}$	Elovich energy for a reaction in a specific sorption Site [J mol^{-1} K^{-1}]
ΔH_{rxn}	Enthalpy of a reaction [kJ mol^{-1} K^{-1}]
γ	Angle between the sample and the incident X-Rays in XRD analysis [°]
δ	Wavelength of the incident X-Rays in XRD analysis [m]
ε	Porosity [-]
η	Dynamic gas viscosity [kg m^{-1} s^{-1}]
η_{rxn}	Internal mass transfer efficiency for a reaction [-]
θ	Particle sites coverage [-]
λ	Thermal conductivity [W m^{-1} K^{-1}]
λ_{eff}	Effective axial heat dispersion
ν	Dynamic viscosity [m^2 s^{-1}]
ρ	Density [kg m^{-3}]
τ	Tortuosity [-]

Φ_k	Rate factor [-]
Ξ_{ik}	Element of correction factor matrix [-]

List of symbols

C_p	Heat capacity [J kg^{-1} K^{-1}]
d_p	Particle diameter [m]
$D_{eff,ax}$	Effective axial diffusion coefficient [m^2 s^{-1}]
$D_{eff,ik}$	Effective binary diffusivity [m^2 s^{-1}]
E_a	Activation energy [J mol^{-1}]
$k_{f,site}$	Freundlich k-parameter for a certain site [mol kg^{-1} bar$^{-n,f}$]
$k_{g,ik}$	Element of mass transfer coefficient at actual response [m s^{-1}]
$k^0_{g,ik}$	Element of mass transfer coefficient at low mass transfer rates [m s^{-1}]
k_{rxn}	Kinetic constant of a certain reaction
$\dot{m}_{g\rightarrow s}$	Mass transfer rate [kg m^{-3} s^{-1}]
$\dot{n}_{g\rightarrow s}$	Molar transfer rate [mol m^{-3} s^{-1}]
n_b	Bulk carbonation reaction exponential factor [-]
n_C	Exponential factor for Site C capacity equation [-]
$n_{f,site}$	Freundlich n-parameter for a certain site [-]
n_i	Mass flux of component *i* [kg mol^{-1}]
n_T	Smooth transition coefficient [-]
n_{tot}	Drift flux [kg m^{-2} s^{-1}]
Nu	Nusselt number [-]
p	Pressure [bar]
Pe_{ax}	Axial Peclet number [-]
Pr	Prandtl number [-]
Q_{max}	Maximum site coverage [mol kg^{-1}]
q_{site}	Adsorbed species concentration in a certain site [mol m^{-3}]
r	Particle radial coordinate [m]
r_B	Position of boundary between reaction and diffusion zone in the particle [m]
$r_{i/j}$	Rate of production of gas/solid species i/j [mol m^{-3} s^{-1}]
R	Gas constant [J mol^{-1} K^{-1}]
Re	Reynolds number [-]
Sh	Sherwood number [-]
t	Time [s]

T	Temperature [K]
v	Velocity [m s^{-1}]
x	Reactor axial coordinate [m]
X_{rxn}	Conversion of a certain reaction [-]
y_i	Molar fraction of gas species [-]
$\overline{y}_{bulk}$	Gas bulk composition vector [-]
w_j	Mass fraction of solid species [-]

Subscripts

A	Relative to Site A
ads	Adsorption reaction
adsA	Free adsorbent in Site A
adsB	Free adsorbent in Site B
adsC	Free adsorbent in Site C
B	Relative to Site B
bulk	Bulk composition/reactions
C	Relative to Site C
carB	Carbonate in Site B
carC	Carbonate in Site C
des	Desorption reaction
g	Gas phase
hydA	Hydrate in Site A
hydC	Hydrate in Site C
i	Component in the gas phase
j	Component in the solid phase
max	Maximum
rxn	Relative to a certain reaction
s	Solid phase

Superscripts

0	Initial composition
eq	Equilibrium composition

References

Anderegga, W. R. L., Prallb, J. W., Haroldc, J. and Schneidera, S. H. (2010) 'Expert credibility in climate change', *Proceedings of the National Academy of Sciences*, 107(27), pp. 12107–12109. doi: 10.1073/pnas.1003187107.

Armaroli, N. and Balzani, V. (2015) 'Solar Electricity and Solar Fuels: Status and Perspectives in the Context of the Energy Transition', *Chemistry – A European Journal*, 22(1), pp. 32–57. doi: doi:10.1002/chem.201503580.

Bauer, R. and Schluender, E. U. (1978) 'Effective Radial Thermal Conductivity of Packings in Gas Flow, Part II: Thermal Conductivity of the Packing Fraction without Gas Flow', 18(2), pp. 189–204.

Birkholz, M. (2006) 'Thin film analysis by X-ray scattering', *Journal of Applied Crystallography*, 39, pp. 925–926. doi: 10.1107/S0021889806034698.

Cavani, F., Trifirbò, F. and Vaccari, A. (1991) 'Hydrotalcite-type anionic clays: preparation, properties and applications', *Catalysis Today*, (11), pp. 173–301.

Coenen, K., Gallucci, F., Cobden, P., Van Dijk, E., Hensen, E. and Van Sint Annaland, M. (2016) 'Chemisorption working capacity and kinetics of CO_2 and H_2O of hydrotalcite-based adsorbents for sorption-enhanced water-gas-shift applications', *Chemical Engineering Journal*, 293, pp. 9–23. doi: 10.1016/j.cej.2016.02.050.

Coenen, K., Gallucci, F., Pio, G., Cobden, P., Van Dijk, E., Hensen, E. and Van Sint Annaland, M. (2017) 'On the influence of steam on the CO_2 chemisorption capacity of a hydrotalcite-based adsorbent for SEWGS applications', *Chemical Engineering Journal*. Elsevier B.V., 314, pp. 554–569. doi: 10.1016/j.cej.2016.12.013.

Coenen, K., Gallucci, F., Mezari, B., Hensen, E. and Van Sint Annaland, M. (2018a) 'An in-situ IR study on the adsorption of CO_2 and H_2O on hydrotalcites', *Journal of CO2 Utilization*. Elsevier, 24(January), pp. 228–239. doi: 10.1016/j.jcou.2018.01.008.

Coenen, K., Gallucci, F., Hensen, E. and Van Sint Annaland, M. (2018b) 'CO_2 and H_2O chemisorption mechanism on different potassium-promoted sorbents for SEWGS processes', *Journal of CO_2 Utilization*. Elsevier, 25, pp. 180–193. doi: 10.1016/j.jcou.2018.04.002.

Coenen, K., Gallucci, F., Cobden, P., Van Dijk, E., Hensen, E. and Van Sint Annaland, M. (2018c) 'Influence of material composition on the CO_2 and H_2O adsorption capacities and kinetics of potassium-promoted sorbents', *Chemical Engineering Journal*. Elsevier, 334(December 2017), pp. 2115–2123. doi: 10.1016/j.cej.2017.11.161.

Coenen, K., Gallucci, F., Hensen, E. and Van Sint Annaland, M. (2018d) 'Kinetic model for adsorption and desorption of H_2O and CO_2 on a hydrotalcite based adsorbent for sorption-enhanced water-gas shift'.

Cullity, B. D. and Weymouth, J. W. (1957) 'Elements of X-Ray Diffraction', *American Journal of Physics*. American Association of Physics Teachers, 25(6), pp. 101–102. doi: 10.1119/1.1934486.

Darunte, L. A., Walton, K. S., Sholl, D. S. and Jones, C. W. (2016) 'CO_2 capture via adsorption in amine-functionalized sorbents', *Current Opinion in Chemical Engineering*. Elsevier, 12, pp. 82–90. doi: 10.1016/J.COCHE.2016.03.002.

Daubert, T. E. and Danner, R. P. (1992) *Physical And Thermodynamic Properties Of Pure Chemicals*. Taylor & Francis. Available at: https://books.google.nl/books?id=pMrKAAAACAAJ.

Dębek, R., Motak, M., Grzybek, T., Galvez, M. and Da Costa, P. (2017) 'A Short Review on the Catalytic Activity of Hydrotalcite-Derived Materials for Dry Reforming of Methane', *Catalysts*. Multidisciplinary Digital Publishing Institute, 7(12), p. 32. doi: 10.3390/catal7010032.

Didas, S. A., Choi, S., Chaikittisilp, W. and Jones, C. W. (2015) 'Amine-Oxide Hybrid Materials for CO_2 Capture from Ambient Air', *Accounts of Chemical Research*, 48(10), pp. 2680–2687. doi: 10.1021/acs.accounts.5b00284.

Edwards, M. F. and Richardson, J. F. (1968) 'Gas dispersion in packed beds', *Chemical Engineering Science*, 23(2), pp. 109–123. doi: 10.1016/0009-2509(68)87056-3.

Fuss, S., Minx, J. C., Lamb, W. F., Max, W., Nemet, G. F., Callaghan, M. W., Stechow, C. V., Minx, J. C., Lamb, W. F., Beringer, T., Garcia, W. D. O., Hartmann, J and Khanna, T. (2018) 'Negative emissions — Part 2 : Costs , potentials and side effects', *Enviromental Research Letters*, (13), p. 63002.

Gunn, D. J. (1978) 'Transfer of heat or mass to particles in fixed and fluidised beds', *International Journal of Heat and Mass Transfer*, 21(4), pp. 467–476. doi: 10.1016/0017-9310(78)90080-7.

Gunn, D. J. and Misbah, M. M. A. (1993) 'Bayesian estimation of heat transport parameters in fixed beds', *International Journal of Heat and Mass Transfer*, 36(8), pp. 2209–2221. doi: 10.1016/S0017-9310(05)80152-8.

Hamers, H. P. (2015) 'Packed bed chemical-looping combustion : experimental demonstration and energy analysis'. doi: 10.6100/IR783193.

Holmes, G. and Keith, D. W. (2012) 'An air-liquid contactor for large-scale capture of CO_2 from air', *Philosophical Transactions of the Royal Society A: Mathematical, Physical and Engineering Sciences*, 370(1974), pp. 4380–4403. doi: 10.1098/rsta.2012.0137.

IPCC (2005) *Special Report on Carbon Dioxide Capture and Storage. Prepared by Working Group III of the Intergovernmental Panel on Climate Change;* Metz, B., Davidson, O., de Coninck, H. C., Loos, M., Meyer, L. A., Eds.;, Cambridge University Press: Cambridge, U.K., and New York.

IPCC (2013) *Climate Change 2013: The Physical Sciences Basis*, University Press, Cambridge New York.

IPCC (2014) 'Climate Change 2014: Synthesis Report', *Contribution of Working Groups I, II and III to the Fifth Assessment Report of the Intergovernmental Panel on Climate Change.* In: Core Writing Team, Pachauri RK, Meyer LA (eds) IPCC, Geneva, Switzerland, 151 p., pp. 1–112.

Jang, H. J., Lee, C. H., Kim, S., Kim, S. H. and Lee, K. B. (2014) 'Hydrothermal synthesis of K_2CO_3-promoted hydrotalcite from hydroxide-form precursors for novel high-temperature CO2 sorbent', *ACS Applied Materials and Interfaces*, 6(9), pp. 6914–6919. doi: 10.1021/am500720f.

Lackner, K. S., Brennan, S., Matter, J. M., Park, A., Wright, A. and Van der Zwaan, B. (2012) 'The urgency of the development of CO_2 capture from ambient air', *Proceedings of the National Academy of Sciences*, 109(33), pp. 13156–13162. doi: 10.1073/pnas.1108765109.

Lackner, K., Ziock, H.-J. and Grimes, P. (2008) 'Carbon capture from air, is it an option?', *The AIDS reader*, 18(6), p. 292. Available at: http://www.ncbi.nlm.nih.gov/pubmed/21904770.

Lee, J. M., Min, Y. J., Lee, K. B., Jeon, S. G., Na, J. G. and Ryu, H. G.(2010) 'Enhancement of CO_2 sorption uptake on hydrotalcite by impregnation with K_2CO_3', *Langmuir*, 26(24), pp. 18788–18797. doi: 10.1021/la102974s.

Moreira, R. F. P. M., Soares, J. L., Casarin, G. L. and Rodrigues, A. E. (2006) 'Adsorption of CO_2 on hydrotalcitelike compounds in a fixed bed', *Separation Science and Technology*, 41(2), pp. 341–357. doi: 10.1080/01496390500496827.

Deen, N. G., Van Sint Annaland, M. and Kuipers, J. A. M. (2016) *Numerical method for Chemical Engineers course material*. Eindhoven, NL: Technical University Eindhoven.

Nataraj, S. *et al.* (2000), European Patent EP1006079A1

National Institute of Standards and Technology website (2018). Available at: www.nist.gov.

Nature website. Available at: https://www.nature.com/articles/d41586-018-05357-w.

Noorman, S., Gallucci, F., Van Sint Annaland, M. and Kuipers, J. A. M. (2011) 'A theoretical investigation of CLC in packed beds. Part 1: Particle model', *Chemical Engineering Journal*. Elsevier, 167(1), pp. 297–307. doi: 10.1016/J.CEJ.2010.12.068.

Noorman, S., van Sint Annaland, M. and Kuipers (2007) 'Packed Bed Reactor Technology for Chemical-Looping Combustion', *Industrial & Engineering Chemistry Research*, 46(12), pp. 4212–4220. doi: 10.1021/ie061178i.

Paterson, W. and Hayhurst, A. . (2000) 'Mass or heat transfer from a sphere to a flowing fluid', *Chemical Engineering Science*. Pergamon, 55(10), pp. 1925–1927. doi: 10.1016/S0009-2509(99)00467-4.

Sanz-Pérez, E. S, Murdock, C. R., Didas, S. A. and Jones, C. W. (2016) 'Direct Capture of CO_2 from Ambient Air', *Chemical Reviews*, 116(19), pp. 11840–11876. doi: 10.1021/acs.chemrev.6b00173.

Smit, J., Van Sint Annaland, M. and Kuipers, J. A. M. (2005) 'Grid adaptation with WENO schemes for non-uniform grids to solve convection-dominated partial differential equations', *Chemical Engineering Science*, 60(10), pp. 2609–2619. doi: 10.1016/j.ces.2004.12.017.

Soares, J. L., Moreira, R. F. P. M., José, H. J., Grande, C. A. and Rodrigues, A. E. *et al.* (2005) 'Hydrotalcite Materials for Carbon Dioxide Adsorption at High Temperatures: Characterization and Diffusivity Measurements', *Separation Science and Technology*, 39(9), pp. 1989–2010. doi: 10.1081/SS-120039307.

Socolow, R., Desmond, M., Aines, R., Blackstock, J., Bolland, O., Kaarsberg, T., Lewis, N., Mazzotti, M., Pfeffer, A., Sawyer, K., Siirola, J., Smit, B. and Wilcox, J. (2011) 'Direct Air Capture of CO_2 with Chemicals Panel on Public Affairs', *American Physical Society - Panel on Public Affairs*, p. 100.

Tzimas, E. and Peteves, S. (2003) *Controlling Carbon Emissions: The Option of Carbon Sequestration*.

Vortmeyer, D. and Berninger, R. (1982) 'Comments on the paper, theoretical prediction of effective heat transfer parameters in packed beds by Anthony Dixon and D. L. Cresswell[AIChE J., 25, 663(1979)]', *AIChE Journal*, 28(3), pp. 508–510. doi: 10.1002/aic.690280321.

Walspurger, S., Walspurger, S., Boels, L., Cobden, P. D., Elzinga, G. D., Haije, W. G., Van den Brink, R. W. (2008) 'The Crucial Role of the K^+ – Aluminium Oxide Interaction in K^+ -Promoted Alumina- and Hydrotalcite-Based Materials for CO_2 Sorption at High Temperatures', *ChemSusChem*, 1(7), pp. 643–650. doi: 10.1002/cssc.200800085.

Yuan, Z., Eden, M. R. and Gani, R. (2016) 'Toward the Development and Deployment of Large-Scale Carbon Dioxide Capture and Conversion Processes', *Industrial & Engineering Chemistry Research*, 55(12), pp. 3383–3419. doi: 10.1021/acs.iecr.5b03277.

Acknowledgments

The six months I spent at the Technische Universiteit Eindhoven for my thesis work have been an incredible experience for both my professional career and my life. First, I want to thank professor Fabrizio Bezzo for all the support he gave me during this time and for the patient revision of this thesis. Special thanks also to professor Paolo Canu, responsible of the Erasmus+ exchange program which allowed me to develop my project in Eindhoven.

During my time in The Netherlands, I met many great people who gave their contribution to the beautiful experience I lived. I want to thank professors Martin Van Sint Annaland and Fausto Gallucci for welcoming me in the SMR group and for the assistance in the development of the very interesting project I was assigned to. I owe special thanks to my daily supervisor Francesco Sabatino, who was literally always available to discuss the issues I was facing and to give useful suggestions. I felt very lucky (and sometimes envied by other students) for having had the opportunity to work with him. Thanks are due also to the other PhD students for the occasional support during the project. I want to thank all the people from the SMR/Erasmus family, who made me feel like at home and enjoy all this time in Eindhoven.

Finally, I want to express my infinite gratitude to my family and my friends for the support and help they gave me during this experience, making me feel always close to them despite the distance.